ABSTRACT

YING, MANQING. Modeling Plume Rise of Air Emissions from Animal Housing Systems: Applications of CFD and AERMOD. (Under the direction of Dr. Lingjuan Wang-Li).

Gaussian-based dispersion models have been applied to simulate the fate and transport of air emissions from animal housing systems. The accuracy of the plume rise and plume shape predictions had been a challenge for Gaussian dispersion models to simulate air emission from AFOs. To meet the research needs, this study was conducted to:

1. Quantify the plume shapes in a single ventilation fan testing setup that generated similar plume fluid field to those in commercial animal houses through visualization and CFD modeling of field measurements;
2. Apply inverse-AERMOD to derive the plume rises of animal house emissions on a commercial layer farm using field measurements of PM_{10} emissions and concentrations at the emission source and in the downwind locations;
3. Identify the impacts of various factors on plume rises of the animal house air emissions based upon the field observations, the inverse-AERMOD results and the CFD simulations.

The single ventilation fan plume field measurements indicated that the plume of a 0.6 m (24 in.) ventilation fan at the full speed (1072 rpm) had a depth about 9 m, a width about 12 m, and a rise (lifting) beyond the highest measurement point, 4.88 m (16 ft). The CFD simulations revealed that: 1) temperature difference between the plume and ambient air had a positive impact on plume rise and a negative impact on plume depth; 2) background wind directly against the fan flow affected the plume rise, plume width and plume rise negatively;

3) background wind across the fan flow reduced the plume depth but enlarged the plume width and plume rise.

In application of AERMOD, in total 87 hourly plume rises were found for 20 days' hourly measurements of PM_{10} concentrations and emissions (5 days per season for 4 seasons from fall 2008 to summer 2009). The mean plume rises for fall 2008, winter 2008, spring 2009 and summer 2009 were 16.2 m (SE = 11.2 m), 7.9 m (SE = 9.5m), 16.5 m (SE = 12.4m), and 14.3 m (SE = 10.0m), respectively. While the diurnal patterns of the plume rises were not consistent among different selective days, they generally followed the diurnal patterns of house ventilation rates. Plume rise for weekends were found to be significantly higher than those for weekdays in fall. The relationships between plume rises and various factors were tested. Multiple linear regression showed a significant positive relationship (p-value = 0.0134) between wind speed and the plume rises. Ambient relative humidity and total ventilation volume flow were also found to be slightly (p-value = 0.171 and 0.217, respectively) related to the plume rises.

Modeling Plume Rise of Air Emissions from Animal Housing Systems: Applications of CFD and AERMOD

by
Manqing Ying

A thesis submitted to the Graduate Faculty of
North Carolina State University
in partial fulfillment of the
requirements for the degree of
Master of Science

Biological and Agricultural Engineering

Raleigh, North Carolina

2012

APPROVED BY:

_____	_____
Lingjuan Wang-Li Committee Chair	Larry Stikeleather
_____	_____
Jack Edwards	Huixia Wang

ACKNOWLEDGMENTS

I would give my greatest appreciation to my advisor, Dr. Lingjuan Wang-Li for her advices and supports throughout my MS period. Those uncountable hours, especially those non-working hours that she sacrificed for my research project would be memorized deep in my heart with thankfulness. And I would like to thank all my committee members, Dr. Larry Stikeleather, Dr. Jack Edwards and Dr. Huixia Wang for their help and suggestions.

This project was supported by the NSF CAREER Award No. CBET-0954673

The ventilation data, meteorological data and source PM_{10} concentrations for the input files in AERMOD modeling were collected under the National Air Emission Monitoring Study (NAEMS).

The help from Roberto Munillia, Steven Badawi, Di Hu, Qianfeng Li and BAE research shop for testing setup construction and field data collection is also thankfully acknowledged.

Last but not least, I would like to thank for the unconditional love and support from my parents.

BIOGRAPHY

In the summer of 2010, Manqing Ying received her Bachelor's degree in the department of Environmental and Resource Science at Zhejiang University, Zhejiang, China. She started her Master of Science degree and has occupied a Research Assistant position in the department of Biological and Agricultural Engineering at North Carolina State University in fall, 2010. Her research focused on applying CFD and AERMOD to model plume rises of air emissions from animal houses.

TABLE OF CONTENTS

LIST OF TABLES……ix

LIST OF FIGURES……xi

CHAPTER 1 INTRODUCTION……1

1.1 Animal agricultural air emissions……1

1.1.1 Animal feeding operations……1

1.1.2 Air emissions of AFOs……2

1.2 National air emission monitoring study……4

1.3 Air dispersions……5

1.3.1 Plume rise……6

1.3.2 The impact of sources on air dispersions……8

1.3.3 The impact of ambient environments on air dispersions……11

1.3.4 Measurements of air dispersions……12

1.3.4.1 Conventional and remote sensing……12

1.3.4.2 Scale of the measurements……14

1.3.4.3 Visualization methods……16

1.3.5 Modeling of air dispersions……16

1.3.5.1 Box model……17

1.3.5.2 Gaussian model……17

1.3.5.3 Lagrangian and Eulerian model……18

1.3.5.4 Computational fluid dynamic model……19

1.4 Summary of current insufficiency……20

1.5 Research objectives……21

CHAPTER 2 MODELING RISE OF PLUME EMITTED FROM AN ANIMAL HOUSING VENTILATION FAN: APPLICATION OF CFD……..……23

2.1 Introduction……24

2.2 Methodology……..26

2.2.1 Ventilation plume testing setup: the mini-tunnel……...……...…….…….27

2.2.2 Ventilation plume measurements……..…….…….……28

2.2.2.1 Instrumentation…….……...28

2.2.2.2 Plume fluid field measurements……..…….30

2.2.3 Data processing……..……..……33

2.2.3.1 Flow vector transformation……..……33

2.2.3.2 Weather data processing……..……34

2.2.4 Plume fluid field 3D velocity plotting: the Tecplot visualization……...……36

2.2.5 Plume fluid field CFD modeling……..…….……..36

2.2.5.1 Definition of the boundary conditions…….....37

2.2.5.2 Computational mesh……..……..……..41

2.2.5.3 Simulation and comparisons……..……..……..42

2.2.5.4 Plume shape observation……..……...……...45

2.3 Results and discussion…….……..……46

2.3.1 Field measurements……...……...……...46

2.3.1.1 Velocity measurement comparisons within test sets……...……..47

2.3.1.2 Plume visualization of field measurements by Tecplot…….……..48

2.3.1.3 Plume shape observation and prediction of field measurements…....50
2.3.2 Plume modeling and visualization by CFD……...…….…….51
2.3.2.1 Modeling and visualization of plume under the field experimental conditions……..……...51
2.3.2.2 Impact of temperature difference on the plume rise…….……...53
2.3.2.3 Impact of background wind on plume shape……...……..55
2.4 Conclusions……..……60
CHAPTER 3 MODELING PLUME RISE OF AIR EMISSIONS FROM ANIMAL HOUSING SYSTEMS: APPLICATION OF AERMOD……61
3.1 Introduction…….……61
3.1.1 Particular matters emitting from animal housing systems……....……..61
3.1.2 Application of air dispersion model in agricultural emission……...……..63
3.1.2.1 Application of AERMOD in AFO emission...……..…….65
3.1.3 Research objectives……...……..73
3.2 Methodology…….……73
3.2.1 Field data collection……...…….....…….74
3.2.1.1 The layer farm and PM monitoring stations……...…..……..74
3.2.1.2 PM data collection……..……..77
3.2.1.3 House ventilation (fan flow) measurements……..…..……..78
3.2.1.4 Meteorological conditions…….…….……81
3.2.2 Data period selection……81
3.2.3 Field data processing……82

3.2.3.1 Meteorological data……82

3.2.3.2 Individual fan flow rates……84

3.2.3.3 Emission rates……86

3.2.4 AERMOD simulation……89

3.2.4.1 Source inputs……89

3.2.4.2 Receptor inputs……93

3.2.4.3 Meteorological data inputs……93

3.2.4.4 Building information inputs……93

3.2.4.5 Plume rise predictions……94

3.2.4.6 Data analysis and statistical modeling of adjusted plume rises……97

3.3 Results and discussion……97

3.3.1 Analysis of the selected data periods for AERMOD simulations……97

3.3.2 Seasonal impact of plume rises……99

3.3.3 Diurnal effect on plume rises……100

3.3.4 The impact of weekday and weekend……104

3.3.5 Multiple linear regression analysis……106

3.3.6 Causes of uncertainties……108

3.4 Conclusions……109

CHAPTER 4 CONCLUSIONS AND FUTURE WORK……110

4.1 Summary and conclusions……110

4.2 Recommendations for future work……111

REFERENCES……114

APPENDICES……..126

Appendix A Tecplot results…….……..127

Appendix B FloEFD results……..…….129

Appendix C AERMOD results……..150

Appendix D Statistical codes……159

LIST OF TABLES

Table 2-1. Exponents for wind profile (Power Law) model……..……..……...35

Table 2-2. Adjustments of coordinate system for testing points by using u, v and w…….....39

Table 2-3. Settings of the computational domain in the FloEFD model……..……...42

Table 2-4. The distribution of wind speeds in stability-related ranges at 10 m …….……44

Table 2-5. Parameter settings for CFD simulations……..…..…….44

Table 2-6. Exit velocities and radial velocities for fan surface determination…….…..…51

Table 2-7. CFD modeled plume shapes under various temperature differences……..…...55

Table 2-8. CFD modeled plume shapes under various background winds…….……..…..57

Table 2-9. Pearson's correlation analysis of relationship between background winds and plume shapes ……58

Table 3-1. Overall building information of the layer farm…….……..……..75

Table 3-2. Data periods selected for modeling PM_{10} dispersion to derive plume rises through inverse AERMOD method……..…….82

Table 3-3. Definition of the air flow streams for tunnel ventilated houses 3 and 4…….....85

Table 3-4. PM_{10} data sources for different tunnel ventilated houses…….……..….88

Table 3-5. List of source information for simulations in AERMOD……..…….……..…..90

Table 3-6. Stack heights and stack diameters for point sources…….…...……..91

Table 3-7. Releasing heights and XY dimensions for area sources……..……..…….92

Table 3-8. Receptor information……..93

Table 3-9. The grouping of the selected data periods……..98

Table 3-10. Mean plume rises by seasons……...……99

Table 3-11. The impact of weekday and weekend on the plume rises……...……105

Table 3-12. The multiple linear regression modeling reults for plume rise…..……..…...107

LIST OF FIGURES

Figure 1-1. Characteristics of axial fan flow (ACGIH, 2004)…..……..……..4

Figure 1-2. Definition of the plume rise (Δh)……7

Figure 1-3. Industrial stack emission (left) (Novel, 2004) and agricultural air emission (right)…….……8

Figure 1-4. Plume of air emissions (mixture of PM + gas + moisture) from two tunnel ventilated poultry houses (Note: the background trees were over 14m high) (Ying et al., 2011)…….…….……9

Figure 2-1.The wooden mini-tunnel with a 0.6m (24in.) axial ventilation fan on the one end and the collimating screen on the other end…….……...28

Figure 2-2. The 3D ultrasonic anemometer assemblies (left: five anemometers on the posts with data loggers and battery power supplies) and illustration of the adjustable heights of the anemometer assembly on the post (right)……..……..29

Figure 2-3. Top view of the 3D plume flow measurement layout……...31

Figure 2-4. The plume fluid field measurement on the3m ring and at 3.05m (10ft) height ...32

Figure 2-5. The coordinate system for plume fluid field velocity computation……..…...33

Figure 2-6. Testing points of the fan surface flow measurements……..…….38

Figure 2-7. 95% confidence intervals of differences of velocity in "w" direction (m s^{-1}) within the first set of tests (left) and second set of tests (right)…….47

Figure 2-8. Contour plots of the vertical velocity "w" at four heights for the testing group 2-05……..48

Figure 2-9. Contour plots of the vertical velocity “w” at three rings for the testing group 2-05……49

Figure 2-10. Contour plots of the vertical velocity “w” at the location of five sensors (side views) for the testing group 2-05……..…….……..49

Figure 2-11 Top-view of CFD modeled contour plot of the flow speeds at a horizontal plane 1.22 m above the ground…..……..……52

Figure 2-12. 3D view (left) and side-view slide (right) of the contour plot of the velocity “w” modeled by the CFD, simulation of field measurement conditions…….....52

Figure 2-13. Side view of the vertical velocity “w” when $\Delta T = 0$……..……...……53

Figure 2-14. Top view of the flow speeds when $\Delta T = 0$ at a horizontal cut plane 6.41 m above the ground……...……...54

Figure 2-15 “w” contour of particle movements with background wind V_x = -0.05 ms^{-1}….56

Figure 2-16 “w” contour of particle movements with background wind V_x = -2.50 ms^{-1} …59

Figure 3-1. Plume with Gaussian distribution in both vertical and horizontal directions (Turner, 1994)…….……67

Figure 3-2. Plume with bi-Gaussian distribution in vertical direction under the CBL (U.S. EPA, 2004b)……67

Figure 3-3. Three plume treatments under the CBL (U.S. EPA, 2004b)……..…68

Figure 3-4. The layer farm layout & the locations of PM monitoring stations (Wang-Li et al., 2012)…….……..75

Figure 3-5. Illustration of the fans in a cross-ventilated house (left) & a tunnel-ventilated house (right)…….76

Figure 3-6. Ventilation stage settings of the tunnel ventilated houses (Wang-Li et al., 2012)……79

Figure 3-7. Ventilation stage settings of the cross ventilated houses……...…80

Figure 3-8. Upwind and downwind illustration……...…84

Figure 3-9. 3D layout of the farm simulated in AERMOD…….……94

Figure 3-10. Flowchart of inverse-AERMOD in predicting plume rises……..…..…..95

Figure 3-11. Diurnal variations of the plume rises……..…..……101

Figure 3-12. Diurnal variation of the plume rises on three selected days…….102

Figure 3-13. Diurnal variation of the plume rises on 11 October 2008……103

Figure 3-14. Diurnal variation of the plume rises on 12 April 2009…….104

Figure 3-15. Diurnal variation of the plume rises on 16 April 2009……104

CHAPTER 1 INTRODUCTION

1.1 ANIMAL AGRICULTURAL AIR EMISSIONS

Living in a time of rapid advance nowadays, people start to care more about the harmonious coexistence with the nature. As a rising concern, environmental pollutions can be divided mainly in to air pollution, water pollution and soil contamination. The pollutions are mainly caused by: 1) industrial productions; 2) agricultural productions The United States (U.S.) has been the greatest agricultural country, producing $100.9 billion net farm income per year (USDA, 2011). While providing Americans' food supplies, animal agricultural productions are generating massive quantities of manure, urine and other wastes leading to serious air pollution problems and public health concerns (U.S. EPA, 2008).

1.1.1 ANIMAL FEEDING OPERATIONS

Animal feeding operations (AFOs) are defined as operations where animals are raised and fed in confined environment for no less than 45 days during a 12-month period (U.S. GAO, 2008). AFOs have become dominant livestock production in the U.S. and other parts of the world. Most of the poultry products consumed by humans have been from AFOs starting in the 1950s, and most cattle and pork products started to come from AFOs since the 1970s and 80s (Burkholder et al., 2007). As Quinn et al. (2001) reported that up to 90% of the massive agricultural air pollutants were from animal agriculture, mainly gases and particulate, their impacts on the local environment are essential.

1.1.2 AIR EMISSIONS OF AFOS

The U.S. Environmental Protection Agency (U.S. EPA) uses emission factors (EF) to express the air emissions. An EF was described by the U.S. EPA (1995) as a representative

value that attempts "*to relate the quantity of a pollutant released to the atmosphere with an activity associated with the release of that pollutant*". The U.S.EPA (1995) classified the EFs into different chapters by the source types of emissions, among which the AFO emissions are included in the chapter 9-Food and Agricultural Industries. Although the compilation of air pollutant EFs has been developed for various emission sources, neither EFs nor estimation methods of emissions were suggested for livestock and poultry operations.

To better control air pollution, an essential part of environmental pollution, the U.S. Congress passed the first Clean Air Act (CAA) in 1963. The CAA of 1970 established the U.S. EPA and "*defined the U.S. EPA's responsibilities for protecting and improving the nation's air quality and the stratospheric ozone layer*"(U.S. EPA, 2012a). The National Ambient Air Quality Standards (NAAQS) were set for pollutants considered harmful to public health and the environment consequently. The main purpose of NAAQS is to regulate six principal pollutants: lead (P_b), ozone (O_3), carbon monoxide (CO), nitrogen dioxide (NO_2), sulfur dioxide (SO_2) and particulate matter (PM). At current stage, the baseline emissions of those criteria pollutants from AFOs are unknown and the AFOs are exempted from the NAAQS permitting requirements.

The main air pollutants from AFOs are PM (i.e. total suspended particulate-TSP, PM_{10}, and $PM_{2.5}$: PM with aerodynamic equivalent diameter less than or equal to 10 and 2.5 micrometers, respectively), ammonia (NH_3), hydrogen sulfide (H_2S), and volatile organic compounds (VOCs) (NRC, 2003). The amount of each pollutant varies among AFOs with different characteristics. Firstly, the types of animals are important. Not only would the species of animals affect the type and amount of air pollutants emitting from animal houses,

but also would the ages of the animals have impact on it. For instance, the broiler production would emit less NH_3 upon the birds' arrival as compared to the amount of NH_3 emission after the birds were raised several weeks (Harper et al., 2010). Secondly, the animal activities would have impact on the emissions. Jeppsson (2001) stated in his study that the NH_3 emission from pig farm follows a clear diurnal pattern with a minimum emission at 6:00 a.m. and a maximum emission at 5:00 p.m. Similar diurnal patterns were also found by Ngwabie et al. (2011). Furthermore, different ventilation systems would lead to different fluid field out of the animal buildings, and thus result in varies emissions.

Mechanical ventilation systems are commonly used currently in AFOs for effectiveness in controlling the indoor thermal conditions of animal houses. This is also an essential factor to influence animal growth and thus affect the air emissions. In general, the house ventilation is fulfilled by fans. There are two main kinds of fans: centrifugal fans and axial fans. The AFO building ventilations usually use the axial ones as they require large volume flow of air that centrifugal ones could not achieve. The axial fan flows would be rotating out instead of emitting in one direction and the distribution of velocities through the fan surface is special. As indicated by American Conference of Governmental Industrial Hygienists (ACGIH) (2004), for an axial fan, the exit flow speeds are shown in Figure 1-1. Specific measurements of air velocities and flow angles should be taken in order to simulate emission and dispersion of air pollutants from animal housing systems.

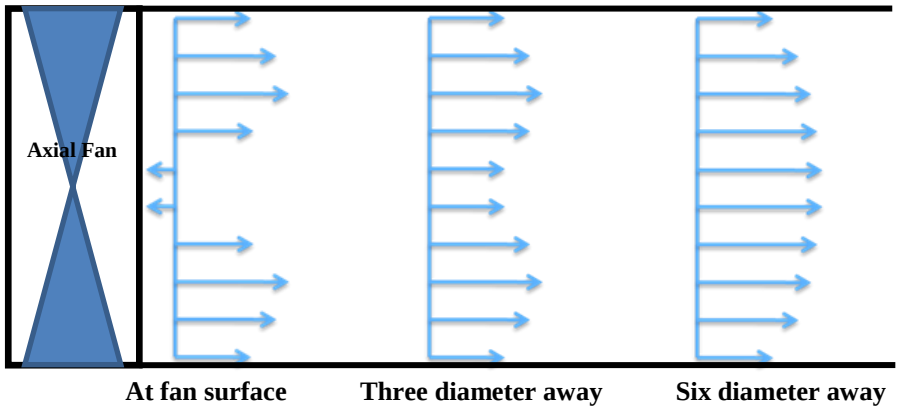

Figure 1-1. Characteristics of axial fan flow in a pipe (ACGIH, 2004)

Like for other kinds of AFOs, researchers have been trying to develop a comprehensive emission inventory for poultry operations, but found it being challenged (Roumeliotis and Van Heyst, 2008; Powers et al., 2005). Roumeliotis and Van Heyst suggested the inconsistency of various studies in NH_3 and PM EFs may be due to the different local climate, ventilation systems of poultry houses and manure management systems. They also concluded that before promoting a new policy or regulation in agricultural air emission related problems, more accurate data that "*clearly illustrate negative impacts*" would be important. Similar findings were reported by Powers et al. (2005), who also pointed out that reliable, accurate and precise technique to measure flow rates from ventilation systems would be necessary to quantify emission rates.

1.2 NATIONAL AIR EMISSION MONITORING STUDY

Insufficient agricultural air emission studies have caused wide concern. In 2003, National Academy of Sciences (NRC, 2003) reported that possible air pollution problems from AFOs

should be highlighted and the existing databases about air emissions from AFOs were not adequate. In response to that, a two-year project called "National Air Emission Monitoring Study (NAEMS)" was conducted to collect baseline emissions of various pollutants under the U.S. EPA Air Compliance Agreement for AFOs (U.S. EPA, 2005). The NAEMS was supported by the AFO industries and overseen by the U.S. EPA, involving in eight universities for data collection.

In the NAEMS project, 14 sites ranging in barn numbers and operation types across the nation were carefully selected to be representative of various AFOs. Pollutants of $PM_{2.5}$, PM_{10}, TSP, NH_3, H_2S and VOCs were measured based on the type of site with technical approaches addressed by a group of invited scientists, producers' representatives and officials from U.S. EPA and USDA (Purdue, 2006a). Based on the data collected by the NAEMS project, the U.S. EPA has developed a draft emissions estimating methodologies report and baseline emission data for broiler operations (U.S. EPA, 2012b). It is anticipated that similar reports will be issued for other animal species under the NAEMS, including egg, swine, and dairy operations.

1.3 AIR DISPERSIONS

After being emitted from the source, pollutants can disperse with air in the atmosphere. Studies of fate and transport of air pollutants requires knowledge about dispersion of the exhausted pollutant plume. Research in air dispersion includes different types of sources, various dispersion plume measurement techniques and models for simulations and so on.

1.3.1 PLUME RISE

As shown in Figure 1-2, plume rise is the rise of the dispersing plume centerline above its original emission source height. It is often added to the physical stack height to form effective stack height in the dispersion models. Currently, the most commonly used equations for estimating plume rise are the Briggs' formula and the Holland's formula (Cooper and Alley, 2002). As described by Briggs (1971), his model predicted "nears the stack the rise of a hot, buoyant plume". Briggs showed the correlation between the heat emission and the plume rise. Also, Holland's formula computes the plume rise by two parts: the rise caused by heat emission and the rise caused by vertical momentum. Despite the fact that most of the later studies of plume rises (Bennet et al., 1991; Bennet et al., 1992; Contini and Robins, 2001; Michioka et al., 2007) are based on Briggs' formula, Awasthi et al. (2006) compared the field measurement data with the results computed from Brigg's and Holland's formula and concluded that the later performed better agreement. Using the formulas provided by Cooper and Alley (2002) to compute the same sample provided in the same chapter, two different values were resulted, by which the Briggs' formula predicted a plume rise twice as much as the Holland's prediction (Ying et al., 2011). Disagreements were also detected for the other formulas provide in the book. Thus, further studies are needed to provide more accurate plume rise estimation for different case scenarios.

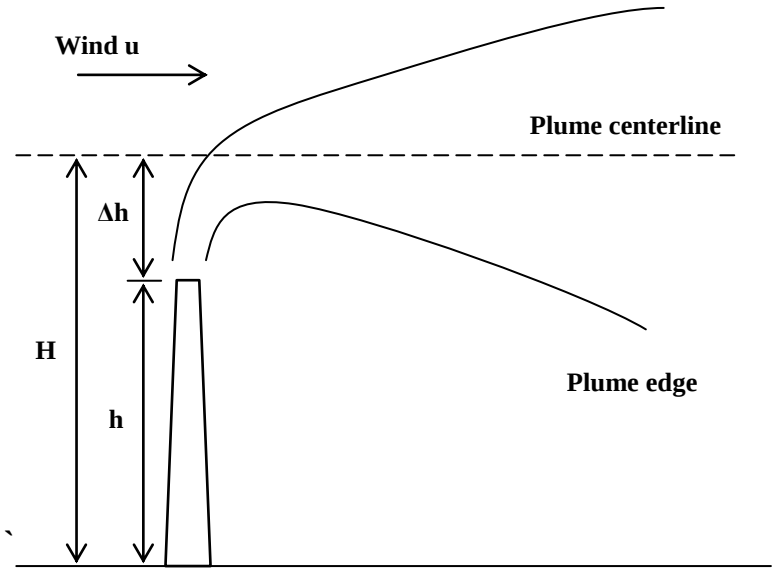

Figure 1-2. Definition of plume rise (Δh) of stack emissions (Cooper and Alley, 2002)

Briggs' (2001) reported a longer horizontal distance before the rise of the plume and a lower vertical dispersion of the plume for dense plume (plume with a density higher than the ambient air) cases; Hanna et al. (1997), on the other hand, found that the plume vertical dispersion would be enhanced for buoyant plume (plume with a density lower than the ambient air).

Applying both Briggs and Holland formulas into the case of animal housing systems, a small plume rise would be expected due to the lack of sufficient vertical momentum and thermal buoyancy. However, field observation showed that the plume rise of exhaust air from animal buildings could reach as high as 10m. Moreover, unlike the plume rise models for industrial stacks used in the existing formulas, for AFO housing system, the emission

"stacks" are much lower with horizontal initial air flow instead of vertical flow as compared to the industrial stacks (Fig. 1-3). Thus, the accuracy of the existing formulas is questionable when applied to current animal housing systems.

Figure 1-3. Industrial stack emission (left) (Novel, 2004) and air emissions from a poultry production house (right)

1.3.2 THE IMPACT OF SOURCES ON AIR DISPERSIONS

Based on the status of the emission plume, the air dispersion plumes can be divided into three primary types--buoyant plumes, dense gas plumes, and passive or neutral plumes. Buoyant plumes are lighter than ambient air either because the temperature of the plume is higher than the ambient, or because the mixture of the plume has a smaller molecular weight than air, or both. On the contrary, dense gas plumes are the plumes heavier than air either because of lower plume temperature, or heavier plume molecular weight, or both. Plumes which are neither lighter nor heavier than air are passive or neutral plumes. The buoyant plumes are the most common case in the industrial emissions and have been studied widely,

including ground level emissions (Hanna et al., 1997; Meroney, 1978) and high stack emissions (Bennet et al., 1992; Briggs, 1969). It was found by Hanna et al. (1997) that the plume vertical dispersion would be enhanced for helium gas as compared to normal air, which means that the buoyancy would add the plume rises. On the other hand, for dense gases, Briggs (2001) reported that the higher density would limit vertical diffusion.

Not only do the characteristics of the sources have an impact on plume rise, the interaction between emission sources is also an important factor. As shown in Figure 1-4, the interaction of emissions from two tunnel ventilated poultry houses can increase plume rise.

Figure 1-4. Plume of air emissions from two tunnel ventilated poultry production houses (Note: the background trees were over 14m high)

Animal houses nowadays mainly use mechanical ventilation systems that include fans, usually with a diameter of 0.61 m (24 in.) or 1.22 m (48 in.), to bring fresh air to animals and to control the indoor temperature and humidity. Other older animal houses may use natural

ventilation systems, controlling the wind flow through the opening of side curtains of the houses. As a result, the air dispersions from animal housing systems may have various initial directions and momentum dictated by the ventilation systems and controls. The relatively lower airflow speed and thermo buoyancy as compared to industrial stack emissions does not weaken the importance of dispersion of the air emissions from AFOs, thus, knowledge about those emission dispersions is needed.

As the odors and PM emitting from AFOs have bothered the residents in the neighborhood (Bunton et al., 2006; Bottcher, 2001), causing health concerns, the fate and transport of air pollutants from AFOs have been a rising research topic. Although air emissions from AFOs have been measured and studied by the NAEMS project and other research (Hiscox et al., 2008; Powers et al., 2005; Roumeliotis and Van Heyst, 2008), the study of air dispersion of AFO air emissions is limited. Quinn et al. (2001) tried to model the dispersion of aerial pollutants from a point source releasing NH_3 above the ridge of an isolated low rise building. They combined two models-an Eulerian diffusion model and a Lagrangian particle tracking technique, with computational fluid dynamics (CFD) and compared the results with field measurements. Their comparison showed that for distances more than three building heights downstream, the predictions from both Eulerian and Lagrangian models were satisfactory; whereas the Eulerian model was less successful in the near wake of the building. The inaccuracies in predicting the NH_3 concentrations were reduced partially after a weighting process of the solutions developed by the authors. By dividing the wind directions into several ranges, this research weighted the concentrations more when the wind direction appears more often in a certain range. "Lack of plume spread" was detected as the main cause

of inaccuracies in the predictions, which indicated that a wider measurement of the plume and more knowledge of plume shape are in need to better model the air pollutant dispersions. In the study of Meroney (1978), wind tunnel simulations of ground level horizontal air dispersion were made. It was concluded that the significant shear flow velocities near the ground led to a delay of the "lift off" of the plume, and the delay would be strengthened by increased wind speed in the direction of plume emission. The description of plume "delay" in Meroney's study support an assumption of our study that when the air emission was horizontal and near the ground, the plume would travel along the ground for a distance, defined as plume depth, and then rise till bending over.

1.3.3 THE IMPACT OT AMBIENT ENVIRONMENTS ON AIR DISPERSIONS

To describe the atmospheric air condition and its impact on dispersion of the air pollutants emitted from the sources, stability classes were developed. The classification of stability may be determined using Turner's method (1994), which is the revised version of the most commonly used Pasquill-Gifford method (Pasquill, 1961; Gifford, 1976). The general factors considered in stability classification are the wind speed at a height of 10 meters, the solar radiation, and the cloud cover. Based on Turner's method, the stability of the ambient air can be divided from A to F, where A stands for the most unstable class, F stands for the most stable one, and D stands for neutral condition. Other meteorological factors are also important for air dispersion modeling. For instance, the wind direction help deciding in which direction the pollutants go; the relative humidity (RH) has impact on the deposition of some kind of pollutants like ammonia (Quinn et al., 2001). Thus, meteorological data is often

measured simultaneously when researchers are trying to measure and model dispersion of air emissions.

Beside the meteorological data, as air emissions from AFOs are often near the ground, the surface roughness and temperature of the ground also have impact on emission dispersion. Other than that, the building structures, surrounding trees, traffics and human activities would also affect the dispersion of the air pollutants.

1.3.4 MEASUREMENTS OF AIR DIRPERSIONS

1.3.4.1 Conventional and remote sensing

As compared to conventional sensing technology, remote sensing is a technique of observing and acquiring some parameters or phenomenon without physically contacting the fluid field. Relatively speaking, for those field measurements that do have interaction with the field, we call them conventional sensing. Both conventional and remote sensing technologies have been used widely in various research projects for dispersion plume measurements.

Conventional *in situ* techniques like instrumented tower, tethered balloon and instrumented aircraft require much field work to acquire enough observations, which may be costly (Singal et al., 1994). As a case of conventional sensing, Quinn et al. (2001) used NH_3 releasing at 16-2.5 $\times 10^{-4}$ m^3 s^{-1}as a tracer gas and denuder tubes fixed on masts to collect samples within 20 degrees from the normal to the long face of the building downwind. The masts were set at nine distances in the range from 7 m to 17 m. At each location, the NH_3 concentration was collected at only one height. Wind data was collected by an ultrasonic anemometer located 25 m upwind of the building on top of a mast (2.5 m) and averaged by

minute. The idea of using NH_3 as a tracer gas has some deficiencies: firstly, as NH_3 is harmful to both humans and the environment, the releasing amount and time were limited such that measuring time and accuracy were limited; secondly, NH_3 could be significantly reduced along the dispersion path due to its quick deposition rate (Asman, 1998; McGinn et al., 2003); although the authors used only data for "dry conditions", which was not defined, the amount of NH_3 loss in "dry deposition" during the travel from the releasing point to the detecting devices was not estimated. Moreover, the limitation of the background wind directions within 20 degrees from the normal to the long face of the building downwind limited the measurements in a very small range, causing inaccuracies. Thus, for conventional field measurement methods of air dispersions, to improve the results, proper ways of quantifying the airflow field, the variation of the wind and more sampling points should be considered. However, the small range of measurements of conventional method is still a limitation for a wider usage. Moreover, the existence of the instruments in the measured field would disturb the flow.

For remote sensing, major technique used in fluid field measurements for various research projects (Bennett et al., 1991; Bennett et al, 1992; Hiscox et al., 2008) is the Light Detecting and Ranging (LIDAR) technology. Similar to LIDAR, another technology that uses sonic wave instead of light for detection of fluid field was Sonic Detection and Ranging (SODAR) (Singal et al., 1994). While being easier to handle, the scanning range of the instrument sets was often fixed in a very small angle-around 5 degrees. Based on Bennett et al. (1991 and 1992) and Hiscox et al.'s descriptions, LIDAR was used to detect industrial tall stack air dispersions that were more than a hundred meters above the ground, so as SODAR. In

Hiscox et al. (2008)'s research, the LIDAR was used to detect downwind PM concentrations from cotton field at ground level, and without much obstacles. It should be noticed that Hiscox et al's study may not apply to other near ground air dispersions where there are often some obstacles like buildings and plants. Moreover, as mentioned by Bennett et al. (1991), the standard error of plume prediction could be less than 20% only when the downwind distances were exceeding 350 m. Similarly, other studies (Hiscox et al., 2008; Singal et al., 1994) also used LIDAR and SODAR to detect plumes hundreds of meters downwind of the source. Limited related research was found in applying the remote sensing technology. The cost of remote sensing instruments is often too high for this technology to be used more widely.

1.3.4.2 Scale of the measurements

For test of air dispersion, researchers (Briggs et al., 2001; Contini and Robins, 2001; Meroney, 1979; Michioka, 2007; Robins et al., 2000) chose to scale down the experimental setting so that they were able to control all the related plume parameters. Wind tunnel has been widely used (Briggs et al., 2001; Meroney, 1979; Michioka, 2007; Robins et al., 2000) to simulate various plume generation environments (boundary layer conditions) in air dispersion measurements and modeling. Another type of experimental setup for plume dispersion simulation was the use of water tank (Contini and Robins, 2001)-a tank full of fresh water as a neutral stability state with salt water released from top of the tank to simulate the plume.

While the scale-down simulations can better control the environmental factors such as boundary conditions, temperature and so on, various complicated computations should be

made to prove that the simulation is valid under the given conditions. Criteria for selections of simulation models along with specific assumptions should be made for the given conditions. In this effort, Robins et al. (2000) has developed three main criteria to examine if the test set fitted the reality in their wind tunnel study of dense gas dispersion. The three main criteria were about 1) Reynolds number,2) mean velocity profiles and turbulence intensities, and 3) the dense gas plume behavior, including six equations. Moreover, to validate the experimentally controlled simulations of dispersion plumes, field measurements of real-world conditions are needed, which would not be conducted under controlled circumstances, requiring more advanced data process and analyzing techniques to compare the model results and the field measurements for model validation.

For measurements with real-scale sources, it is common to consider the ambient environmental factors by measuring them simultaneously and then analyze the data case by case. Test sets measuring indoor air dispersions (Blanes-Vidal et al., 2008; Zhao et al., 2011) were more often developed as compared to open area dispersions. For those studies measuring real scale air dispersions, Quinn et al. (2011) tested a simpler case under confined circumstances such as dry condition, stable emission, small angle of wind direction, and so on. In the study of Hiscox et al. (2008) , they measured near-field PM concentrations from cotton field with two methods-field PM samplers and LIDAR measuring PM_{10} and TSP and found the results from the *in situ* samplers and the LIDAR matching well for both PM_{10} and TSP, but they did not discuss the dispersion of the air emission. For real scale data collection in air dispersion studies in outdoor area, the main challenge would be collecting

comprehensive and accurate field data with consideration of the various effects resulted from the changing environmental factors.

1.3.4.3 Visualization methods

To get a more specific impression and better understanding of the dispersion of the plume, studies often try to visualize the plume dispersion. Tracer gases are often used for visualization in air dispersion studies. In experimental scale simulations, it would be a relatively easier step as the amount tracer gas would be much smaller as compared to real scale experiments. Meroney (1979) used $TiCl_4$ as smoke tracer in his wind tunnel study; Contini and Robins (2001) used a blue vegetable dye in their water tank measurements; Zhao et al. (2011) used helium filled bubbles illuminated by a two dimensional light sheet in their indoor airflow measurement in a full-scale ventilation room. One point that the above mentioned studies shared in common is that their tests were all performed within a confined space. However, for the dispersion studies, it would cost too much to use these visualization methods. Cost-effective and reliable ways of visualizing open area air dispersions are needed.

1.3.5 MODELING AIR DISPERSIONS

Air pollution dispersion models can be divided mainly into four types--Box model, Gaussian model and Lagrangian model and Eulerian model. In the applications of these models, combinations of the model were also used in some cases (Holmes and Morawska, 2006). Also, in recent years, computational fluid dynamics (CFD) modeling has been applied to simulate air dispersions and was found in good agreement with the field measurements (Gidhagen et al., 2004).

1.3.5.1 Box model

In box model, the testing domain was treated as a controlled box. Based on the conservation of mass, it was assumed that the air pollutants, once released, homogeneously distributed inside the box. As compared to other types of models, the box model is relatively simple. The advantage of the box model is that although the meteorology input is simplified, it specifies more chemical and physical reaction schemes and more aerosol dynamics (Holmes and Morawska, 2006). However, neglecting, for example, the impact of local environmental factors such as buildings and other obstacles, makes this kind of model unsuitable for many air pollution dispersion applications, including AFOs.

1.3.5.2 Gaussian model

Gaussian dispersion model assumes that the pollutant distribution across the plume cross sections is normally distributed. Gaussian model can be applied in a wide range of plume dispersions, from continuous to non-continuous (puff), from ground-level to elevated sources. Consequently, various applications of Gaussian dispersion model have made it the basis for most of current air dispersion modeling of continuous, buoyant air pollution plume (Awasthi et al., 2006; Cooper and Alley, 2002).For instance, the preferred and recommended air dispersion model by the U.S. EPA-AERMOD modeling systems is based on Gaussian dispersion model, so are many alternative models (Holmes and Morawska, 2006).

As the Gaussian model is commonly used, the study of this model has been relatively more thorough, leading to a better understanding of its insufficiencies. The main limitations of Gaussian dispersion model include the following (Holmes and Morawska, 2006): 1) as steady state approximations was used, Gaussian dispersion model does not consider the time of the pollutant transporting to the receptor; 2) chemical reactions as well as some physical

interactions are often not included in the calculations; 3) interactions between plumes are not taken into consideration, which would be significant if the emission sources are close enough. Contini and Robins (2001) suggested as large as 30% extra-plume rise could appear a few tens of stack diameters downwind of the sources in cross-winds when there were two sources as close as several stack diameters away emitting simultaneously. More importantly the Gaussian based dispersion models focus on the dispersions of emissions from industrial stacks, which is not the case for AFO plume dispersions.

1.3.5.3 Lagrangian and Eulerian model

As compared to other models, the Lagrangian model has the distinctive characteristic that its coordinates move as the parcels in the air travel during dispersion. Like the Box model, Lagrangian model treats a region of air as a box with pollutants. But as the pollutants travel, the box moves downwind. It works well for both homogeneous and inhomogeneous conditions, and is suitable in both stationary conditions over the flat terrain and unstable media conditions for the complex terrain (Holmes and Morawska, 2006). Although the Eulerian model shares the idea of tracking parcel movements similar to the Lagrangian model, it uses fixed instead of moving coordinates. . As a result of the similarity of the two models, they are often used in combination. For instance, the Institute for Internal Combustion Engines and Thermodynamics (Graz, Austria) has developed a dispersion model named Graz Lagrangian Model (GRAL) using a coupled Eulerian-Lagrangian method to model the dispersion of inert compounds in inhomogeneous wind fields (Holmes and Morawska, 2006). Quinn et al. (2001) compared the two during their research and found

Eulerian model less successful when the downwind measuring points were close to the building of emission sources.

The major drawback of these kinds of models is that they are computationally very expensive since they take time-step into consideration. Also, chemical reactions are often not included in the calculations.

1.3.5.4 Computational Fluid Dynamic model

The CFD model uses governing equations in fluid dynamics, mainly the Navier-Stocks equations for mass, momentum, and energy conservation, to analyze the fluid flow with the help of computers. The application domain of CFD can be as tiny as a magnitude of millimeters and as larger as a city canyon. It has the flexibility of including or excluding various factors such as background wind, temperature differences and obstacles or other environmental factors. Moreover, by adding additional equations to the existing governing equations, researchers have the ability to customize CFD models to fit specific research needs. However, the coding of CFD models requires a strong knowledge of mathematics, physics, and computer science, so this requires the work of specialists in that field. . Thus, for the cases in air dispersion studies, many researchers (Blanes-Vidal et al., 2008; Kim, 2007; Quinn et al., 2001) chose commercial packages such as FLUENT and FloEFD with user friendly interfaces. Although the solving steps are not designed by the users, current commercial packages are considered to be capable of meeting the research needs in exploring the fluid flow during air dispersions.

As Quinn et al. (2001) reported, the performance of the modeling systems highly depended on the fluctuation of the wind conditions. While it is essential to simulate appropriate wind

conditions, it takes hours, or even days to compute a single scenario under a certain wind condition in CFD modeling. Thus it is time consuming to simulate various wind conditions in CFD models. This probably explains the fact that while there are many publications about both CFD modeling and field measurements of industrial fan flows (Aličet al., 2010; Gates et al., 2004; Wang et al., 2011), there is seldom comparison between them, especially for closer downwind fluid field studies.

1.4 SUMMARY OF CURRENT INSUFFICIENCY

Through the literature review of relevant areas, several insufficiencies were observed and summarized as follows:

Although air emissions from AFOs are essential, application of the current national ambient air quality standards may be challenged due to lack of knowledge about air dispersions of AFO air emissions.

Although current air dispersion models with consideration of plume rises were used to predict fate and transport of air pollutants, the plume rise formulas in current Gaussian dispersion models do not take the characteristics of AFO emissions into consideration. Also there is not good agreement with among them.

Most air dispersion studies have focused more on industrial stack emissions and there is a lack of research about plume dispersion of air emissions from AFO housing facilities which are characterized by ground-level, horizontal emissions with diurnal and seasonal variations. Among the few studies meeting the above stated characteristics, the measurements and comparisons have been limited to a small spread, leading to inaccuracies. More

comprehensive measurements of plume dispersion from AFOs with wider spread, more points and longer duration are needed.

There is a need to develop a way to better measure near source characteristics of the fluid field out of animal buildings.

For real scale data collection in air dispersion studies in outdoor area, the main challenge is to collect comprehensive and accurate plume fluid field data while accounting for the various effects resulting from the changing environmental factors. Also, a way of cost effective visualization of the plume in real scale needs to be developed.

Air dispersion models for AFO housing emissions are needed.

1.5 RESEARCH OBJECTIVES

The major goal of this research is to model the shapes (rise, depth and width) of exhaust plumes emitted from animal housing systems under different ventilation and meteorological conditions. Specific objectives are to:

1. Measure the plume shapes in a single ventilation fan testing setup that generates similar plume fluid field to those in commercial animal houses;
2. Conduct CFD modeling to simulate the plume flow pattern of the single fan testing system under different scenarios and identify the impact of temperature difference and background wind on plume shapes;
3. Apply inverse-AERMOD to derive the plume rises of animal house emissions on a commercial layer farm using field measurements of PM_{10} emissions and concentrations on the farm and in the vicinity;

4. Identify the impacts of various factors on plume rises from the animal houses based upon the inverse-AERMOD results and the field observations.

CHAPTER 2 MODELING RISE OF PLUME EMITTED FROM AN ANIMAL HOUSING VENTILATION FAN: APPLICATION OF CFD

ABSTRACT

Gaussian dispersion models have been applied to simulate the fate and transport of air emissions from animal housing systems to meet the increasing need for knowledge in this area. However, the accuracy of the models may be challenged due to the unknown plume rise and plume shape. This chapter reports a combination of theoretical and field study of the plum rise and shape of air flow from a ventilation fan commonly used in mechanically ventilated animal houses. The theoretical modeling of the plume shape was conducted using a commercial Computational Fluid Dynamics (CFD) package named FloEFD; the field measurements of the plume field was conducted using five 3D ultrasonic anemometers to simultaneously measure the air flow in the plume at various locations (four heights and five downwind distances). The Tecplot package was used to visualize the plume flow field based upon anemometer measurements. The plume shape of the field measurements was found to be left-shifted by the Tecplot visualization due to the background wind effect. The plume field measurements indicated that the plume of a 0.6 m (24 in.) ventilation fan at full speed had a depth about 9 m, a width about 12 m, and a rise (lifting) beyond the highest measurement point, 4.88 m (16 ft). Various factorial simulations were conducted using the CFD model to find that: 1) temperature difference between plume and ambient air had a positive impact on plume rise and a negative impact on plume depth; 2) background wind against the fan flow had a negative impact on plume depth, plume width and plume rise; 3) background wind across the fan flow reduced the plume depth, but increased the plume width and plume rise.

2.1 INTRODUCTION

Animal products are more and more in need to feed the rapidly growing population. It has been reported (USDA, 2005) that there were 450,000 AFOs in the U.S. Along with the significant economic and social benefits produced by the AFO industry, however, serious environmental concerns have been raised due to massive production of animal waste and air emissions from the operations. In assessment of impact of AFO air emissions on local and regional air quality, knowledge of the fate and transport of those emissions is required, and yet has not been well studied and understood.

While estimations of air emissions from AFO facilities have been studies intensively (Heber et al., 2008; NRC, 2003), investigation of the fate and transport of the AFO emissions is a relatively newer research topic in recent years (Carney and Doddt, 1989; Henihan et al., 2003; Sarr et al., 2010). In the literature, estimations of downwind pollutant concentrations in responses to AFO emissions have been commonly conducted through Gaussian dispersion modeling approach (Gorgy, 2003, Schauberger et al., 2000; Sarr et al., 2010).The Gaussian dispersion model was originally developed based upon observations of industrial "stack" emissions with vertical momentum and thermal buoyancy (Cooper and Alley, 2002). The accuracy of the Gaussian dispersion model may be challenged when it is applied for assessing dispersion of air emissions from animal housing system where there is lack of vertical momentum and sufficient "stack" height. This challenge mainly comes from unknown of plume rise and plume shape of the horizontal emissions from the housing ventilation fans.

In an effort to assess the emission plume, Holmes et al. (2006) reported that the flow patterns of gas and PM emissions agreed well in open environments unless there was severe turbulence or the emission sources were too complicated. Understanding of fluid filed of the exhaust plume from animal housing ventilation fans may lead to quantification of rises of the emission plumes. In theory, fluid dynamic equations, which are mostly in the forms of partial differential equations, may be used to express the fundamental principles of any fluid field. To predict fluid field behavior under any given boundary conditions (Wendt and Anderson, 2009) and to find a numerical description of the fluid field that meets the fundamental principles and the given boundary conditions, as much as millions of iterations could happen. To facilitate such high computational demand, the computational fluid dynamics (CFD) has been commonly used in fluid field calculation and modeling.

In the application of the CFD modeling, fluid field measurements are usually required to validate and calibrate the model outputs. While there are many publications about both CFD modeling and field measurements of industrial fan flows (Aličet al., 2010; Gates et al., 2004; Wang et al., 2011), there is seldom comparison between them, especially for closer downwind fluid field studies. This is probably because, as Quinn et al. (2001) reported, the performance of the modeling systems depends highly on the fluctuation of the wind conditions.

As a commercial package of CFD, FloEFD had been used in the research in various areas (Remsburgb et al., 2010; Kawamorita et al., 2012; Wang et al., 2009). For the convenience of the customers, an engineering database was built to offer some default input files such as types of materials of surfaces. The database also allows users to build and store their own

input files such as characteristics of exhaust fans. However, despite the freedom of defining fans, the specific exit velocities at different radii were defined by the system and cannot be changed. It assumes the exit velocities across the fan diameter to be parabola. On the other hand, the pattern of exit velocities across the fan diameter varies from a bimodal curve to a parabola based on the distance away from the fan as reported by ACGIH (2004). The fact that there is seldom study about the velocities at fan surfaces leads to a research need of measuring the velocities at the fan surfaces.

In addition to CFD method for fluid field modeling, Tecplot is another fluid dynamic package to visualize and model the fluid field behavior when the fluid field measurements are available (Tecplot, 2011). It has been applied in visualization of various research fields such as heat transfer process (Kun et al., 2011), flow field measurements (Gong et al., 2009) and even chemical reactions (Muramalla et al., 2005).

This study compared the fluid filed measurements with the CFD model out puts of the fluid field of the exhaust plume from a ventilation fan commonly used in AFO housing systems. The specific objectives of this chapter were to (1) measure the fluid field of the exhaust plume from an animal housing ventilation fan; (2) visualize and quantify the shape and rise of the plume through CFD modeling and visualization.

2.2 METHODOLOGY

In this study, two approaches were taken to model and visualize rise of the plume emitted from a ventilation fan testing setup. The first approach measured the fluid field of the ventilation plume under the controlled setting. The fluid field measurements were then applied to visualize the exhaust plume shapes defined by plume height, depth and width. In

the second approach, a commercially available CFD package (FloEFD 11 for Creo, Mentor Graphics) was used to simulate the fluid field of the plume emitted from the ventilation fan testing setup. Various influencing factors including air temperature, background wind speeds and wind directions, were taken into consideration in CFD plume field simulation. Through the plotting of the CFD model predictions of the plume approach, the impact of these factors on plume shape was then assessed.

2.2.1 VENTILATION PLUME TESTING SETUP: THE MINI-TUNNEL

To be consistent with field observation, a wooden mini-tunnel with an axial ventilation fan was constructed to simulate ventilation flow that would be typically observed in a poultry housing system. This testing mini-tunnel has a dimension in 1.22 m x 0.91 m x 2.44 m (4 ft x 3 ft x 8 ft) with an axial ventilation fan (0.6 m, 24-in. in diameter, AT24ZCP, Aerotech) installed on the one end. To ensure similar air flow patterns in the testing tunnel as it is in a typical poultry house, a collimating screen was installed at the entrance end of the tunnel. This collimating screen not only stabilized the airflow in the tunnel with short traveling distance, but also generated a pressure drop around 12.50 Pa (0.05 in-H_2O) (Fig. 2-1). The wooden mini-tunnel was placed in an open area on the Lake Wheeler Field Laboratory of North Carolina State University for the plume testing.

Figure 2-1. The wooden mini-tunnel with a 0.6 m (24-in.) axial ventilation fan on the one end and the collimating screen on the other end

2.2.2 VENTILATION PLUME MEASUREMENTS

2.2.2.1 Instrumentation

The plume field velocity measurements were conducted using five 3D ultrasonic anemometer assemblies with adjustable heights (Fig. 2-2). Each assembly consisted of a 3D anemometer (Model 81000, R. M. Young Company, Traverse City, Michigan), a battery and a 4-channel data logger (U12-006, Onset Computer Corporation, Cape Cod, MA) to record measurements of 3D velocities and temperature. The data logger can store 14 hours of data with a 10 second recording interval. Before the field testing, some default settings of the anemometers were changed to fit the experimental design. These changes include: "serial output form"— changed to "u, v, w", "T_s (sonic temperature)" and "internal voltage"; The velocities were denoted by u_0, v_0 and w_0, among which $+u_0$ values = wind from the east; $+v_0$ values = wind from the north; $+w_0$ = wind from below (updraft).

"voltage output format"—"scaling" was changed to 15 m s^{-1}.

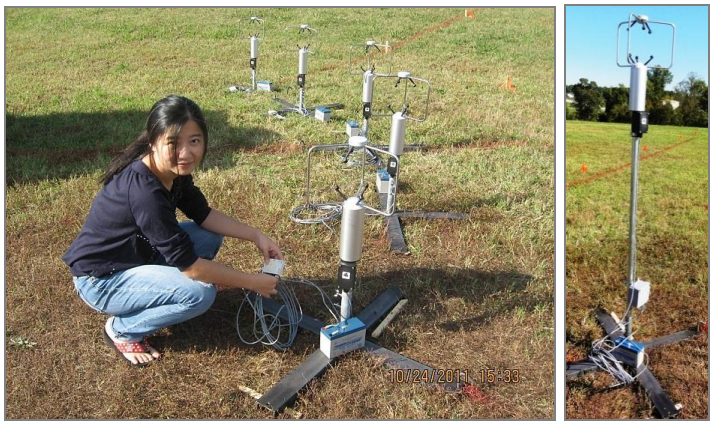

Figure 2-2. The 3D ultrasonic anemometer assemblies (left: five anemometers on the posts with data loggers and battery power supplies) and illustration of the adjustable heights of the anemometer assembly on the post (right)

In addition to the tunnel plume field measurements, the local meteorological data were monitored to count for background wind effect. The meteorological data collection was conducted using a 10 meter weather tower installed about 30 meters away from the mini-tunnel testing field. Wind speed, wind direction and solar radiation, air temperature, RH were monitored by the sensors on the tower (Onset Computer Corporation, Cape Cod, MA) including a wind speed/direction smart sensor (S-WCA-M003), a solar radiation shield (RS3), a temperature/RH smart sensor (S-THB-M00x), a multi-channel logger (U30) to record data every minute and a U-shuttle (U-DT-2) for reading data from the logger and transfer to a host computer.

2.2.2.2 Plume fluid field measurements

Before the measurements of the plume fluid field, preliminary smoke tests were done to visualize the width and depth of the plume for placement of the anemometers. The preliminary smoke tests showed that the plume at full rpm capacity went as far as 15 m before rising up and could reach as high as 4.57 m (15 ft) after rising up and bending over. Based upon the observations of the smoke tests, the plume fluid field was divided into five rings (3, 6, 9, 12 and 15 m) away from the fan and four heights (0.30 m = 1 ft, 1.22 m = 4 ft, 3.05 m = 10 ft, 4.88 m = 16 ft). The top view of testing field is displayed in Figure 2-3. As the flow generated by the fan was constant at a given fan speed (rpm), the exhaust fluid field was considered unchanged without the impact of background wind. For each dimension of the 3D velocities, the background wind vector can be subtracted using field wind measurements. Thus, the plume field air velocity measurements were conducted one ring one height at a time.

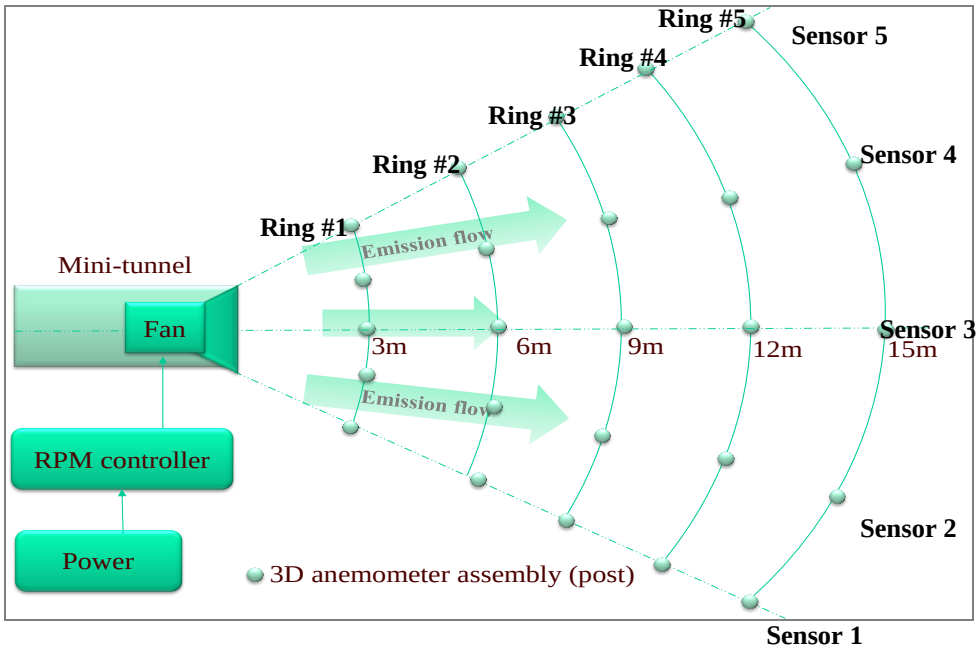

Figure 2-3. Top view of the 3D plume fluid field measurement layout

The experiment was started on 18 November 2011 with the first set of plume field tests from 18 November to 4 December 2011, the second set of tests from 17 to 23 December 2011, and the third set of tests from 5 to 8 January 2012.

For the first set of tests, measurements at five locations were simultaneously taken at one height in one ring in each test with data collection for two hours at 10 second interval. Total of 12 tests were conducted for four heights (0.30 m = 1 ft, 1.22 m = 4 ft, 3.05 m = 10 ft, 4.88 m = 16 ft) and three rings (#1, #3, #5). Figure 2-4 illustrates the setup for one test at the height of 3.05 m (10 ft).

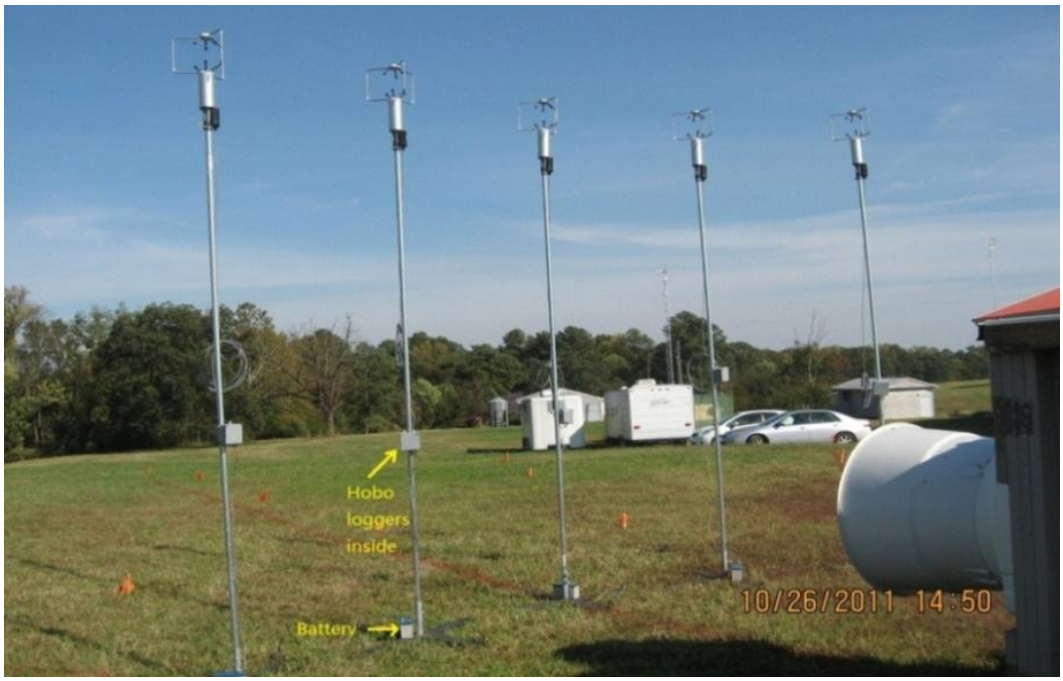

Figure 2-4. The plume fluid field measurement on the ring #1 and at 3.05 m (10ft) height

For the second set of tests, the experimental design was the same as the first set of tests. Thus, another 12 tests were conducted for four heights (0.30 m = 1 ft, 1.22 m = 4 ft, 3.05 m = 10 ft, 4.88 m = 16 ft) and three rings (#1, #3, #5).

In these two sets of tests, background wind data measured by the weather station on the 10 m tower were used to count for background wind effect on the plume filed velocity measurements.

In the third set of tests, to be more precisely factor out the background wind effect on the plume flow measurements, the background wind measurements in the testing field were also conducted. For each test, plume field 3D air velocities were taken for 10 minutes when the

fan was on, then, the background 3D wind velocities in the same field were taken for another 10 minutes when the fan was turned off. In this set, total of 20 tests were conducted for four heights (0.30 m = 1 ft, 1.22 m = 4 ft, 3.05 m = 10 ft, 4.88 m = 16 ft) and five rings (#1-5).

2.2.3 DATA PROCESSING

2.2.3.1 Flow vector transformation

To better describe plume shape (i.e. depth, width and rise) in line with the testing setup, a coordinate system was built based on the testing tunnel/fan position to transfer 3D velocity measurements from the North-South and West-East coordinates to a new coordinate system. As shown in Figure 2-6, in the new coordinate system, the +x was aligned with the fan pointing towards the flow direction; the +y was perpendicular to the x axial toward the left side of the fan; the +z was perpendicular to the x-y plane pointing upward from the ground. Based on the historical weather records, the prevailing wind at the field was in south-west direction, thus the fan was aligned 57 degrees clockwise from the north direction (Fig.2-5).

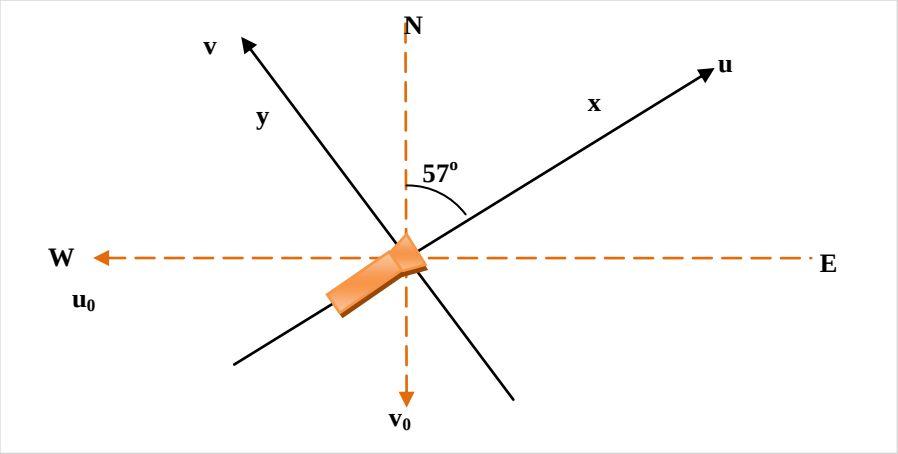

Figure 2-5. The coordinate systems for plume fluid field velocity computation

The 3D velocities measured by the anemometers and the background wind velocities measured by the weather tower were transferred to the new coordinate system by:

$$u = -u_0 \cdot \sin 57° - v_0 \cdot \cos 57° \qquad (2\text{-}1)$$

$$v = -v_0 \cdot \sin 57° + u_0 \cdot \cos 57° \qquad (2\text{-}2)$$

The 3D velocity measurements were then averaged to every 10 minutes. For the third set of tests, by subtracting 10min background 3D background wind velocity measurements (fan off), the measurement of the plume flow field as impacted only by the fan was resulted. For the first two sets of test, the background 2D (east-west & north-south) wind velocities measured by the weather tower were used for subtraction to obtain the plume field measurements as impacted only by the ventilation fan.

2.2.3.2 Weather data processing

For the first two sets of tests, since no in field background wind was measured, the wind speed/direction data from the weather station were used. As the weather data were recorded every minute, it was first averaged to every 10 minutes. Thus, u_0's and v_0's (Fig.2-5) were averaged separately and were transformed by equations 2-1 and 2-2 to u's and v's (Fig.2-5) at the measurement height of 10 meter. The measured wind directions were assumed to be within the horizontal plane, which suggested that there was no vertical impaction from the weather. Appling the power law (Cooper and Alley, 2002), the wind speeds in two directions (u & v) were then converted to the speeds at the heights of the 3D anemometers at the time for taking the plume field measurements. The power law takes the following form:

$$\frac{u_1}{u_2} = \left(\frac{z_1}{z_2}\right)^p \qquad (2\text{-}3)$$

where,

z_1, z_2 = elevations 1 and 2. In this study, z_1 and z_2 are elevations of the 3D anemometers and the tower at10m, respectively.

u_1, u_2 = wind speeds at z_1 and z_2

p = exponent

The power "p" in equation 2-3 varies with atmospheric stability class and surface roughness. It may be determined from the Table 2-1 below:

Table 2-1. Exponents for wind profile (Power Law) model (U.S. EPA, 1995)

	Exponent (p)	
Stability Class	Rough Surface (urban)	Smooth Surface (rural)
A	0.15	0.07
B	0.15	0.07
C	0.20	0.10
D	0.25	0.15
E	0.30	0.35
F	0.30	0.35

In this study, the smooth surface was chosen for calculation. Turner's (1994) method has been used to define atmospheric stability classes. This method is the revised version of the most commonly used Pasquill-Gifford method (Pasquill, 1961; Gifford, 1976). The classification of the stability classes requires information about the solar altitude, wind speed and the cloud cover. Detailed procedure for determining the stability classes are reported in Cooper and Alley (2002). After transforming the weather data, the converted wind velocities were used as background wind for plume filed final flow calculation to identify plume profile as impacted solely by the ventilation fan.

2.2.4 PLUME FLUID FIELD 3D VELOCITY PLOTTING: THE TECPLOTVISUALIZATION

After subtracting the background wind impact for all the tests, the resulted 3D velocities were considered to be the plume caused simply by the fan flow.

Once the 10 minute averages of 3D velocity obtained for each set of tests, a plot of velocity vectors and contour of the measured plume field was generated by the software-Tecplot 360, 2011 (Tecplot, Inc. Bellevue, Washington). Procedure for plotting in Tecplot include the following

1. sorting the data into 6 columns, denoting “x”, “y”, “z”, “u”, “v”, “w”, respectively;
2. exporting the data into a text file with the first row “variables = x, y, z, u, v, w” and the second row “zone i=3 for test set one and two, 5 for test set three, j=5, k=4”;
3. listing the 6 columns of field data from the third row;
4. importing the text file into the Tecplot;
5. customizing the plot and generating contour map of the fluid field.

2.2.5 PLUME FLUID FIELD CFD MODELING

The commercial CFD software, FloEFD was used to simulate the plume flow field of the axial fan by solving the governing equations. Additional to the Navier-Stocks equations for mass, momentum, and energy conservation laws, specific equations describing the fluid could be customized by users based on the study case.

In the CFD models, the codes were developed to solve Navier-Stocks equations for both laminar and turbulent flows. Specifically, the FloEFD used the k-ε model to express the transport equations for the turbulent kinetic energy and its dissipation rate. In this study, as a common case was expected to be simulated, the settings of the turbulence parameters were

kept as default (C_μ = 0.09, $C_{\varepsilon 1}$ = 1.44, $C_{\varepsilon 2}$ = 1.92, σ_k = 1.0, and σ_ε = 1.0, where C_μ, $C_{\varepsilon 1}$, $C_{\varepsilon 2}$ are constants for k-ε turbulence model, σ_k is the turbulent Prandtl number for k, σ_ε is the turbulent Prandtl number for ε).

2.2.5.1 Definition of the boundary conditions

The boundaries of the plume field were the ground, the fan and the fan discharge cone. The model default set of the boundaries was adiabatic. As the ground in the testing field was covered with grass, the roughness of the boundaries was set to be 0.03 m as commonly used by other researchers (Linacre and Geerts, 1999).

As discussed in the introduction, while the default assumption of exit velocities across the fan diameter in FloEFD was in a shape of parabola, literature has shown a variation based on the distance away from the fan. Thus, the default input files of fans may not be suitable. To better simulate the fan flow, the fan flow was assumed to be swirling out from a lid in a same diameter with the edge of the fan cone (0.76 m diameter). FloEFD required a rotational speed, a radial speed and an exit speed to define the flow. An experiment was set to measure the 3D velocities at 21 different points at a distance of 0.2 m away from the edge of the fan cone. The layout of each measurement point is shown in Figure 2-6:

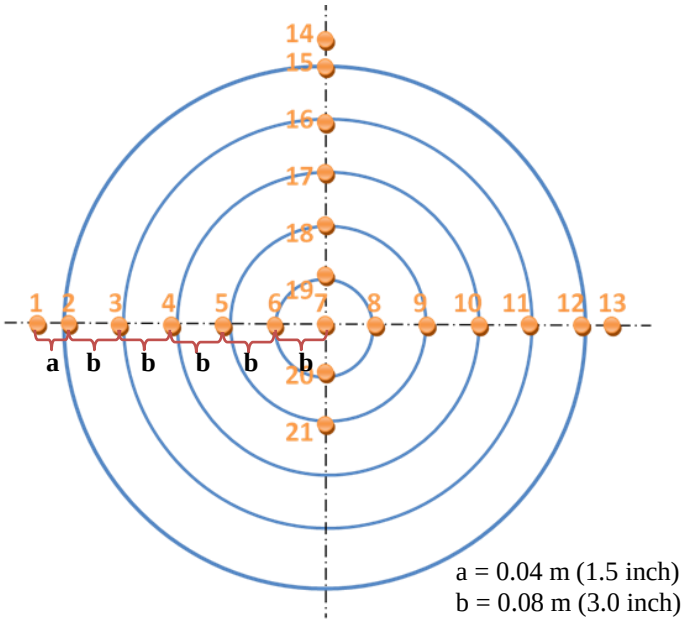

Figure 2-6. Testing points of the fan surface flow measurements

As shown in Figure 2-6, the 21 points of 3D velocities were tested along the vertical and horizontal diameter of the fan surface at six different distances away from the center, forming six concentric circles. One anemometer was used at each point to record the 3D velocities for one minute. After being recorded, the velocities were transferred into cylindrical coordinate system with radial velocity (V_r), rotational velocity (w_0) and exit velocity (u, the velocity pointing away from fan surface). The transferring process of the coordinate system is shown in Table 2-2:

Table 2-2. Adjustments of coordinate system for testing points by using u, v and w

# of point	V_r	w_0	u
1-6	-v	w	u
8-13	v	-w	u
14-19	w	v	u
20-21	-w	-v	u

It was assumed that the points at a same radius had the same speeds of the 3-D velocities. Thus, the speeds of the 3-D velocities at each circle were computed by averaging the measured testing points. However, the cumulative volume flow rate may not be exactly the same as the actual fan flow rate due to the disturbance of the sensor and other reasons. To better simulate the fan flow, exit velocities (u) were adjusted by the ratio between the measured flow rate and the one designed by the manufacturer (2.83 $m^3 s^{-1}$). On the other hand, as the tests were set at 0.2 m away from the edge of the fan cone, the tested area was larger than the fan opening area. Since the volume flow rate was constant, the exit velocities at different cross session areas were assumed to follow the equation below:

$$A_1 \cdot u_1 = Q_1 = Q_2 = A_2 \cdot u_2 \qquad (2\text{-}4)$$

where,

A_1= the surface area at fan cone (0.79 m in diameter)

A_2 = the surface area at the testing distance (0.2m away from cone surface with 0.84 m in diameter)

u_1, u_2 = exit velocities at the cross-section of the fan cone surface and the surfaces 0.2m away from the cone surface, respectively

$Q_1 = Q_2$= flow rate across the fan surface = 2.83 $m^3 s^{-1}$

The adjustment of radial velocities was obtained by the following equation 2-5:

$$V_{r2} \quad at \quad r_2 = V_{r1} \quad at \quad r_1 = \sqrt{\frac{A_1}{A_2}} \cdot r_2 \cdot V_{r2} \qquad (2\text{-}5)$$

Since the measurements of the 6th circle were out of the edge of the fan cone, it was not suitable to use the measurements at this circle to represent the radial velocities within the cone area, those points on this circle were not used for the computation of radial velocities. The dimensions of the fan cone were 0.66 m in depth, 0.62 m in i.d., and 0.79 m in o.d.. The cone was made of plastic. The roughness of typical plastic surface is 0.0015 m, as it is very small, the cone was considered ideal wall, which here means adiabatic, frictionless wall. As a maximum temperature difference of 10K was selected in the CFD simulations, calculations were done to see the significance of the cone in thermal activities. The total heat energy in the flow (q_{flow}) and heat loss (q_{loss}) due to the cone were computed as:

$$q_{flow} = h \cdot m_{da} = h \cdot (Q \cdot \rho_{da}) \qquad (2\text{-}6)$$

$$\rho_{da} = \frac{P_b - RH \cdot P_s}{R_a \cdot (273.15 + t_{db})} \qquad (2\text{-}7)$$

$$q_{loss} = \frac{A}{R} \cdot \Delta T \qquad (2\text{-}8)$$

where,

t_{db} = dry bulb temperature of ambient air, here the average of field measurements was used, 15^{o}C

RH = ambient air average relative humidity during the field measurements, 55%

h = enthalpy of air at the t_{db} = 15^{o}C, RH = 55%, 42.3 kJ kg^{-1} dry air;

Q = average fan flow rate at full RPM, 2.87 m^3 s^{-1};

ρ_{da} = density of dry air component of moist air, kg m^{-3};

P_b= atmospheric pressure, 101.325 kPa;

P_s = saturation pressure of water vapor at t_{db} = 15^{o}C, RH = 55%, 1.792 kPa;

R_a = individual gas constant of air, 0.287 kPa-m^{3}kg^{-1} k^{-1};

A = surface area of the plastic cone, 0.404 m^2;

R = typical thermal resistance of plastic, 1.14 $m^2\ ^oC\ w^{-1}$ for a cone with 0.01 m thickness

ΔT = temperature difference between fan flow and ambient air, 10 ^oC

With the help of psychometric chart, q_{flow} was resulted to be 147.348 kW while q_{loss} was only 3.544 W, which is 0.002% of q_{flow}. Thus, the heat loss by the fan cone was considered insignificant in this study.

As it was assumed that neither the fan flow nor the boundary conditions would change, the system simulating the fluid field of fan outflow was defined by FloEFD as a "steady external" system. In such systems, the inputs of initial thermodynamic parameters (static pressure, static temperature and static density) and velocity parameters (x, y, z components of the velocity vectors) were defined by ambient conditions, and the default turbulence parameters (constants, Prandtl numbers). Also, based on the manual of the software, the above mentioned ambient initial conditions were applicable to define the boundary conditions at the computational domain boundaries. The thermodynamic and velocity parameters were kept as default except for changes of temperature in temperature difference study, and changes of initial flow velocities in x and y directions in the study of background wind impact.

2.2.5.2 Computational mesh

A computational domain was first developed to define the region of model calculation. In this study, the origin was set on the centerline of the fan system right at the edge of the discharge cone (the same as the one shown in Fig.2-5). The orientation of the coordinate system is also the same as the one in the field measurement (Fig.2-5). The edges of the computational domain are listed in Table 2-3:

Table 2-3. Settings of the computational domain in the FloEFD model

Min x	Max x	Min y	Max y	Min z	Max z
-1 m	50 m	-25 m	25 m	0 m	40 m

The refinement of the computational mesh was conducted automatically during the simulation process. The principle was to evenly split the current mesh to eight child cells when interface was observed until the mesh size reached the threshold defined by the users. In this study, the mesh refine degree was selected ranging from seven (the range is one to eight, greater number means smaller mesh size) to three (minimum refine degree) for simulations without background wind to test the lowest refine degree that would satisfy the research need in this study. , It was found that at a refine degree as low as three would present satisfying results. Thus, minimum refine degree (three) was selected for simulations with background wind as the initial mesh refinement done by the system was fine enough for obtaining the results.

2.2.5.3 Simulation and comparisons

For simulations without background wind, the end of simulation was set to be after 100 iterations as the mean and maximum velocities did not vary a lot after that. The model outputs were then obtained. For simulations with background wind, the model was set to stop when the calculation reached the maximum travels (set as auto and value equals 4, meaning that the calculation period required for a flow disturbance to cross the computational domain 4 times) or convergence with the default analysis interval level of 0.5, meaning that the system will check if its solution has converged every 0.5 travel.

For this study, the following set of CFD model simulations were conducted to observe the impact of various temperature differences ($\Delta T = T_{fan} - T_{ambient}$), RPMs and background wind speeds on the plume shapes for the single fan testing system. In total, 14 CFD simulations were conducted to define the plume field in the computational domain with dimensions listed in Table 2-3.

The plume rise models for industrial stacks indicate that a positive ΔT would add the plume rise (Cooper and Alley, 2002). Meanwhile, it is often seen that the air emission from animal houses is warmer than the ambient air. Thus, in order to see more significant plume rises, for the simulations with various background winds and RPMs, the fan flow temperature was fixed at 288K and the ambient temperature was set at 278K to simulate the cases when plume rise tend to be more significant. The background wind velocities, V_x and V_y (against and across the fan flow direction, respectively) were chosen for same reason (i.e. more significant plume rise case scenarios). Based on Turner's (1994) method of stability classification, the wind speeds measured at 10 m above the ground were divided into four ranges. Table 2-4 summarizes the distribution of wind speeds measured in each range during the flow testing periods. As it is shown, around 30% of the measured background wind speeds were in 0-2 m/s, and 88% measured wind were in 0-5 m/s range (the first three ranges). The averaged wind speeds for the three ranges were chosen to simulate the background wind effects in the CFD.

Table 2-4. The distribution of measured wind speeds in stability-related ranges at 10 m above ground

Wind speed range m/s	Avg. wind speed m/s	# of wind speeds by minute	% of wind speed by minute
0-2	1.0	1062	32.8
2-3	2.5	885	27.4
3-5	4.0	893	27.6
>5		395	12.2

Table 2-5. Parameter settings for CFD simulations

Variables		Setting	Note
Temperature difference between plume flow and the ambient air temperature, ΔT (^oC)		0	
		10, -10	
Background wind with $\Delta T = 10\ ^oC$ only	V_x (m s^{-1})	0.00	The plume field was measured under the following combined setting: RPM=Full (1074) $\Delta T=0\ ^oC$ No background wind
		-0.05	
		-0.10	
		-1.00	
		-2.50	
		-4.00	
	V_y (m s^{-1})	0.00	
		-0.05	
		-0.10	
		-1.00	
		-2.50	
		-4.00	

Table 2-5 shows detailed parameter selections for CFD simulations, including various temperature differences, background wind speeds and wind directions.

After each CFD run, a plane parallel to the ground was set to view the resultant 3D velocities of the model outputs at various heights. Then probe tool was used to capture the 3D velocities at the points where the anemometer measurements in the field were taken. Paired two-sample t-tests were done to analyze the difference between the model and one set of field data in winter. Also, the velocities observed by the probes in CFD were recorded in the text and excel file and plotted in Tecplot for visual check of the plume.

2.2.5.4 Plume shape definition and observations

In this research, the plume shape was defined by the plume depth ("x" direction in Fig.2-5), width ("y" direction in Fig.2-5) and rise ("z" direction). The plume depth is defined as the downwind distance from the exhaust fan surfaces to the point where the plume started to lift quickly. Based upon filed observations, the plume depth was observed as following: when the plume lifting velocity, w, increased along the "x" direction to a point where it started decreasing, the distance x at this point was defined as the plume depth.

Cooper and Alley (2002) suggested that the pollutant concentration across the plume would follow a normal distribution, and the concentration lines of 5% of the maximum concentration in the plume center were then defined as the edges of the plume. Since the gas pollutants or fine particles (e.g. PM_{10}, or $PM_{2.5}$) follow the air flow well, it was considered to be the edge of the plume when the 3D velocity at one point was less than 5% of the highest 3D velocity of the cross section of the plume. The plume widths at the height when the plume stopped rising were thus recorded.

As the rise of the plume is caused by the vertical velocity, w, the maximum w was observed by the probe tool in the FloEFD. As the plane parallel to the ground moved from

the ground to upper heights, a series of w's were recorded, noted as w_{m1}, w_{m2}, w_{m3}... w_{mn}. Among these w's, the maximum w, noted as w_{max} was identified through ranking. When w_{mn} = 5% * w_{max}, it was considered the end of plume rise. In some cases, w_{max} was too small that 5% * w_{max} were less than 0.001 ms^{-1}, in that case, the point when w_{mn} = 0.001 m $s^{-1}$was defined as the end of plume rise. Sometimes the addition of background wind caused the plumes going beyond the computational domain. In those cases, w_{mn}'s at several heights that were within the computational domain were obtained, then regression on these points on heights versus w_{mn}'s was conducted to predict the plume rises through the resultant regression equations.

Particle tracer was also used in CFD simulations to visualize the dispersion of the plume and to check the definition of plume shape by the contour plots at cut planes. The particle material was isolator and the diameter was set at 10 μm—the maximum diameter of the particles of interest (PM_{10}) in this study. The mass flow rate of the particles was set at 1 g s^{-1},. The initial temperature and velocity of the particles were set the same as the fan flow.

2.3 RESULTS AND DISCUSSION

2.3.1 FIELD MEASUREMENTS

Due to some sensor and data logger connection problems, for the first set of tests, only eight groups of measurements were valid and named as group 1-01 through 1-08. For the second set of tests, 12 groups of results were valid and named as group 2-01 through 2-12. Each group had 60 data points of 10-minute average 3D velocities. For the third set of tests, one scenario was generated with 100 points of 10-minute average 3D velocities and named as group 3.

2.3.1.1 Velocity measurment comparisons within test sets:

The comparisons of velocities among the groups within the first and second test sets were conducted by the statistical software R. The TukeyHSD test was applied to compare the means of the velocities in three directions. Figure 2-7 shows an example of comparisons of the velocity in W direction (vertically up) for the first and second test sets.

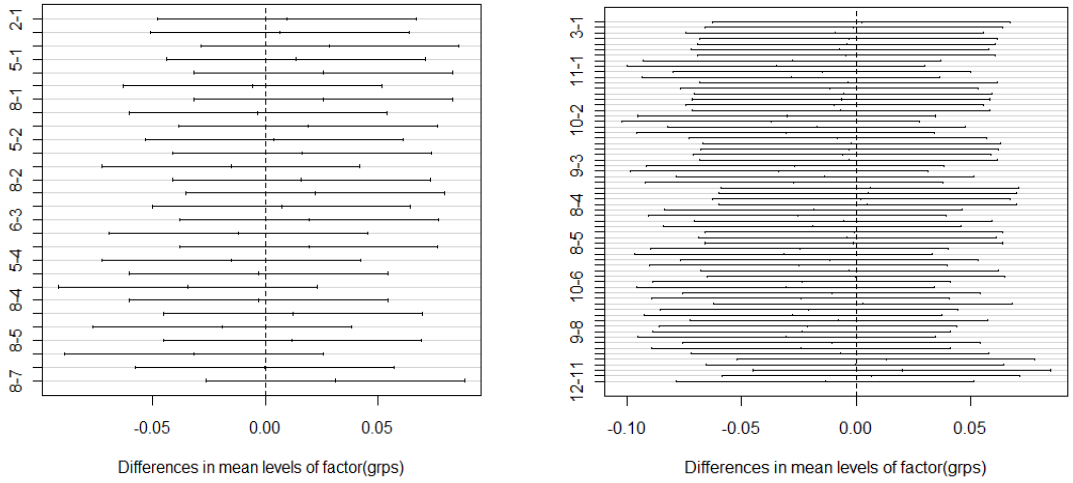

Figure 2-7. 95% confidence intervals of differences of velocity in w direction (m s^{-1}) within first set of tests (left) and second set of tests (right)

The TukeyHSD tests revealed that there were no significant differences in u, v and w velocities among groups in both test sets. The flow velocities in the vertical direction, w, was chosen as a representative because it was related to the plume lifting, thus to the rise of the plume, the target parameter this research is investigating.

The same TukeyHSD tests were also conducted on u, v and w between the first and the second sets of tests. The results showed no significant differences at 0.05 levels. The third set

of tests, however, was found to be significant different from the first two sets of data. This indicated that the adjustment of the fluid field measurements by subtracting the background wind in horizontal plane did not significantly change the consistence of the fluid field measurements, but the method of background wind measurement caused significant differences in fluid field computation, thus had significant effect on fluid field measurement results.

2.3.1.2 Plume visualizationof field measurements by Tecplot

Tecplot was used to generate the 3D contour plot for each group of test sets. As the vertical lifting was the main focus, the velocity in vertical direction, w's were plotted for visualization of the plume field for all the testing groups. Since no significant difference was found among test groups within first and second sets of tests, randomly selected plots are shown in Figure 2-8 - 2-10 for illustration. The contour plots by Tecplot for other groups are included in Appendix I. These figures show the displays of the 3D domain from different angles. By the "slices" function in Tecplot, planes could be inserted to display the contour plot at certain planes.

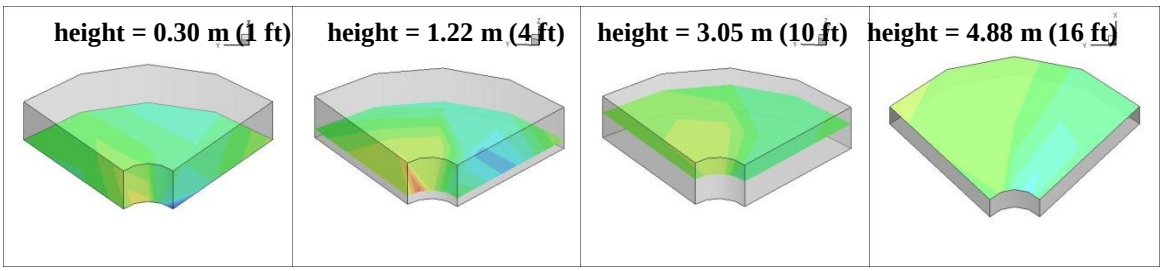

Figure 2-8. Contour plots of the vertical velocity "w" at four heights for testing group 2-05

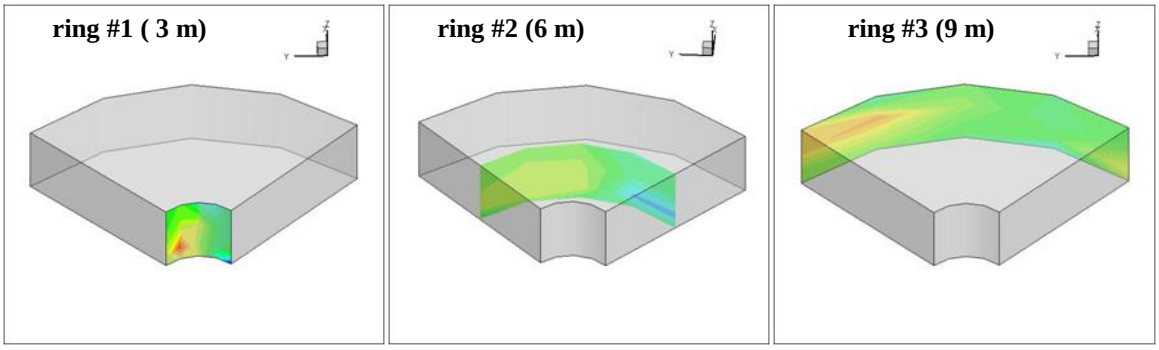

Figure 2-9. Contour plots of the vertical velocity "w" at three rings for group 2-05

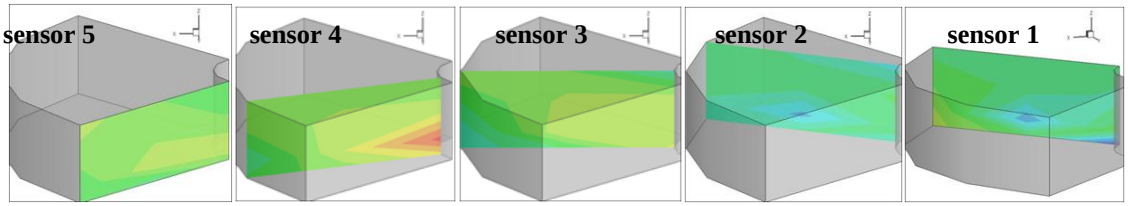

Figure 2-10. Contour plots of the vertical velocity "w" at the location of five sensors (side views) for group 2-05

The plotting results showed that the plume was shifted to the left in general. This was different from the initial expectation of a symmetric plume under no background wind interference. The measurement-based plotting results for all three sets of tests show a similar left-shifted plume. It was suspected that the background wind was the cause of the left-shifting plume.

While the first two sets showed reasonable flow patterns, the contour plots of the third set did not show a shape of the plume. Meanwhile, paired two-sample t-test between test set three and test set two indicated significant differences between the two. This might be due to

the variation of the background wind since the background wind and fan flow velocities were not measured simultaneously. Since only one group of test was done for the test set three, further experiments should be conducted to justify this method.

2.3.1.3 Plume shape observation and prediction of field measurements

To quantify plume depth, the first two sets of "w" data were sorted from the smallest to the largest and each data set was ranked. After data sorting and ranking, it was discovered that, the maximum of "w" appeared at the lower left part (x = 2.10-3.00 m, y = 0.00-2.14 m, z = 0.30-1.22 m) on the ring #1, followed by points at the center (x = 8.3 m, y = 3.49 m, z = 1.22 m) on the ring #2. On the ring #3, the biggest "w" appeared at the upper left part (x= 10.49-13.83 m, y = 5.81-10.72 m, z = 3.05-4.88 m), but these points had smaller w's as compared to the first two rings (#1 & #2). This suggests that at 3 m (ring #1) away from the fan, there was a strong lifting momentum; at around 9 m (ring #3) away from the fan, the lifting momentum was still big, but not as strong as at the 3 m ring.

Combining the data examination with the plots visualization, it was discovered that the plume depth was approximately 9 m away from the fan where the plume started to lift.

Similar method was used to examine the plume width and it was discovered that the plume width was about 12 m.

For plume rise examination, the filed measurement was conducted with the furthest distance at 15 m and top height at 4.88 m. The field smoke test indicated that the plume went beyond 15 m away from fan and rose over 4.88 m. Limitation of the measurement height and distance prevented a numerical development of the plume rise at this time. Further experiment is planned to extend field measurement to a greater scope.

2.3.2 PLUME MODELING AND VISUALIZATION BY CFD

2.3.2.1 Modeling and visualization of plume under the field experimental conditions

The fan surface tests showed an average rotational speed (w_0) of 6.83 rad s^{-1}. The exit velocities and radial velocities are shown in Table 2-6.

Table 2-6. Exit velocities and radial velocities at the fan surface

Radius (m)	V_r (m s^{-1})	u (m s^{-1})
0	/	1.482
0.072	-0.082	1.938
0.143	-0.479	4.129
0.215	-0.510	7.931
0.286	0.194	8.749
0.358	0.086	4.508
0.394	/	1.711

Upon obtaining the CFD outputs, paired two-sample t-test was used to test the difference between the CFD simulation and the field measurements. The results showed significant differences for comparing the model outputs in vertical velocities (w) with all groups' measurements of the velocities, while no significant difference was found between the horizontal velocities (u and v) of the field measurements and the CFD simulations. The mean of the w velocities in CFD model was 0.1 m s^{-1} higher than the mean w of a randomly chosen group of the field measurements. The top-view of the plume at 0.3 m above the ground and the computational meshes modeled by FloEFD is presented in Figure 2-11.

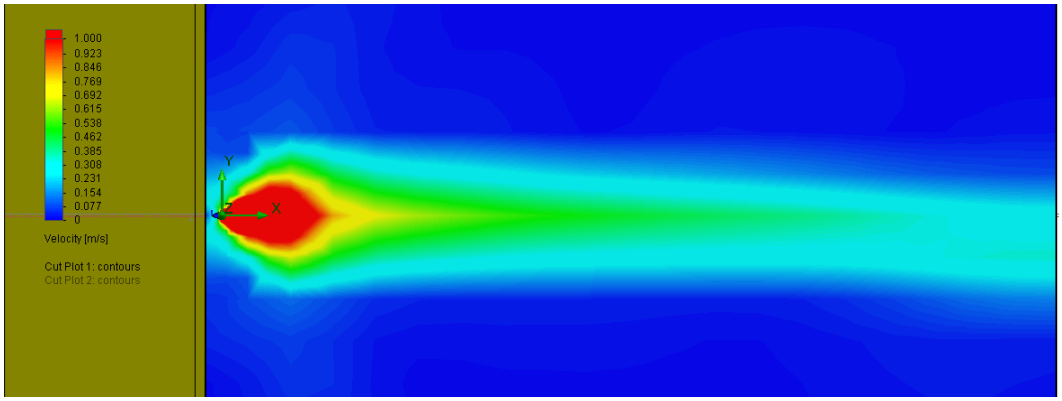

Figure 2-11 Top-view of CFD modeled contour plot of the flow speeds at a horizontal cut plane 1.22 m above the ground

The contour of the CFD model also provided similar velocity profile as illustrated by the Tecplot. As an example, Figure 2-12 shows left side view of the CFD contour plot.

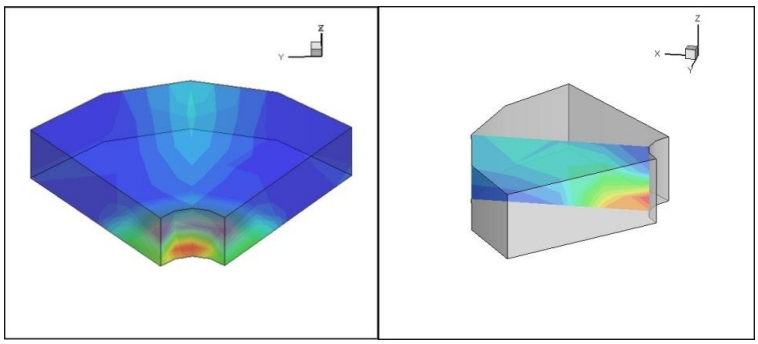

Figure 2-12. 3D view (left) and side-view slide (right) of the contour plot of the velocity "w" modeled by the CFD, simulation of field measurement conditions

2.3.2.2 Impact of temperature difference on the plume shape

To investigate the thermal lifting effect, the model simulation was set at no background wind & a full fan RPM, the temperature difference between the fan flow and the ambient air was the only variable. The 15^{o}C of fan flow temperature was selected based on the average temperature measured during the field experiment. By using the probe function in FloEFD, the coordinates, velocities and other parameters at a certain point could be chosen. Figure 2-13 illustrates two points showing the 3D coordinates and vertical velocities (w) in the case of $\Delta T = 0$. The left point was the location when w stopped increasing and started to decrease along x axis. The x coordinate at that point was defined as the plume depth and 0.496 m s^{-1} was the w_{max}. The right point shows a vertical velocity 5% of the w_{max}. The z coordinate of this point was thus considered to be the plume rise. The top view was used to verify if these points at y = 0 m were showing the highest w at the same heights.

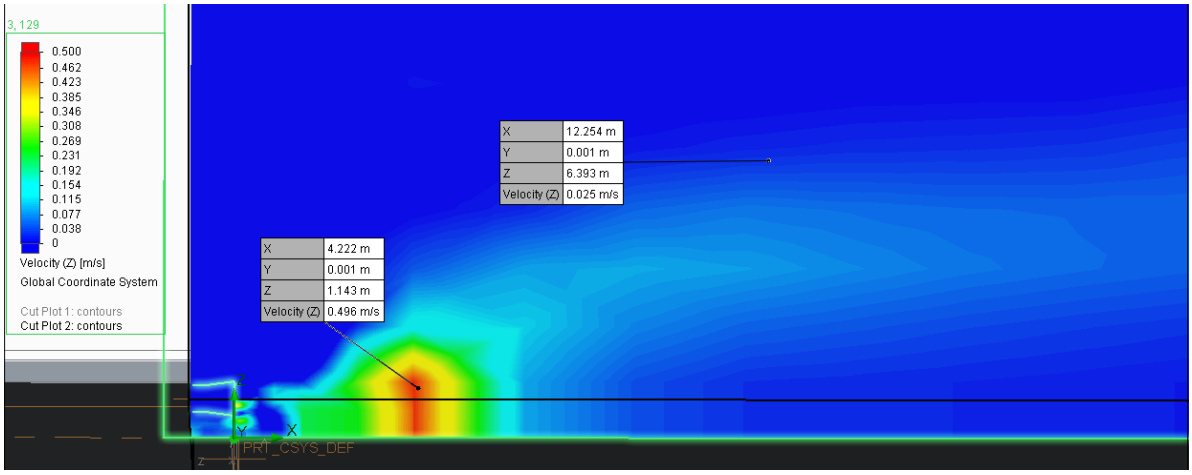

Figure 2-13 Side view of the vertical velocity "w" when T = 0 at a vertical cut plane along with the centerline of the fan

Figure 2-14 illustrates the process of finding plume width. After the plume rise was determined, a top-view cut plot at the height of plume rise was generated, showing the 3D velocities of the computational domain. By using the probe, the point that had the biggest 3D velocity was found. Two points on each side of the center point along the y direction was found with the flow speeds 5% of the highest value. The distance between the two points was defined as the plume width.

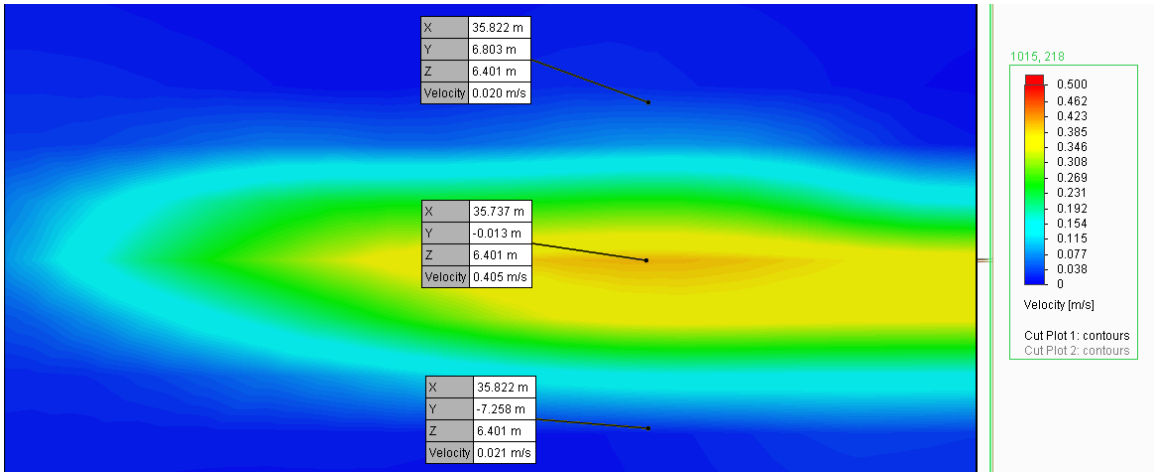

Figure 2-14 Top view of the flow speeds velocity when T = 0 at a horizontal cut plane 6.41 m above the ground

By using the same method, the plume shapes of all three cases with different temperature differences were defined. Figures showing the determination process for all the simulations, including the background simulations in later discussions, are listed in Appendix II. The simulated resultant plume shapes are listed in Table 2-7:

Table 2-7. CFD modeled plume shapes under various temperature differences

Fan flow temp. (^oC)	Ambient temp. (^oC)	T(^oC)	Plume depth (m)	Plume width (m)	Plume rise (m)
15	15	0	4.2	14.0	6.4
15	25	-10	14.3	>100	6.0
15	5	10	9.5	/	>40

The results showed that the temperature differences, no matter positive or negative, added the plume depth. Especially when $\Delta T < 0$, indicating a warmer ambient temperature, the plume depth was three times as large as it was when $\Delta T = 0$. Meanwhile, under the situation that $\Delta T < 0$, the plume rise also decreased. When the exit temperature of the plume was lower than the ambient, the plume was considered to be dense plume. These results agreed with the finding of dense plume dispersion study by Briggs (2001) that higher density of the plume would limit vertical diffusion, but meanwhile, add the distance before rising up.

In the case when $\Delta T > 0$, the plume met the definition of buoyant plume — defined as plumes lighter than ambient air either because the temperature of the plume is higher than the ambient, or because the mixture of the plume has a smaller molecular weight than air, or both. More obvious than the increase of plume depth, the plume rise increased so much that it was out of the computational domain. Thus, the exact plume width meeting the definition of this study was not able to be determined. This observation agreed with the enhancement of plume reported by Hanna et al. (1997) for buoyant plume.

2.3.2.3 Impact of background wind on the plume shape

Based upon the same CFD simulation/plume shape determination procedure, the plume shapes as impacted by various background winds were defined. In the plume shape

determination for simulation results with low background winds (-0.05 and -0.10 m s^{-1}) in x direction, it was observed that w_{max}'s were at the edge of the computational domain, indicating a possibility that the current computational domain was not large enough. To further observe the plume shape in such cases, a new simulation was set with a background wind V_x = -0.05 m s^{-1} and a computational domain twice as long as the original one in x direction (100m). The result showed that the w_{max} still appeared at the edge of the new boundary of the enlarged computational domain. According to the field measurements of wind speeds, there was only 0.2% of time that the wind speed was less than 0.10 m s^{-1}, further exploration of background winds at such low speeds was not conducted.

Particle tracer was taken to better visualize the movements of the plume. The result, as shown in Figure 2-15, indicated that the particle plume from the fan kept its movement in x direction and was not quite affected by the background wind at 0.05 ms^{-1} against it. However, the definition of plume shape by contour plot of cut planes did show the increase of "w" velocity near the end of the computational domain. This was probably due to the swirl of the ambient air caused by the fan flow.

Figure 2-15 "w" contour of particle movements with background wind V_x = -0.05 ms^{-1}

Similarly, w_{max}'s were found to be around the edge of the computational domain for the simulation with background wind V_x = -0.10 m s^{-1}. As the particle tracer simulations showed that the particles in the plume were moving towards the fan plume original direction, not appear to be affected by the background wind at low speed against the plume. Therefore, in this study, the plume shapes of simulations with low background wind (-0.05 and -0.10 m s^{-1}) were considered to be the same as the case when there is no background wind.

For higher background winds, particle tracer simulations were also taken. In general, the resultant plume shapes through particle simulation agreed with the plume shapes defined by cut planes in air flow simulation. The plume shapes are listed in table 2-8:

Table 2-8. CFD modeled plume shapes under various background winds

V_x (ms^{-1})	V_y (m s^{-1})	Plume depth (m)	Plume width (m)	Plume rise (m)
0.00	0.00	4.2	14.0	6.4
0.00	-1.00	9.2	49.0	12.3
0.00	-2.50	6.1	49.4	12.0
0.00	-4.00	4.9	49.4	14.0
-1.00	0.00	24.7	49.8	19.6
-2.50	0.00	9.0	28.84	13.4
-4.00	0.00	4.1	29.0	12.7

Pearson's correlation coefficients (ρ) were calculated to test the linear relationship between the strength of background winds in –x or –y directions, and the 3D dimensions of the plume. Table 2-9 shows the statistical test results. The coefficient varies from -1 to 1, meaning the relationship varies from negatively related to positively related.

Table 2-9. Pearson's correlation analysis of relationship between background winds and plume shapes

Wind direction	Plume dimension	Correlation coefficient	Conclusion
-y	Plume depth	-0.969	Negatively related
-y	Plume width	0.866	Positively related
-y	Plume rise	0.788	Positively related
-x	Plume depth	-0.957	Negatively related
-x	Plume width	-0.862	Negatively related
-x	Plume rise	-0.908	Negatively related

As the background wind rise from -1.00 to -4.00 m s^{-1}, the plume depth became shorter. This is because that as the plume went out of the fan, it lost its momentum in x direction gradually. The background wind would accelerate the dissipation of x momentum. Figure 2-16 shows the movement of particles along with the plume at V_x = -2.50 m s^{-1}. As the plume went out of the fan, it would keep its original momentum in +x direction at first, then gradually change its direction towards –x direction due to the background wind.

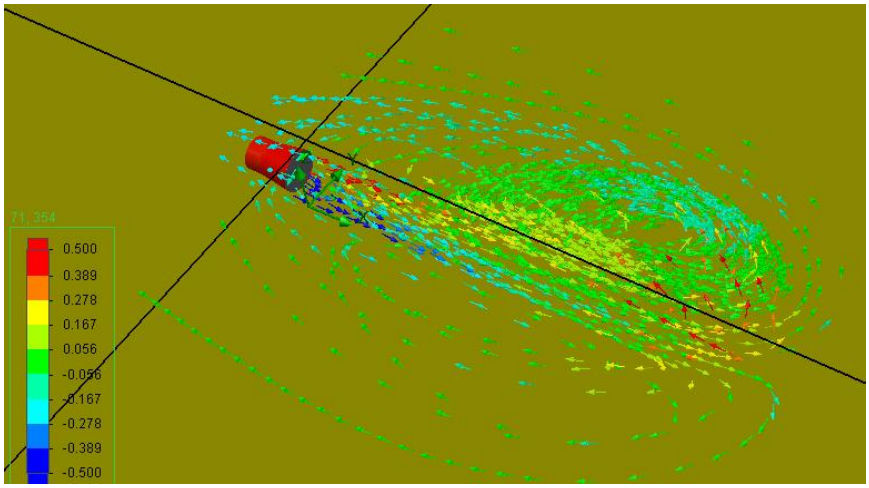

Figure 2-16 "w" contour of particle movements with background wind V_x = -2.50 ms^{-1}

The plume width and rise were positively impacted by the background wind in –y direction and yet they were negatively impacted by the background wind in –x direction. This is probably because in -x direction, the background wind was directly against the fan flow, causing stronger interaction than other directions. Stronger background wind ($-V_x$) around the fan flow might consequently limit the width and rise of the plume. As only three results can be used for discussion, it is not enough to give out reliable results of linear relationship test. More simulations with various background winds are needed for more convincing conclusions.

Based on the above results, the background wind was found to have a strong impact on the plume shape, including all the three dimensions—depth, rise and width. In reality, the background wind varies in speed and direction at high frequency. The plume shapes would be affected more in such cases and become more complicated.

2.4 CONCLUSIONS

In this research, a combination of theoretical and field study was conducted to measure and simulate the plume rise and shape of air flow from a ventilation fan. The theoretical modeling of the plume shape was conducted using a commercial CFD package named FloEFD; the field measurements of the plume field were conducted using five 3D ultrasonic anemometers to simultaneously measure the air flow in the plume at various locations. The Tecplot package was used to visualize the plume flow field based upon anemometer measurements.

The plume field measurements indicated that the plume of a 0.6 m (24 in.) ventilation fan had a depth about 9m, a width about 12 m, and a rise (lifting) beyond the highest measurement point, 4.88 m (16 ft) when no background wind interference and thermal lifting occurred. Further filed data collection is needed to extend measurement height to capture the true plume lifting height.

While the plume shapes were found to be left-shifted by the Tecplot visualization, the simulation of CFD did not show a shifting trend. A negative temperature difference (ΔT) between the plume flow and the ambient air was found to increase the plume depth, but reduced the rise of the plume. A positive T, on the contrary, led to a big increase of plume rise. Stronger background wind against the fan flow had shortened the plume depth, reduced the plume rise and plume width. The strength of background wind in perpendicular to the fan flow and the plume shape was found to reduce the plume depth, but increase the plume width and plume rise.

CHAPTER 3 MODELING PLUME RISE OF AIR EMISSIONS FROM ANIMAL HOUSING SYSTEMS: APPLICATION OF AERMOD

ABSTRACT

In application of AERMOD, this study used the trial and error method to find the rise of the plume emitted from a commercial layer farm by comparing the predicted ambient PM_{10} concentrations with the field measurements. In total 87 hourly plume rises were found for 20 days (five days per season for four seasons, from fall 2008 to summer 2009). The mean plume rises for fall 2008, winter 2008, spring 2009 and summer 2009 were 16.2 m (SE = 11.2 m) 7.9 m (SE = 9.5 m) 16.5 m (SE = 12.4 m), and 14.3 m (SE = 10.0 m), respectively. The relationships between plume rises and various factors were tested. While the diurnal patterns of the plume rises were not consistent among different selective days, they generally followed the diurnal patterns of house ventilation rates. Plume rise for weekends were significantly higher than those for weekdays in fall. Multiple linear regression showed a significant positive relationship (p-value = 0.0134) between wind speed and the plume rises. Ambient relative humidity and total volume flow were also found to be slightly (p-value = 0.171 and 0.217, respectively) related to the plume rises.

3.1 INTRODUCTION

3.1.1 PARTICULAR MATTER EMITTING FROM ANIMAL HOUSING SYSTEMS

Particulate matter, mainly generated from the entrainment of the dried manure, feed, soil, animal dander and other materials in the ambient air (U.S. EPA, 2004a), can travel deep into the lungs. Heart and lung malfunction, asthma attacks, irregular heartbeats and heart attacks may occur when exposure to high level PM (U.S. EPA, 2008). As the pollutants regulated by

the NAAQS, the PM concentrations, including PM_{10} and $PM_{2.5}$, in AFOs' ambient air are of concern. To better prevent PM as well as other air pollutants from affecting the ambient environment and human health, the emission, fate and transport of these air pollutants should be understood first.

Holmes et al. (2006) suggested that the flow patterns of gas and PM emissions meet well in open environments when there is no severe turbulence and the emission sources are not too complicated. Thus, study of the PM concentrations at a source (e.g. animal housing systems) and in its surrounding area can be representative to show the fate and transport of air pollutants from the emission source. Through simultaneously measuring the PM concentrations at the source and downwind locations, dispersion of the PM emission dispersion could be analyzed.

While the filter-based gravimetric measurement of PM concentrations had been established by the U.S. EPA as federal reference method (FRM), tapered element oscillating microbalance (TEOM) had been a very popular method. This is because that TEOM was able to measure the PM concentrations in real time, saving the manual operation time and operating costs (Green and Fuller, 2006). However, the PM concentrations measure by TEOM was found to have wide variations with the FRM (Allen et al., 1997). Although its measurements may be affected by volatile compounds (Green and Fuller, 2006; Li et al., 2012), TEOM was accepted by the U.S. EPA as an equivalent method of PM_{10} measurement (U.S. EPA, 1990). Although more studies continued to report difference between TEOM and traditional gravimetric method (Charrona et al., 2003; Jaques et al., 2004; Lee et al., 2005)

and tried to address the differences and to make corrections, Li et al. (2012a) found that the disagreement of these two techniques remains to be a great challenge.

Studies about the PM emission from AFOs have been done by lots of researchers (Cambra-Lopez et al., 2011; Redwine et al., 2002). The NAEMS also includes the measurements of baseline PM emissions from AFO buildings. As a case of study about PM emissions, Cambra-Lopez et al. (2011) reported the main source of PM in poultry houses was the feathers of the birds, followed by the manure as the second biggest source. This indicated that for high-rise egg production houses where the hens and the manure are set at different floors, the PM emission at different emission height would be different. Redwine et al. (2002) reported the PM emissions from broiler production houses to be related to the bird age and would increase in summer time than winter time. Roumeiliotis et al. (2010) had measured the hourly $PM_{2.5}$ and PM_{10} for continuous 35 days in four seasons. In their study, prominent diurnal trends were found for both $PM_{2.5}$ and PM_{10} emissions. It was proved to be greatly depended on the photoperiod or activity level of the birds.

3.1.2 APPLICATION OF AIR DISPERSION MODEL IN AGRICULTURAL EMISSIONS

Along with the characteristics of PM emissions, the dispersion of PM had been another concern. Dispersion models were often used to predict the fate and transport of air pollutants after emitted from the sources. As discussed in chapter one, box model, Gaussian model, Larangian and Eulerian model as well as computational fluid dynamics model are four main kinds of models widely used in pollutant dispersion studies.

As a widely used air dispersion model, Gaussian dispersion model have been applied to not only industrial dispersions but also agricultural dispersions as early as 1989 (Carney and

Doddt, 1989). Their study used the basic Gaussian equation for the prediction of downwind pollutant concentrations:

$$C(x, y, z, H) = \frac{ER}{\pi \sigma_y \sigma_z u} \{\exp[-0.5(\frac{z-H}{\sigma_z})^2] + \exp[-0.5(\frac{z+H}{\sigma_z})^2]\} \qquad (3\text{-}1)$$

where,
C = downwind pollutant concentrations at point (x, y, z), μg m^3
H = effective stack height = physical stack height (h, m) + plume rise (Δh, m)
ER = emission rate, μg s^{-1}
u = wind speed, m s^{-1}
x, y, z = 3-D distances of the receptor away from the source, m
σ_y, σ_z = standard deviation of the plume concentration in the horizontal and vertical direction at a distance x, respectively, m

After the prediction, the results were used to be compared with field measurement. They found the model and the field measurement in good agreement. Based on equation 3-1, plume rise was needed for the prediction of downwind concentration of air pollutants. However, Carney and Doddt (1989) did not specify the way to measure or compute the effective stack height. The unknown plume rise and plume shape is a vital week point for the accuracy of predictions by Gaussian dispersion model in application of AFO emission and pollutant dispersions. Research about plume rise from animal housing systems is needed to make contribution to more reliable prediction of current Gaussian dispersion models.

McGinn et al. (2010) used a modified backward Lagrangian stochastic (BLS) model to simulate the disperion of PM. However, their simulation of the source was not based on measurement. Instead, they assumed a total amount of particles evenly distributing out of the surface, which may not be the reality and could not be justified by field measurements.

Along with the various types of model applied in agricultural emission, the modeled source type varies from poultry litter combustion (Henihan et al., 2003) to odor from poultry production units (Hayes et al., 2006), to staphylococci from a broiler barn (Seedorf et al., 2005). In the study of Henihan et al. (2003), Atmospheric Dispersion Modeling System (ADMS), a widely used Gaussian dispersion model was used for prediction of pollutant dispersion. Although it was stated that the ADMS was validated to be a good model in the previous studies (Hanna et al., 1999), the allowed inputs in ADMS did not include the emission direction of the source. Hayes et al. (2006) used the Industrial Source Complex (ISC) model—another Gaussian-based model in their study, but stated the lack of peer-reviewed data on model validation regarding odor had made the choice of dispersion model problematic (Curran et al., 2002). Gaussian model was used for plume dispersion and Lagrangian model was used for particle dispersion in the study of Seedorf et al. (2005). However, the results of the two models were reported to be generally contradictory. The above studies showed that to get satisfactory and convincing results of dispersion models, not only should the emission source input be specifically defined, but also adjustments of the current existing models shall be done before application, Furthermore, to validate the model prediction, field measurements were often used to compare with the modeled results. However, in reality, different types of sources are always combined together, making it hard to simulate the fate and transport of the air pollutants.

3.1.2.1 Application of AERMOD in AFO emissions

The AERMOD was developed by the American Meteorological Society (AMS)/U.S. EPA Regulatory Model Improvement Committee, known as AERMIC, as an improved model of

ISC model. Inverse-AERMOD was often applied to predict the emission of pollutants as a substitution of emission measurement when the direct measurements of emission rates are not practical.

In addition to the main body of the AERMOD, there are two pre-processors required by AERMOD system: (1) AERMET for providing meteorological data of planetary boundary layer (PBL) turbulence structure and scaling concepts, and (2) AERMAP for characterizing the terrain and generating receptor grids for the dispersion model. By inputting surface characteristics and standard meteorological observations, AERMET is able to calculate the boundary layer parameters needed by AERMOD, including friction velocity (u^*), Monin-Obukhov length (L), convective velocity scale (w^*), temperature scale (θ^*), Mixing height (zi –, convective z_{ic} and mechanical z_{im}) and surface heat flux (H). AERMAP helps to provide the receptor information (location, height above mean see level, specific terrain height scale) after the receptor grids were created by the system.

AERMOD allows simulations in both the stable boundary layer (SBL) and the convective boundary layer (CBL). Simulations under the SBL condition assume the Gaussian concentration distribution in both the vertical and horizontal directions (Fig. 3-1), whereas simulations under the CBL condition assume Gaussian distribution in horizontal direction but a bi-Gaussian probability density function in vertical direction (Fig. 3-2). Additionally, in the CBL condition, a portion of plume mass, released from a buoyant source, rises to and remains near the top of the boundary layer before becoming mixed into the CBL. There are five types of plume depending on the atmospheric stability and on the location in and above the boundary layer: 1) direct, 2) indirect, 3) penetrated, 4) injected and 5) stable.

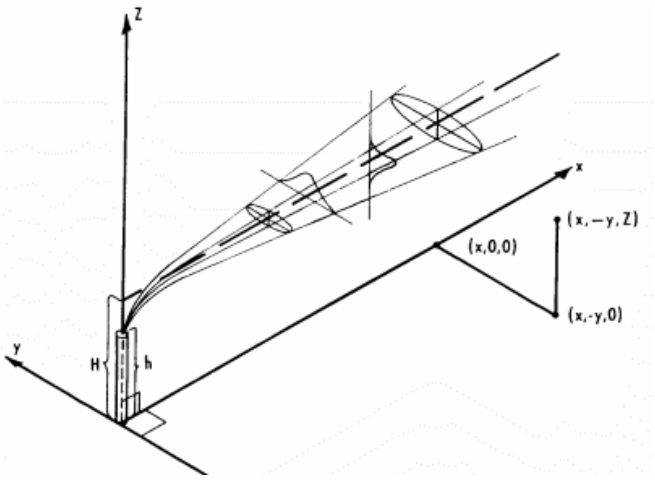

Figure 3-1. Plume with Gaussian distribution in both vertical and horizontal directions (Turner, 1970)

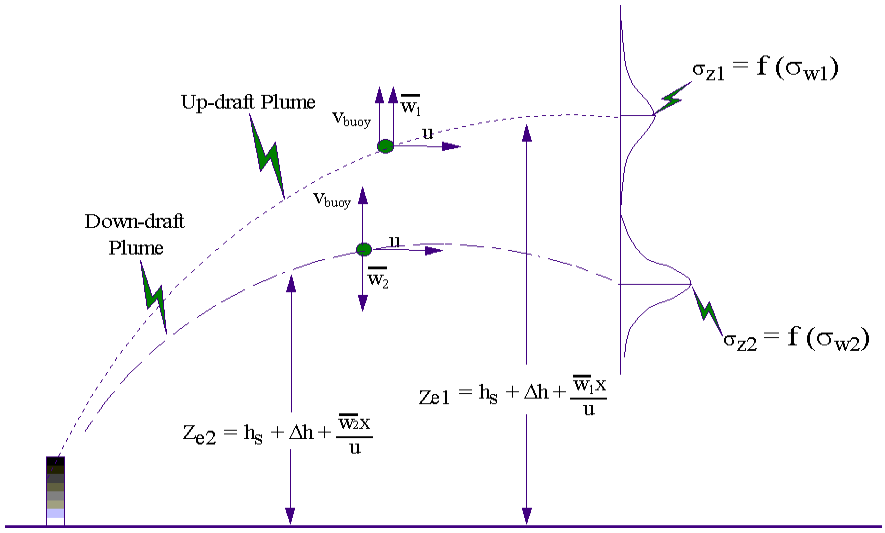

Figure 3-2. Plume with bi-Gaussian distribution in vertical direction under the CBL (U.S. EPA, 2004b)

In AERMOD, under the CBL condition, the downwind concentration predictions are attributed to the three plume treatments, i.e., direct, penetrated and indirect sources (U.S. EPA, 2004b). The direct source is the portion of the plume mass reaching the ground and all subsequent reflections of that mass with the mixing layer. The penetrated source is the plume segments initially penetrating the elevated inversion above the mixing layer. The indirect source is referred to the plume segment initially rising in updrafts above the mixing layer (Fig. 3-3).

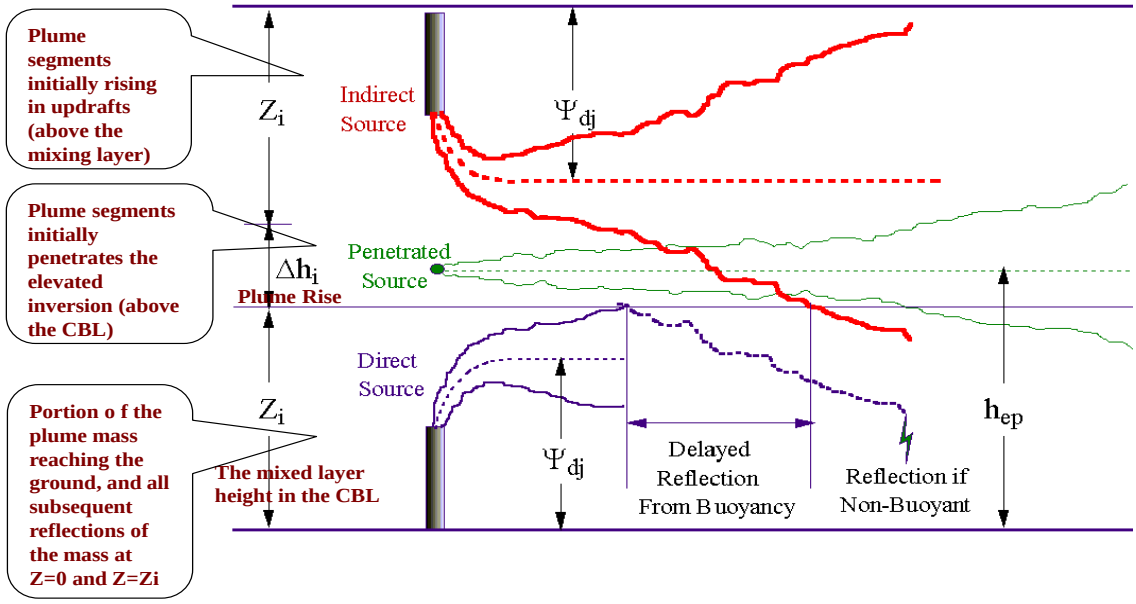

Figure 3-3. Three plume treatments under the CBL (U.S. EPA, 2004b)

Under the CBL condition, the downwind concentration prediction is the summation of these three source contributions. The computational models for the contributions of direct

source, indirect source and penetrated source are in equations 3-2, 3-3 and 3-4, respectively (U.S. EPA, 2004b).

$$C_d\{x_r, y_r, z\} = \frac{Qf_p}{\sqrt{2\pi}\tilde{u}} F_y \cdot \sum_{j=1}^{2}\sum_{m=0}^{\infty}\frac{\lambda_j}{\sigma_{zj}}[\exp(-\frac{(z-\psi_{dj}-2mz_i)^2}{2\sigma_{zj}^2}) + \exp(-\frac{(z+\psi_{dj}+2mz_i)^2}{2\sigma_{zj}^2})] \quad (3\text{-}2)$$

where,

$\psi_{dj} = h_s + \Delta h_d + \frac{\bar{w}_j X}{u}$ = total height of the direct source plume, m

$\bar{w}_j$ = mean vertical velocity, m s^{-1}

h_s = stack height corrected for stack tip downwash, m

Δh_d = plume rise for the direct source, m

j = 1 for updraft and 2 for downdraft distributions

Q = source emission rate, g s^{-1}

f_p = fraction of plume mass contained in CBL

u = wind speed at stack top, m s^{-1}

$\tilde{u}$ = effective wind speed, m s^{-1} = average wind speed of vertical variations

F_y = lateral distribution function with meander

λ_j = weighting coefficient

z_i = mixing height, m

σ_{zj} = total vertical dispersion for both the direct and indirect sources

$$C_r\{x_r, y_r, z\} = \frac{Qf_p}{\sqrt{2\pi}\tilde{u}} F_y \cdot \sum_{j=1}^{2}\sum_{m=1}^{\infty}\frac{\lambda_j}{\sigma_{zj}}[\exp(-\frac{(z+\psi_{rj}-2mz_i)^2}{2\sigma_{zj}^2}) + \exp(-\frac{(z-\psi_{rj}+2mz_i)^2}{2\sigma_{zj}^2})] \quad (3\text{-}3)$$

where,

$\psi_{rj} = \psi_{dj} - \Delta h_j$ = total height of the indirect source plume, m

Δh_i = plume rise for the indirect source,

$$C_p\{x_r, y_r, z\} = \frac{Q(1-f_p)}{\sqrt{2\pi}\tilde{u}\sigma_{zp}} F_y \sum_{m=-\infty}^{\infty} [\exp(-\frac{(z-h_{ep}+2mz_{ieff})^2}{2\sigma_{zj}^2}) + \exp(-\frac{(z+h_{ep}+2mz_{ieff})^2}{2\sigma_{zj}^2})] \quad (3\text{-}4)$$

where,
h_{ep} = penetrated plume height, taken as the height of the plume centroid above the mixed layer, m
z_{ieff} = the height of the effective mechanical mixed layer, m

Under the SBL, the concentration due to the stable plumes can be computed as follows (U.S. EPA, 2004b):

$$C_s\{x_r, y_r, z\} = \frac{Q}{\sqrt{2\pi}\tilde{u}\sigma_{zs}} F_y \sum_{m=-\infty}^{\infty} [\exp(-\frac{(z-h_{es}-2mz_{ieff})^2}{2\sigma_{zs}^2}) + \exp(-\frac{(z+h_{es}+2mz_{ieff})^2}{2\sigma_{zs}^2})] \quad (3\text{-}5)$$

where,
h_{es} = plume height = $h_s + \Delta h_s$, m
Δh_s = plume rise for stable source, m
σ_{zs} = total dispersion for the stable source, m

As it can be seen from the equations above, in order to calculate downwind concentrations, it is required to model the dispersion plume rise first. The AERMOD defines the plume rises based upon atmospheric boundary conditions (U.S. EPA, 2004b). Under the CBL condition, the plume rise models include direct plume rise (equation 3-6), indirect plume rise (equation 3-7) and penetrated plume rise (equations 3-8 and 3-9). Under the SBL condition, the plume rise models include: transitional rise (equation 3-10), final rise (equation 3-11), neutral limit (equation 3-12) and near-calm conditions (equation 3-13) (U.S. EPA, 2004b):

$$\Delta h_d = \left(\frac{3F_m x}{\beta_1^2 u_p^2} + \frac{3}{2\beta_1^2}\cdot\frac{F_b x^2}{u_p^3}\right)^{1/3} \qquad (3\text{-}6)$$

where,
F_m = plume momentum flux, $m^4\ s^2$
F_b = plume buoyancy flux, $m^4\ s^2$
u_p = wind speed at the height of plume rise, ms^{-1}
$\beta_1 = 0.6$ = entrainment parameter

$$\Delta h_i = \left(\frac{2F_b z_i}{\alpha_r u_p r_y r_z}\right)^{1/2}\frac{x}{u_p} \qquad (3\text{-}7)$$

where,
$\alpha_r = 1.4$
r_y, r_z = the lofting plume half-widths in the lateral and vertical directions

For $f_p = 0$, $$h_{ep} = h_s + \Delta h_{eq} \qquad (3\text{-}8)$$

For $f_p > 0$, $$h_{ep} = h_s + 1.5\Delta h_{eq} \quad or \quad h_{ep} = (h_s + z_i)/2 + 0.75\Delta h_{eq} \qquad (3\text{-}9)$$

where,
Δh_{eq} = equilibrium plume rise in a stable environment, m

$$\Delta h_s = 2.66\left(\frac{F_b}{N^2 u_p}\right)^{1/3}\cdot\left[\frac{N' F_m}{F_b}\sin\left(\frac{N' x}{u_p}\right) + 1 - \cos\left(\frac{N' x}{u_p}\right)\right]^{1/3} \qquad (3\text{-}10)$$

with a final rise $$\Delta h_s\{x_f\} = 2.66\left(\frac{F_b}{N^2 u_p}\right)^{1/3} \qquad (3\text{-}11)$$

where,
N = Brunt-Vaisala frequency, s^{-1}
N' = 0.7 N, s^{-1}
x_f = the distance of the final rise, m

$$\Delta h_s = 1.2 L_n^{3/5}(h_s + 1.2L_n)^{2/5} \qquad (3\text{-}12)$$

where,

L_n = neutral length scale = $F_b / (u_p u_*^2)$, m
u_* = surface friction velocity, m s^{-1}

$$\Delta h_s = 4F_b^{1/4} / N^{3/4} \qquad (3\text{-}13)$$

Although AERMOD has a good development of plume rise computations, it does not fit all the cases with different emission source characteristics. There is an option to select horizontal point source in AERMOD, there is no option to define the emitting direction of the exit flow. It is highly suspected that the formulas for plume rise calculations are not suitable for emissions at ground level with horizontal direction and limited thermo buoyancy, e.g., AFO housing emissions. Accuracy of AERMOD simulation of emissions from AFO houses would be challenged if no correction of plume-rise modeling is applied.

While AERMOD is not perfect for modeling air dispersion, it is an U.S. EPA regulatory mode, and it is the best available tool for prediction of short range steady state dispersion. This tool has been used for various AFO air dispersion modeling studies. In the study by O'Shaughnessy and Altmaier (2011), AEMOD was used to determine a hydrogen sulfide emission factor. They followed the default requirements of emission source input files—emission factors, source dimensions (diameter for point sources, length and width for area sources, etc.) and source emission heights. In the study of Sarr and Go ïa (2010), AERMOD, was used to predict ambient NH_3 concentrations around pig farm operations and the result was used to assess a buffer distance. Due to lack of consideration of AERMOD limitation and suitability to the AFO scenarios, the accuracy of O'Shaughnessy, Altmaier and Sarr's study may be challenged.

3.1.3 RESEARCH OBJECTIVES

Literature reviews showed that the modeling PM emissions from animal production systems with multiple types of animal housing designs was not well studied, and current air dispersion models are not suitable for prediction of emission from AFOs because of lacking consideration of characteristics of AFO emissions.

The objectives of this study were to: apply inverse-AERMOD to derive the plume rises of animal house emissions on a commercial layer farm using field measurements of PM emissions and concentrations on the farm and in the vicinity; and to identify the impacts of various factors on plume rises from the animal houses based upon the inverse-AERMOD results and the field observations.

3.2 METHODOLOGY

In this study, plume rises for animal housing systems were predicted using inverse AERMOD approach. The PM_{10} dispersion from a commercial layer farm (consisting of nine animal houses, with six mechanically ventilated and three naturally ventilated ones) was modeled. The plume rises for the source types (i.e. ventilation types) were adjusted and the results of model predicted hourly downwind PM_{10}concentrations were compared with field observations at four ambient stations. When the model predictions agreed with the field measurements within ±20% relative differences, the plume rise for that hour were considered valid. In total, 480 hourly PM_{10}data for four seasons with five days per season for four seasons were selected for this modeling study.

3.2.1 FIELD DATA COLLECTION

The field PM data were collected at a commercial layer farm in the Southeast of the U.S.. Brief descriptions of the farm as well as the collecting process of PM concentrations, flow rates of the ventilation systems and meteorological data are presented in the following sections.

3.2.1.1 The layer farm and PM monitoring stations

As shown in Figure 3-4, the layer farm consisted of nine layer houses and an egg packing building. Based on the type of ventilation systems, the layer houses were divided into four tunnel ventilated high-rise layer houses (houses 1-4), two cross ventilated high-rise layer houses (houses 5-6), and three naturally ventilated shallow pit layer houses (houses 93, 102-103).In the high-rise houses, laying hens were caged on the second floor in 6 rows (houses 1-4) or 8 rows (houses 5-6) and manure was stored in the first floor and was completely cleaned out once a year. In the naturally ventilated houses, hens were caged in 4 tires and manure was flushing out to lagoons twice a day. The dimensions of the houses are listed in Table 3-1.

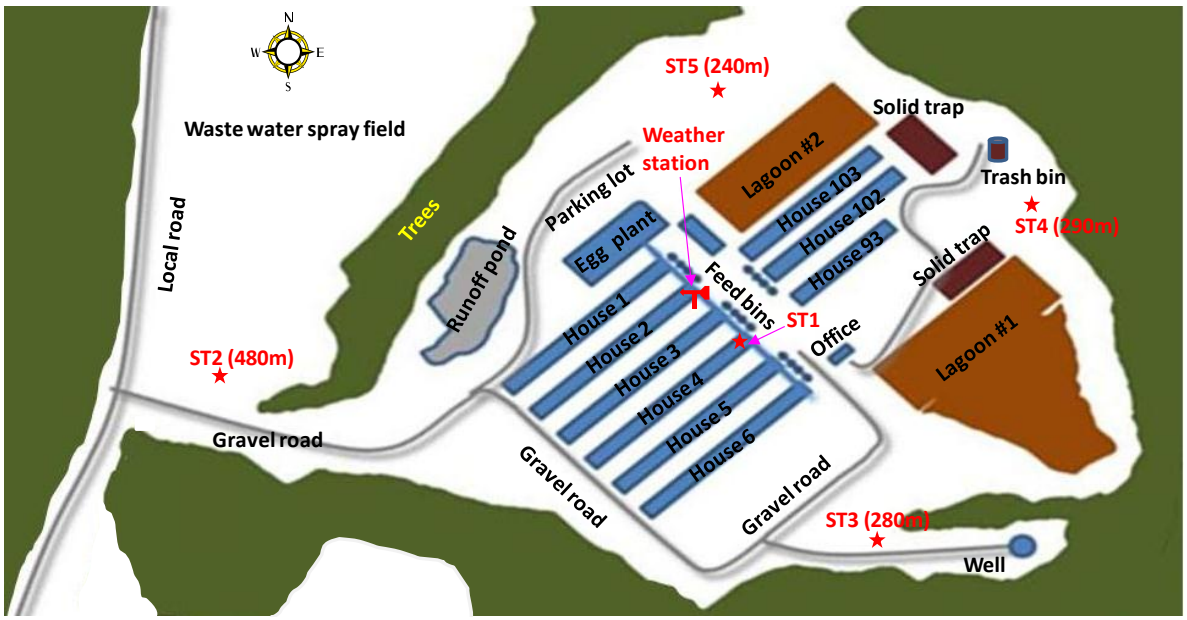

Figure 3-4.The layer farm layout & the locations of PM monitoring stations (Wang-Li et al., 2012).

Table 3-1. Overall building information of the layer houses

Names	Length (m)	Width (m)	Height (m)	Ventilation system	Hen population
Houses 1-4	176.8	17.8	5.5 (eave) 8.4 (ridge)	Tunnel ventilated	~96,000 per house
Houses 5-6	176.8	21.0	5.5 (eave) 8.4 (ridge)	Cross ventilated	~13,000 per house
Houses 102-103	152.4	17.8	3.0 (eave) 5.5 (ridge)	Naturally ventilated -type 1	~70,000 per house
House 93	107.0	17.8	2.5 (eave) 5.0 (ridge)	Naturally ventilated -type 2	~30,000 per house
Egg plant building	82.3	38.1	5	/	

Tunnel ventilated houses used 17 belt-driven ventilation fans (upper 8 and lower 9, 1.22 m in diameter) on end wall of each house (Fig.3-5). Houses 5-6 were cross-ventilated houses with 27 belt-driven ventilation fans (1.22 m in diameter) arrayed on each side wall of each house (Fig.3-5). Houses 93,102,103 were naturally ventilated with curtain openings on the side walls, and twenty winter vents evenly distributed on the building ridge.

Figure 3-5. Illustration of the fans in a cross-ventilated house (left) & a tunnel-ventilated house (right).

The PM concentrations were monitored at five locations, of which one was in-house monitoring station (ST1 in Fig. 3-4) and the other four were ambient monitoring stations (ST2-5 in Fig.3-4). The ST1 was designed to measure in-house PM concentration for determination of PM emission rate from the tunnel ventilated houses, whereas ST2-5 were designed to measure downwind and upwind PM concentrations for the dispersion modeling study. The distances from ambient stations to the emission sources are also marked in Fig. 3-4.

3.2.1.2 PM data collection

At each ambient PM monitoring station, one tapered element oscillating microbalance (TEOM) equipped with a federal reference method (FRM) PM_{10} or a federal equivalent method (FEM) $PM_{2.5}$ sampling head was used to take continuous PM_{10} or $PM_{2.5}$ measurements (Wang-Li et al., 2012). At ST1, two TEOMs were installed at the first floor in the east end of house 3 and house 4 to simultaneously take PM_{10}measurements at 30-min. interval from September 2007 to February 2009. In March of 2009, the TEOM in house 3 was moved to the second floor in the east end of house 4 to simultaneously measure PM concentrations in two floors of the house for assessment of spatial variations. Monitoring of the PM concentrations at ST1 was part of the NAEMS. Detailed information about the monitoring site specifics, PM monitoring plan and quality assurance and quality control (QA/QC) practices are reported in Wang-Li et al. (2012) and Li et al. (2012b). For PM monitoring at ST2-5, PM data collection were conducted from October 2008 through September 2011. More information the ambient PM monitoring plan and results is reported in Li et al. (2012c). . The TEOMs at all five stations were maintained following U.S. EPA approved standard operation procedure (SOP) and QA/QC procedure (Purdue University, 2006b) for the whole duration of the study.

In this reported study, only PM_{10} measurements were used for modeling. In PM_{10} concentration measurements, the TEOMs were set at 50 ℃ to minimize moisture impact, and then the measurements were converted to the dry standard conditions (i.e. 25 ℃, 0% RH and 1atm). Thus, to fit dry standard conditions, conversion was done in the emission rate calculation (Lim and Bogan, 2007).

Due to budget limitation, PM emissions from other two types of housing systems (i.e. cross ventilated and naturally ventilated) were not monitored. Emission rate from tunnel ventilated houses were used as a base to estimate emission rates from these types of houses. More detailed information about the estimation of these emission rates is reported in the following section.

3.2.1.3 House ventilation (fan flow) measurements

In addition to PM concentration measurements, other variables that affected PM emissions were also simultaneously monitored under the NAEMS. These influencing variables include house ventilation rate, air temperature and RH inside the houses and at the exhaust fans, and ambient air temperature, RH, etc. The detailed measurement methods are included in a report by Wang-Li et al. (2012).

For the two types of houses with mechanical ventilation systems, the on/off of the fans are controlled by the stage settings based upon the house temperature measurements. The fans stage settings of the mechanical ventilation houses are shown in Figures 3-6 and 3-7.

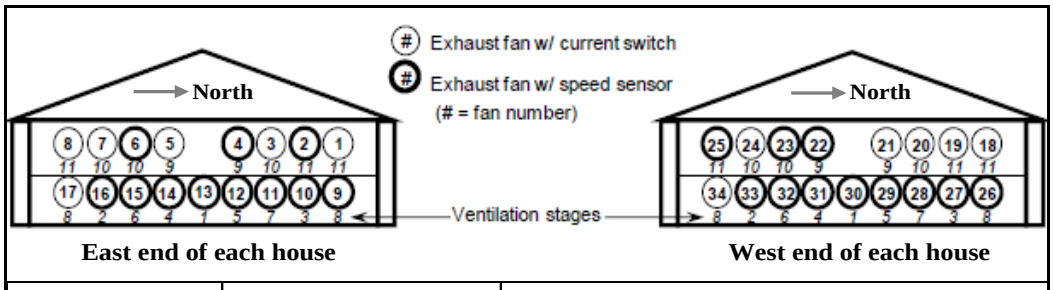

Stage	Quantity	Fan Number
1	2	13, 30
2	2	16, 33
3	2	10, 27
4	2	14, 31
5	2	12, 29
6	2	15, 32
7	2	11, 28
8	4	9, 17, 26, 34
9	4	4, 5, 21, 22
10	6	3, 6, 7, 20, 23, 24
11	6	1, 2, 8, 18, 19, 25

Figure 3-6. Ventilation stage settings of the tunnel ventilated houses (Wang-Li et al. 2012).

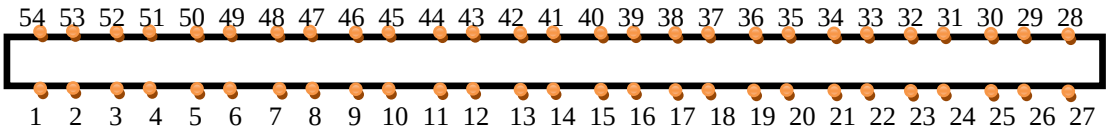

Stage	Quantity	Fan Number
1	4	1, 14, 41, 54
2	2	27, 28
3	2	21, 34
4	2	26, 29
5	2	13, 42
6	2	18, 37
7	2	2, 53
8	2	10, 45
9	2	15, 40
10	2	24, 31
11	2	4, 51
12	2	5, 50
13	2	23, 32
14	2	20, 35
15	2	8, 47
16	4	11, 25, 30, 44
17	4	3, 17, 38, 52
18	4	9, 22, 46, 33
19	8	6, 12, 16, 19, 36, 39, 43, 49

Figure 3-7. Ventilation stage settings of the cross ventilated houses

Under the NAMES project (Wang-Li et al. 2012), ventilation fan status of houses 3 and 4 was monitored using either fan speed sensors (RPM sensors, Cherry Sensor, Model MP100701) or current switches (CR9380-NPN, CR Magenetics Inc.) (Fig. 3-6). In addition to continuous monitoring of the fans' on/off status or speed and the static pressure, *in-situ* airflow measurements were also conducted in November 2007, June 2008 and July 2009 using a portable fan assessment numeration system (FANS) (Gates et al., 2004).

3.2.1.4 Meteorological conditions

For this dispersion modeling study, meteorological data were also monitored using a 10 meter weather tower (see Fig. 3-4 for the location of the tower). Wind speed, wind direction, solar radiation, air temperature, and RH were monitored at a one-minute interval by the sensors on the tower. These meteorological parameters were then averaged to hourly interval for being used by AERMOD.

3.2.2 DATA PERIOD SELECTION

In this reported dispersion modeling study, four periods of field data for each season from fall 2008 to summer 2009 were selected and used. Each period was selected to be consecutive five days. In order to find the potential impact of human activities, the five days included three weekdays and two weekends (Table 3-2). In data selection process, dates with rainfall, snowfall or other extreme weathers that have strong impacts on the air dispersion from the animal buildings were excluded. As the data may not be always proper, some invalid observations, for example, negative PM concentrations measured by the TEOMs due to humidity impact, were also excluded. Thus, the selection of the five days was set to be the periods with the least data points being excluded.

Table 3-2. Data periods selected for modeling PM_{10} dispersion to derive plume rises through inverse AERMOD method

Season	Year	Date period
Fall	2008	11to 15 October
Winter	2008	4 to 8 February
Spring	2009	12 to13 April & 16 to 18 April
Summer	2009	18 to 22 June

3.2.3 FIELD DATA PROCESSING

After the data were collected, calculations were made to transfer the data to the form that would be ready for inputting into the AERMOD software. The specific data processing steps were discussed in the following subsections.

3.2.3.1 Meteorological data

Supporting software named AERMET generating meteorological data files suitable for AERMOD was used to convert field measurement data into hourly means in the format for AERMOD. For missing parameters, AERMET was able to search and obtain data from the nearest surface weather station. After formatting the meteorological data, PFL files and SFC files were formed to be inputted into AERMOD. The formatted metrological files consisted of 20 parameters at hourly intervals.

Reading the hourly wind directions from the AERMET files and based on the relative locations of the center of the whole farm source locations and the ambient stations (ST2-5), the upwind and downwind stations were defined. Since the farm has multiple emission sources, the source inputs for AERMOD included various the source types and their locations.

In addition, emission rate of each source (i.e., exhaust of the houses) varied over time in response to changes in ventilation rates to maintain optimal in-house temperature/RH under different ambient conditions. Consequently, it was hard to define a central location to represent whole farm emission sources for upwind-downwind determination. For summer time, as the curtains of the naturally ventilated houses were fully open, house 93, 102 and 103 had more emission contributions to ambient locations, the center of source locations was defined at the east end of house 3; for winter time, the center of source locations was defined at the middle of the north side wall of house 3; for spring and fall times, the center of source locations was assumed to be located at the middle the above two points.

Once the center point of the whole farm emission source was determined, a plot shown in Fig. 3-8 was generated to determine upwind and downwind locations of each ambient PM monitoring stations. As shown in this plot, $\alpha$was the angle of the receptor-source vector from the north clockwise, θ was the wind direction from the north clockwise. If $|\alpha-\theta|$ was less than 22.5 degrees for any of the ambient stations, PM concentrations from that ambient station was considered upwind concentration, otherwise the upwind concentrations were the average of two ambient stations on both sides of the wind direction. The downwind stations were defined similarly.

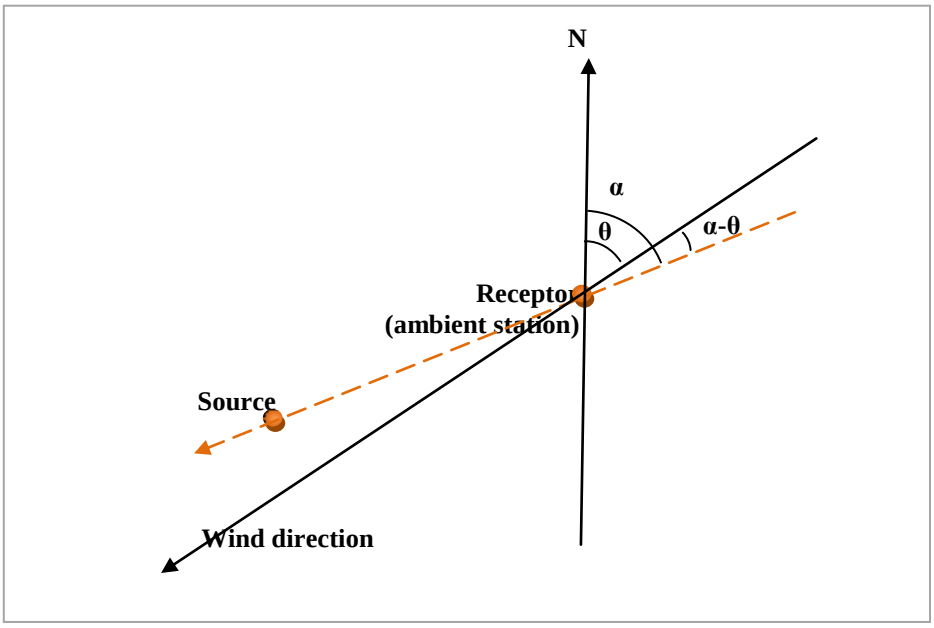

Figure 3-8. Upwind and downwind illustration

3.2.3.2 Individual fan flow rates

The field data collection of PM emission was conducted under the NAEMS project. The fan flow rates for tunnel ventilated houses 3 and 4 were computed and recorded in the form of the air flow streams. For the NAEMS project, the ventilation streams were defined through two versions, named as "NAEMS-old version" and "NAEMS-new version". For the ease of computation, another version of stream classification was done by this study, named "NCSU-version". The definitions of the flow streams are listed in Table 3-3. For the "NCSU-version", four streams were defined, each standing for a bank of fans on one floor at one end of a layer house. Thus, for each individual fan, its fan flow rate was:

$$Q = Q_{NCSU} - S_x \cdot \frac{RPM_i}{\sum_i RPM} \qquad (3\text{-}14)$$

where,

S_x = Stream number for groups of fans

x = 1 for fan 1-8; x = 2 for fan 9-17; x = 3 for fan 18-25; x = 4 for fan 26-34 (see Fig.3-6 for fan number ID)

RPM_i = RPM measured for the individual fan i, for fans without RPM measurement, the RPM for other fans at the same fan stages were used.

Table 3-3. Definitions of the air flow streams for the tunnel ventilated houses 3 and 4

Version description	Streams	Fans included	Equations
NAEMS-old version	Steam 1-- Q_{OS1}	fans 1-8 (east-2nd floor)	
	Steam 2-- Q_{OS2}	fans 9-17 (east-1st floor)	
	Steam 3-- Q_{OS3}	fans 18-34 (west – 1st floor + 2nd floor)	
NAEMS-new version	Steam 1-- Q_{NS1}	fans 1-8 + fans 18-25 (2nd floor – east + west)	
	Steam 2-- Q_{NS2}	fans 9-17 (east-1st floor)	
	Steam 3-- Q_{NS3}	fans 26-34 (west – 1st floor)	
NCSU-version	Steam 1-- $Q_{NCSU-S1}$	fans 1-8 (east-2nd floor)	$Q_{NCSU-S1} = Q_{OS1}$
	Steam 2-- $Q_{NCSU-S2}$	fans 9-17 (east-1st floor)	$Q_{NCSU-S2} = Q_{OS2}$
	Steam 3-- $Q_{NCSU-S3}$	fans 18-25 (west – 2nd floor)	$Q_{NCSU-S3} = Q_{NS1} - Q_{OS1}$ or $Q_{NCSU-S3} = Q_{OS3} - Q_{NS3}$
	Steam 4-- $Q_{NCSU-S4}$	fans 26-34 (west – 1st floor)	$Q_{NCSU-S4} = Q_{NS3}$

Although the ventilations of cross-ventilated houses were not measured, the farm used the same size and kind of fans for both cross- and tunnel-ventilated houses and monitored the performances of all the fans with the same management plan. Thus, the ventilation capacities of the fans for two kinds of houses were assumed to be the same. In addition, the two types of houses shared the same operational practices. Consequently it was assumed that if 50% of

the fans in tunnel-ventilated houses were on, then 50% of the fans in cross-ventilated houses were on. Based on the fan stages described in Figures 3-6 and 3-7, the on/off of fans for cross ventilated houses were determined for each hour.

The ventilation of naturally ventilated houses was basically through the curtains on the side walls. The air flow was relatively small as compared to the mechanically ventilated houses. The air flow velocity (V) was assumed to be the same as the wind speed vector in the direction perpendicular to the side walls of the naturally ventilated houses. The curtains were assumed to be fully opened for summer times, half opened for spring and fall times and fully closed in winter times.

For the naturally ventilated houses 102 and 103, there were 20 vents on top of building ridges. The flow from the vents was insignificant as compared to the opening of the curtains on the side walls in spring, summer and fall times. However, in winter times, the 20 ridge vents of the naturally ventilated house were of the exhausts for air emissions, and were thus taken into account in winter times. As lacking measurement, it was assumed that the exit velocities of the flow coming out of the vents were equal to the wind velocities. Since the house 93 did not have vents on the ridge, and also considering the relative small population (~30,000 in house 93 and ~70,000 in house 102 & 103), it was assumed that the emission from house 93 was insignificant in winter times.

3.2.3.3 Emission rates

For tunnel-ventilated houses, the PM_{10} emission rate of house 4 was calculated based upon field measurements using equation (3-15). It was assumed that emission rates from other three tunnel houses (1-3) were the same as it was from the house 4 due to identical house

configurations, ventilation system controls as well as house management practices and hen types/ages/populations

$$ER = C \cdot Q \tag{3-15}$$

where
ER = emission rate of the PM_{10}, $\mu g\ s^{-1}$
C = PM_{10} concentration at the source (ST1), $\mu g\ m^{-3}$
Q = ventilation flow rate of individual fan, $m^3\ s^{-1}$

In fall and winter of 2008, PM_{10} concentrations were monitored on the east end of the first floor for both house 3 and house 4. The TEOM in house 3 was then moved to the east end of the second floor of house 4 since the beginning of 2009.For the selected period in winter 2008, all the fans on the second floor of the tunnel ventilated houses were off all the time, there was no need to know the PM_{10} concentrations for emission simulations. For fall 2008, no PM measurement was conducted on the second floor of house 4. As the fan stages were depended on the ambient temperature and the fan flow rates would affect the PM concentrations, the PM_{10} concentrations on second floor was simulated by the data collected in fall of 2009 when the daily average of ambient temperature matched well with the selected dates in fall 2008.The detailed data source clarification for the tunnel ventilated houses is listed in Table 3-4.

Table 3-4. PM_{10} data sources for different tunnel ventilated houses

Locations		Seasons 08 fall	08 winter	09 spring	09 summer
First floor	House 1	House 3	House 3	House 4	House 4
	House 2	House 4	House 4	House 4	House 4
	House 3	House 3	House 3	House 4	House 4
	House 4	House 4	House 4	House 4	House 4
Second floor	House 1	House 4 in 09 fall	/	House 4	House 4
	House 2	House 4 in 09 fall	/	House 4	House 4
	House 3	House 4 in 09 fall	/	House 4	House 4
	House 4	House 4 in 09 fall	/	House 4	House 4

Since cross-ventilated houses share the same management plan with tunnel-ventilated ones, only to add 2 rows of layers in one house (6 rows in tunnel-ventilated houses and 8 rows in cross ventilated houses), the emission rate of cross-ventilated ones were assumed to be (6+2)/6 times the emission rate of tunnel-ventilated houses.

For naturally ventilated houses, the ERs would be much less because of wet base manure management practice. Thus, it was assumed that the PM concentrations were 80% of the PM concentrations at the first floor of the tunnel ventilated houses for spring, summer and fall times. For winter times, as the estimation of ventilation was assumed with more uncertainty, instead of considering equation 3-15, the ER of naturally ventilated houses was considered to be directly correlated to the ER of tunnel ventilated houses. The ERs from house 102 and 103 in winter times were computed by the following equation:

$$ER_{nat.} = f_1 \cdot f_2 \cdot f_3 \cdot ER_{tun.} \qquad (3\text{-}16)$$

where
f_1 = factor due to wet base = 0.8
f_2 = factor due to ventilation = 0.4
f_3 = factor due to population = 70,000 hens in house 102 & 103 / 96,000 hens in house 4
ER_{tun} = total emission rate in tunnel ventilated house, ug s^{-1}

3.2.4 AERMOD SIMULATION

AERMOD in this study was provided by BREEZE Software (Dallas, TX), enabling AERMOD to be more user friendly to the customers. AERMOD was used to predict the downwind concentrations of certain pollutants at given emission conditions. Although AERMOD allows multiple choices of time periods and variable emission rates in the simulation process, it does not allow various stack height input for point sources. Thus, for each simulation, one hour of dataset was input into the system. There were 24 hourly runs for each date with total of 480 hourly runs for the selected five days per season for four seasons.

3.2.4.1 Source inputs

Each fan in the mechanical ventilation systems was considered as an individual horizontal point source. The emissions from side wall curtains of the naturally ventilated houses in spring, summer and fall were considered as area sources; whereas in winter time the 20 ridge vents were considered as 20 capped point sources for houses 102 and 103. No such ridge vents was found for house 93, considering its smaller ventilation and less population as compared to other houses, the emission from house 93 in winter time was not taken into account. The grouping of the sources is provided in Table 3-5.

Table 3-5.List of source information for simulations in AERMOD

Group ID	IDs of the sources	Source type	# of sources	Description
TUN_11	TUN11_1-17	Horizontal point source	17	West end of house 1
TUN_12	TUN12_1-17	Horizontal point source	17	East end of house 1
TUN_21	TUN21_1-17	Horizontal point source	17	West end of house 2
TUN_22	TUN22_1-17	Horizontal point source	17	East end of house 2
TUN_31	TUN31_1-17	Horizontal point source	17	West end of house 3
TUN_32	TUN32_1-17	Horizontal point source	17	East end of house 3
TUN_41	TUN41_1-17	Horizontal point source	17	West end of house 4
TUN_42	TUN42_1-17	Horizontal point source	17	East end of house 4
CRO_11	CRO11_1-27	Horizontal point source	27	North side of house 5
CRO_12	CRO12_1-27	Horizontal point source	27	South side of house 5
CRO_21	CRO21_1-27	Horizontal point source	27	North side of house 6
CRO_22	CRO22_1-27	Horizontal point source	27	South side of house 6
NAT_11	NAT11_01	Area source	1	Summer time of house 102
NAT_12	NAT12_01	Area source	1	Spring & fall times of house 102
NAT_13	NAT13_01-20	Capped point source	20	Winter time of house 102
NAT_21	NAT21_01	Area source	1	Summer time of house 103
NAT_22	NAT22_01	Area source	1	Spring & fall times of house 103
NAT_23	NAT23_01-20	Capped point source	20	Winter time of house 103
NAT_31	NAT31_01	Area source	1	Summer time of house 93
NAT_32	NAT32_01	Area source	1	Spring & fall times of house 93

Other than the information listed in Table 3-5, AERMOD required XY coordinates, elevation, emission rate, stack height (releasing height for area source), stack temperature, stack velocity and stack diameter (XY dimensions for area source). The elevations were 58 to 59 meters for all sources. The stack heights and stack diameters of point sources are listed in Table 3-6. Here the stack height was the physical stack height, in the process of finding the plume rises using trial-and- error method, the effective stack height (physical stack height plus plume rise) was input in the same cell to model dispersion.

Table 3-6. Stack heights and stack diameters for point sources

Source description	Stack height (m)	Stack diameter (m)
Fans on the first floor of house 1-4	1.35	1.22
Fans on the second floor of house 1-4	3.84	1.22
Fans of house 5-6	1.35	1.22
Vents of house 102 & 103	5.5	1.54[a]

[a]. Rectangular vents with an area of 1.86 m^2. A stack diameter of 1.54 m was used as it provides a same area.

For naturally ventilated houses, the dimensions of the opening of the curtains were the dimension of the area source. However, the AERMOD system did not allow a length/width ratio to be greater than 100. Compromised dimension of the sources was used to provide same area. The releasing heights and XY dimensions for area sources are listed in Table 3-7.

Table 3-7. Releasing heights and XY dimensions for area sources

Source description	Releasing height (m)	X dimension (m)	Y dimension (m)
House 102 & 103 in summer	1.68	3.0	112.48
House 93 in summer	1.37	2.0	83.22
House 102 & 103 in spring & fall	1.13	1.5	112.48
House 93 in spring & fall	0.97	1.0	83.22

The stack velocities for horizontal point sources were computed by equation 3-17:

$$V = Q \cdot \frac{4}{\pi D_s^{\,2}} \qquad (3\text{-}17)$$

where D_s = the stack (fan) diameter

For capped point sources, the stack velocities were assumed to be the same as wind velocities; for area sources, the exit velocities were assumed to be the wind velocities in the direction perpendicular to the side walls.

The stack velocities and temperature were used in AERMOD to compute the plume rise using embedded plume rise models. Since the plume rise model embedded in the AERMOD was developed for industrial stack emission, the plume rise model does not apply for the animal housing emission. To prevent the calculation of embedded plume rise, a plume-rise manipulation process was used to disable automatic calculation of plume rise by the AERMOD. In this process, the exhaust temperature was set to be the same as the ambient by inputting zeros in the cells. The stack velocities were intended to be set as zeros for all cases and the emission rate would also be set as zero when the fan was off. However, the system

did not allow either zero exit velocity or zero emission rate. Thus, a near zero number was used (10^{-9} g s^{-1} for emission rate and 0.001 m s^{-1} for stack velocity).

3.2.4.2 Receptor inputs

In this research, the receptors were defined to be the four ambient PM monitoring stations (ST2-5).The inputs of receptor information are listed in Table 3-8.

Table 3-8. Receptor information

Station ID	Elevation (m)	Height (m)
ST2	68	1.85
ST3	57	1.83
ST4	52	2.46
ST5	49	2.46

3.2.4.3 Meteorological data inputs

The AERMET-formatted files were directly used as the meteorological input files for surface weather and profile weather data. For each run, in the "data period" options, "start/end" was selected to limit the time period within one hour.

3.2.4.4 Building information inputs

The building information is given in Table 3-1.The BREEZ AERMOD only has the option for rectangular, circular and polygon buildings, all buildings were set to be rectangular with their side wall heights instead of ridge heights. Also, by field observation, a row of tree was in between of the sources and ST2, which may have impact on the PM concentrations at ST2 and is not negligible. As there was no exact way of inputting barrier information, the trees were assumed to be a building with a dimension of 245 m (length) x 58 m (width) x 5 m

(height) and an elevation of 60 m. Figure 3-9 shows the 3D view of the layer farm, including sources, receptors and buildings.

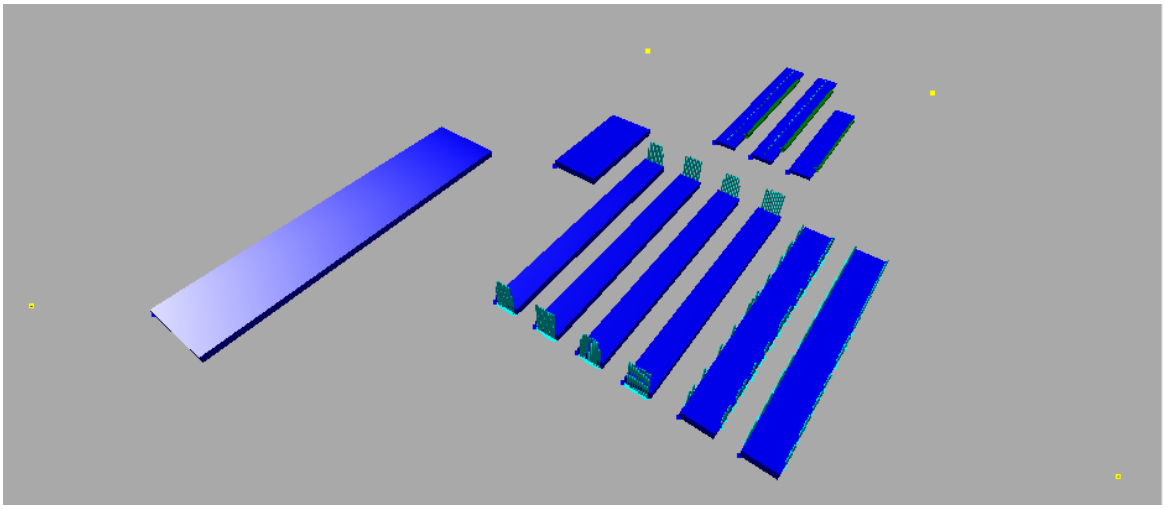

Figure 3-9. 3D layout of the farm simulated in AERMOD

3.2.4.5 Plume rise predictions

After completion of all the input files, hourly AERMOD simulations were conducted to derive plume rises for the selected data periods specified in Table 3-2. These hourly simulation followed the processes in Figure 3-10.

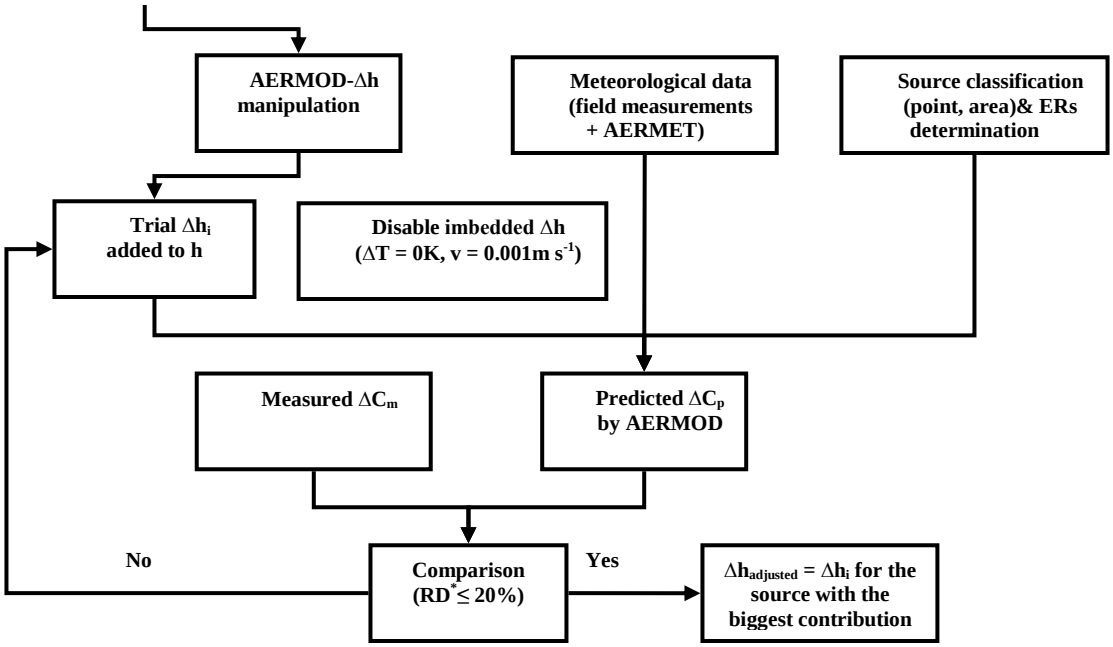

*RD=relative difference between model production and field measurement

Figure 3-10. Flow chart of inverse-AERMOD modeling in predicting plume rises

The detailed trial-and-error steps for determining the valid plume rises are as follows:

1. Go to "Data" in AERMOD and input the hourly emission data for a selected hour into the system;
2. Go to "Project"—"Meteorology"—"Data Period" in AERMOD and narrow the period to the selected hour for reading out the metrological data for the given hour;
3. Click "Model Run" in AERMOD, read the predictions of ambient station PM_{10} concentrations from the output sheet named "PM_{10}, all, 1-hr, 1st high. plt" and record them as C_p;

4. Compare the model predicted data (C_p) with the field measurements (C_m) by the following equation 3-18:

$$RD(\%) = \frac{\left|\Delta C_p - \Delta C_m\right|}{\Delta C_m} \qquad (3\text{-}18)$$

where
ΔC = PM_{10} concentrations of downwind station –average PM_{10} concentrations of the upwind stations.
If the downwind direction was in between two stations, compare both of the stations, respectively. Record the difference and the plume rise. If it was the first run, record plume rise as zero.

5. Set a plume rise value (Δh_{max}) for the horizontal point source with the highest exit velocity (V_{max}) and compute other plume rises by equation 3-19:

$$\Delta h_i = \Delta h_{\max} \cdot \frac{V_i}{V_{\max}} \qquad (3\text{-}19)$$

where
V_i= exit velocity of a given source, m s^{-1};

6. Update the stack heights (hi) with (hi+Δhi) and run the model again;
7. Repeat step 4-6 until RD (equation 3-8 was found to be as small as possible, no bigger than 20%.
8. Record the Δh_{max} for that hour, which was the valid plume rise for this hour.
9. Observe the source that contributes most to the downwind stations. If the horizontal point sources contribute more, record the average plume rise for the operating fans in cross ventilated houses as adjusted plume rise ($\Delta h_{adjusted}$); if the area or capped point sources contributes more, use the plume rise of area or capped point sources.

3.2.4.6 Data analysis and statistical modeling of adjusted plume rises

After all the hours were run and the $\Delta h_{adjusted}$'s were determined, recording the hours when values of $\Delta h_{adjusted}$ were found, other parameters for those hours were listed along with the $\Delta h_{adjusted}$'s. The parameters included source and ambient temperature, wind speeds, wind directions, exit velocities, solar radiations, etc. Seasonal, diurnal and weekly changes of adjusted plume rises were then analyzed using statistical methods. Also, multiple linear regression analysis was done to investigate the impact of various factors on the magnitude of adjusted plume rises.

3.3 RESULTS AND DISCUSSION

The AERMOD modeling results and related factors for different seasons are summarized in tables listed in Appendix III.

3.3.1 ANALYSIS OF THE SELECTED DATA PERIODS FOR AERMOD SIMULATIONS

Although the periods of time were selected to contain less invalid hours caused by either extreme weather like rain and snow, there were still 45 hours of missing AERMET data and invalid PM field data in the 480 selected hours. Consequently, only 435 valid hours were finally selected for the modeling practices.

After the trial and error process for predicting the plume rises, 87 plume rises out of the 435 hours that had the potential to result in a value were found. The reasons that the rest of the hours were not able to give out a plume rise value can be divided into three kinds:

1. The ΔC_m for that hour was negative, meaning that the measured PM concentration of any possible downwind station was lower than the upwind station;
2. The ΔC_p for that hour was always higher than ΔC_m;

3. The ΔC_p for that hour was always lower than ΔC_m.

Table 3-9 summarizes the numbers of hours for each kind of situation stated above in each selected day.

Table 3-9. The grouping of the selected data periods

	Date	Valid	Invalid	High prediction	Low prediction	Negative ΔC_m	Sum
Fall 2008	October 11	9		10		5	24
	October 12	7		6		11	24
	October 13	2	7		12	3	24
	October 14	1	18		3	2	24
	October 15	1	6		10	7	24
Winter 2008	February 4	3		1	13	7	24
	February 5	3	1		13	7	24
	February 6	5		1	2	16	24
	February 7	2	5	2	6	9	24
	February 8	2			18	4	24
Spring 2009	April 12	8		2	3	11	24
	April 13	4		3	2	15	24
	April 14	8		1	1	14	24
	April 15	7	3	2	9	3	24
	April 16	6	6	2	10		24
Summer 2009	June 18	3	4	7	4	6	24
	June 19	6	1	2	3	12	24
	June 20	3	1	9	4	7	24
	June 21	2		5	8	9	24
	June 22	5		3	5	11	24
SUM		87	56	52	126	159	480

As shown in Table 3-9, other than the valid hours of data, there are four reasons in total for a simulation to be unable to get a plume rise. The hours with negative ΔC_m was the biggest group among the five data groups, followed by the hours with low model predictions ($\Delta C_p <$

ΔC_m) to be the second biggest group. As both of the groups had numbers of hours more than twice as much as other groups that failed to give out plume rises, they were considered the main causes of not getting plume rise values.

3.3.2 SEASONAL IMPACT OF PLUME RISES

Based on the prediction, all plume rises in each season were averaged and compared to see if the seasons would affect the magnitude of the plume rises. The average plume rises for each season are listed in Table 3-10 bellow.

Table 3-10. Mean plume rises by seasons

Seasons	Fall 2008	Winter 2008	Spring 2009	Summer 2009
# of plume rises	20	15	33	19
Avg. plume rises (m)*	16.2^a	7.9^b	16.5^a	14.3^c
Standard error (m)	11.2	9.5	12.4	10.0
Avg. ventilation ($m^3\ s^{-1}$)	1421	324	1033	2277
Avg. ΔT (℃)	4.6	18.5	9.0	1.5

*Means with different letters are significant at 0.05.

The average plume rises in Table 3-10 show that for fall 2008 and spring 2009, there were similar average plume rises. All the means were tested by SNK method using SAS with a significant level of 0.05. The SAS code is presented in Appendix IV. The plume rises of spring and fall were higher than the other two seasons. In winter time the average plume rise was much lower than other three seasons. This is probably because in winter times, the ventilation was not as high as other seasons. Also, there were only 15 plume rises to be averaged, among which only three hours were during the daytime, the plume rises may be

affected by diurnal pattern. The average of these 15 plume rises may not well represent the seasonal mean. For summer 2009, as the thermo buoyancy was small (small T in table 3-10), the main plume rises were mainly due to the ventilation. However, despite the fact that summer had the highest ventilation, the plume rise in summer 2009 was not as much as those in fall 2008 and spring 2009. The plume rises for summer times need to be further investigated.

The standard errors in Table 3-10 show that in spring and fall, the variation of plume rises is the highest. This is probably because that in spring and fall, the varying in-house temperature leads to the variation of ventilation, which may cause the plume rise to change. On the other hand, in summer and winter, the ventilation is relatively stable, leading to smaller standard errors for plume rises.

3.3.3 DIURNAL EFFECT ON PLUME RISES

To investigate diurnal variations of the plume rise, the plume rises and the time of a day were sorted together from earlier of the day till the latest ones. The plume rises were then grouped by each two hours from 0:00 to 23:00 and averaged within each group. In results, 12 mean plume rises were obtained and shown in Figure 3-11.

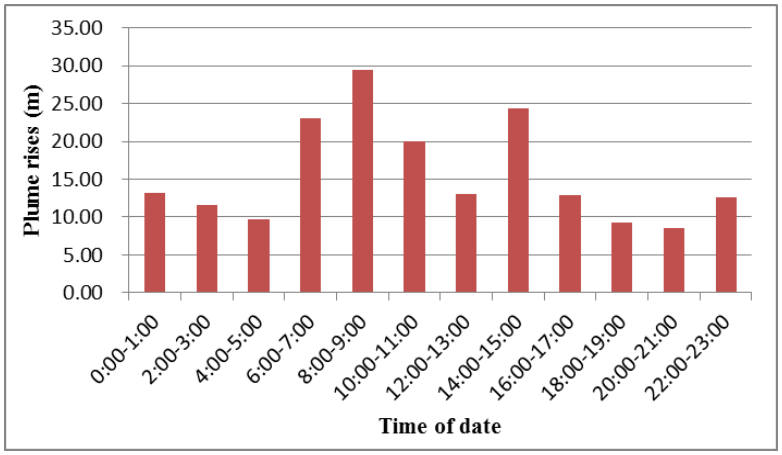

Figure 3-11. Diurnal variations of the plume rises

Based on Figure 3-11, the lowest plume rise appeared at 2:00-3:00 or 18:00-21:00, the highest plume rise appeared at 8:00-9:00. There was no obvious diurnal impact on the plume rises by sorting the whole set of data. This was probably because that as the weather changed for different seasons, the ventilation varied, thus changing the diurnal patterns. By picking dates when there were more valid plume rises predictions, figure 3-12 was generated, showing the time of day variations of the plume rises on those dates when the most valid hourly plum-rises were produced. It seemed that the time when the peak plume rise appears may be a matter of other parameters such as ventilation.

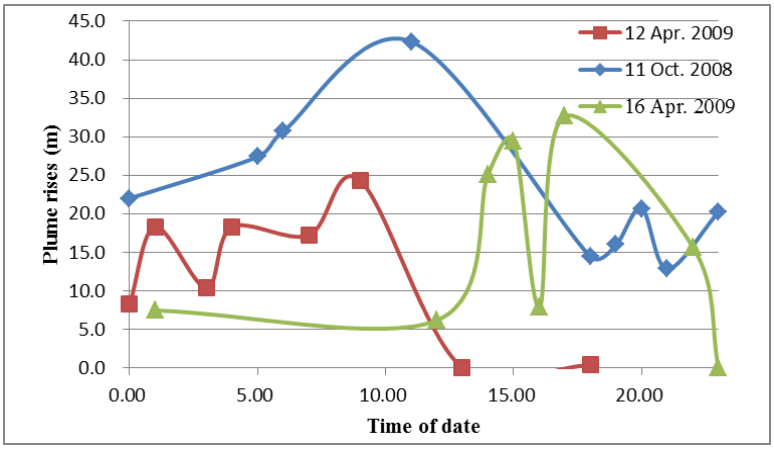

Figure 3-12. Diurnal variation of the plume rises on three selected days

To analyze the relationship between plume rises and ventilation, both ventilation rates and the plume rises for the selected three dates were plotted in Figure 3-13 to 3-15. In general, the plume rises responded to the ventilation rates well. The higher the ventilation rate was, the higher the plume rise occurred. Pearson's correlation coefficients (ρ) tests were also applied for the selected three days. For 11 October 2008, as it is obviously shown in Figure 3-13, the relationship between ventilation and plume rises is quite firm ($\rho = 0.9766$) and the diurnal pattern of the plume rise followed very well with the diurnal pattern of the ventilation rate. For 12 and 16 April 2009, however, the relationship between the two is very poor ($\rho = 0.4001$ and 0.4391, respectively). Although it seems high plume rises occurred at high ventilation rate, the plume rise was abnormally low at 16:00 on 16 April 2009 while the ventilation rate was not. A careful check of all possible related parameters at that hour was conducted for explanation. It was discovered that, except for the ranking of PM concentration levels among the four ambient stations, other factors (parameters) were not significantly

different from the hourly data before and after this specific hour. At 15:00, 17:00 and even 14:00 of that day, the PM concentrations of the ambient stations all followed the order in ST4>ST2>ST5>ST3; while at 16:00 the order was ST2>ST4>ST3>ST5. It is unknown if this change of PM concentration ranking among station would have any impact.

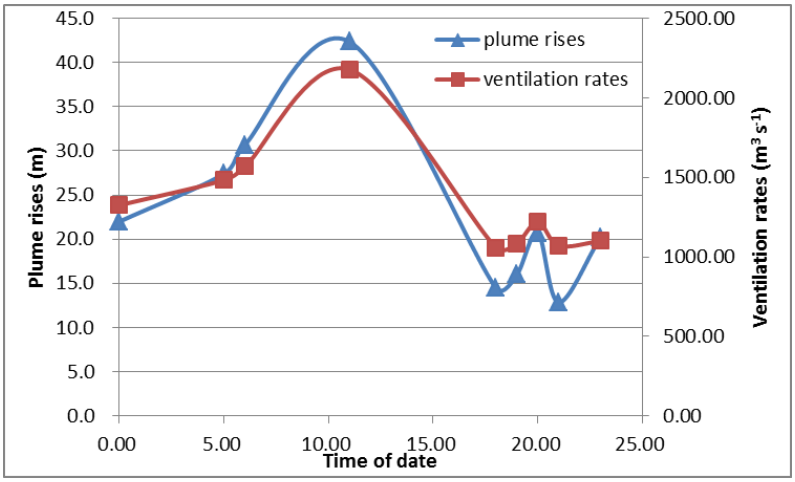

Figure 3-13. Diurnal variation of the plume rise and ventilation rate on 11 October 2008

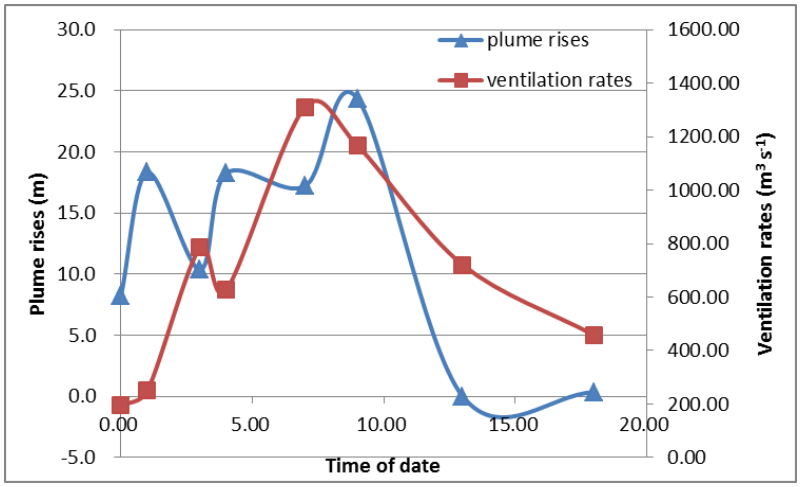

Figure 3-14. Diurnal variation of the plume rise and ventilation rate on 12 April 2009

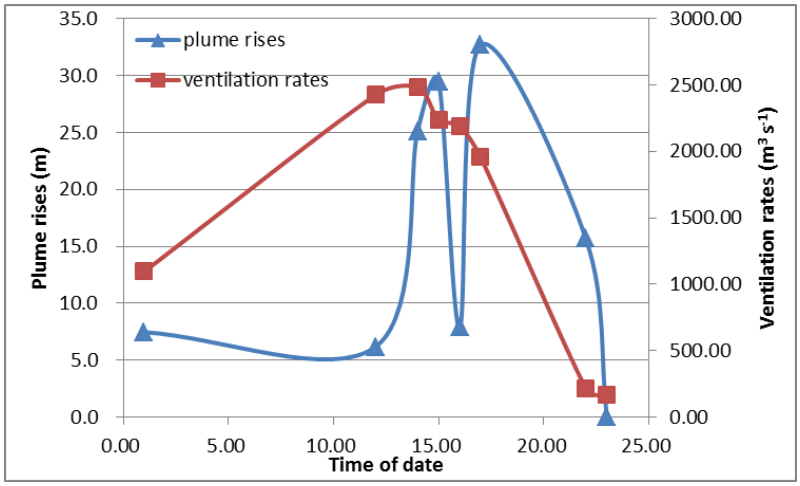

Figure 3-15. Diurnal variation of the plume rise and ventilation rate on 16 April 2009

3.3.4 THE IMPACT OF WEEKDAY AND WEEKEND

As indicated in the previous discussion, the seasonal difference may have impact on the magnitude of plume rises, it is better to compare the weekdays and weekends within one season. The average plume rises for weekdays and weekends are shown in Table 3-11.

Table 3-11. The impact of weekday and weekend on the plume rises

Seasons	Average plume rises during weekdays (m)	Sample size	Standard error (m)	Average plume rises during weekends (m)	Sample size	Standard error (m)
08 fall	2.02	4	2.02	19.76	16	9.53
08 winter	6.23	11	9.79	12.60	4	7.93
09 spring	12.78	23	10.20	24.91	10	13.39
09 summer	14.10	14	10.80	14.90	5	8.30

At a significance level of 0.05, the plume rises during weekdays were compared to those during weekends by paired t-tests for different seasons. As shown in table 3-11, for fall, the plume rises during weekends were significantly higher than those during weekdays (*p*-value = 0.0019); for spring, winter and summer, the difference between the two groups was not significant (*p*-value = 0.1551, 0.4779 and 0.8763, respectively). As fall 2008 and spring 2009 had similar input files of wind speeds, ventilation and other parameters, they should have similar plume rises. The statistical results show not significant difference between the weekend plume rises for the two seasons — 19.76 m and 24.91m; but there was a six times' difference for the weekday plume rises between these two seasons —2.02 m and 12.78 m. Since the sample size of spring 2009 was much higher than that of fall 2008, the results for spring 2009 and weekends of fall 2008 seem to be more reliable than the prediction of plume rises for the weekdays of fall 2008. The fact that winter 2008 and spring 2009 had the plume rise ratios of $\Delta h_{weekends} / \Delta h_{weekdays}$ in 2.02 and 1.95 implies the plume rises for weekends were about twice as much as the plume rises for weekdays.

For those hours providing valid plume rises, the PM concentrations of AERMOD predictions for ambient stations were observed to be smaller as the plume rise become larger. This means that if the ambient stations measured greater PM concentrations than the true contributions of the farm house emissions only, the inverse-AERMOD would produce smaller plume rise. This may explain the observation that the weekday plume rises tend to be smaller than weekend plume rise since there were some traffics around the farm, contributing PM to ambient stations. The PM contribution from traffics were included in PM measurements and yet not included in emission rate for model simulation.

3.3.5 MULTIPLE LINEAR REGRESSION ANALYSIS

Based on field observations, previous analysis and literature review, the magnitude of plume rises may be affected by various parameters. As the simulations in Chapter 2 indicated, the wind direction, wind speed and the temperature differences between ambient and the emission plume flow may affect the magnitude of plume rises, these factors were chosen for multiple linear regression analysis. Also, the cloud cover and solar radiation were closely related to the stability class of the ambient environment, and were thus taken into consideration as influencing factors (predictors). Since momentum and thermal buoyancy had been the most important factors affecting plume rises, the total volume flow of the exhaust fans was then chosen to represent the momentum of the source. After selecting the possible factors affecting plume rises, a multiple linear regression analysis was conducted to identify the significance of each selected factor. The regression results are shown in Table 3-12.

Table 3-12.The multiple linear regression modeling results for the simulated plume rises

	Estimate	Standard error	*p*-value
Intercept	426.6	192.4	0.0296
Wind direction	0.01474	-0.01214	0.2285
Wind speed	3.283	1.297	0.0134
Ambient temperature	297.2	789.2	0.7075
Source temperature	-298.6	789.3	0.7062
Temperature difference	296.5	789.1	0.7081
Ambient RH	0.1239	0.08902	0.1709
Cloud cover	0.2050	0.3617	0.5726
Solar radiation	-0.003875	0.01159	0.7391
Total volume flow	0.003245	0.02608	0.2173

The *p*-values of the multiple linear model shows that the wind speed had the strongest relationship with plume rise (*p*-value = 0.0134 < 0.01). Other than that, wind direction, ambient RH and total volume flow had a little relationship with the plume rises (*p*-value = 0.2285, 0.1709 and 0.2173, respectively). The possible reason for wind speed to be the most important factor would be the fact that due to lacking measurement of emission, the exit velocities for naturally ventilated houses were estimated by the wind speeds, which strengthened the relationship between wind speeds and plume rises. Moreover, as AERMOD did not provide the input of initial direction of horizontal emissions from ventilation fans, they were then was assumed to be along with the wind direction by the system, which also made wind speed and wind direction to be a stronger factor. Furthermore, the ground temperature could also be a possible factor affecting the plume rise of close to ground level

emissions. However, no measurement of the ground temperature was done during the field data collection.

3.3.6 CAUSES OF UNCERTAINTIES

The uncertainties of the modeling results are suspected to be the followings:

1. The BREEZ AERMOD does not allow input of emission direction for horizontal point sources. Instead, the software considered the exit velocities to be in the same direction with the wind. Whereas in reality, all the emission sources except for the capped point sources, were having exit velocities in a direction perpendicular to the end walls of the buildings.
2. The weather data were averaged into one-hour period. However, the wind direction and wind speed varied a lot minute by minute. Consequently the downwind location determined by one hour average wind data may be at unwind location for some minutes in a given one hour period, vice versa, the upwind location of one hour period may have minutes at downwind location. It is more desirable to conduct the dispersion modeling in a smaller time interval in the future work.
3. Due to lack of data for the cross and naturally ventilated houses, the emission parameters such as the PM concentrations and exit velocities were all set by assumptions. This caused additional uncertainty in the whole farm emission estimation, thus, in model predictions of the downwind concentrations.
4. The PM measurement from ST2 may have more uncertainty. As it may be seen, there was a local road close to the ST2 (Fig.3-4). The local traffic as well as the traffics getting onto and out of the farm may contribute to the PM concentrations at this station. Moreover,

between the ST2 and the layer houses, there was a runoff pond and a short tree line (Fig.3-4), which would affect the PM_{10} concentration predictions at ST2 as well. If one of the four ambient stations were inaccurate, since PM concentrations from at least two stations were needed to compute PM concentration differences, it was highly possible that the negative ΔC_m would occur.

5. The on farm traffic (feed/egg delivery trucks, workers cars, etc.) also contributed PM emissions, but was not considered in emission estimation.

3.4 CONCLUSIONS

1. Based on the 87 predictions of plume rises of AERMOD simulations for the selected periods for four season, the mean plume rises were16.2 m (SE = 11.2 m), 7.9 m (SE = 9.5 m), 16.5 m (SE = 12.4 m), 14.3 m (SE = 10.0 m) for fall, winter, spring and summer, respectively. More data are needed to support the prediction, especially for winter times.
2. The relationship between time of a day and the plume rises from animal housing systems did not demonstrate consistent diurnal patterns by observing data from three selected days. However, in general, diurnal patterns of the plume rise followed the patterns of the ventilation rates.
3. The plume rises during weekends were significantly higher than that during weekends.
4. Wind speed had a very strong positive effect (p-value<0.01) on the plume rises, whereas other parameters (i.e. temperature, RH, ventilation, solar radiation and cloud cover) did not show significant impact (p-value > 0.1) on the magnitude of the plume rises.

CHAPTER 4 CONCLUSIONS AND FUTURE WORK

4.1 SUMMARY AND CONCLUSIONS

Gaussian dispersion models have been applied to simulate the fate and transport of air emissions from animal housing systems. The accuracy of the plume rise and plume shape predictions had been a challenge for dispersion models to simulate air emission from AFOs. This study was conducted to:

1. Quantify the plume shapes in a single ventilation fan testing setup that generates similar plume fluid field to those in commercial animal houses by field measurements, visualization and CFD modeling.
2. Apply inverse-AERMOD to derive the plume rises of animal house emissions on a commercial layer farm using field measurements of PM emissions and concentrations on the farm and in the vicinity;
3. Identify the impacts of various factors on plume rises from the animal houses based upon the field observations, the inverse-AERMOD results and the CFD simulations.

The following conclusions were drawn from this research:

The plume field measurements indicated that the plume of a 0.6 m (24 in.) ventilation fan at full speed had a depth about 9 m, a width about 12 m, and a rise (lifting) beyond the highest measurement point, 4.88 m (16 ft). Various factorial simulations were conducted by the CFD model to find that: 1) the differences between plume flow and ambient air temperatures (T) had a positive impact on plume rise and a negative impact on plume depth; 2) background wind directly against the fan flow affected the plume rise, plume width

and plume rise negatively; 3) background wind across the fan flow reduced the plume depth but enlarged the plume width and plume rise.

In application of AERMOD, in total 87 hourly plume rises were found for 20 days' hourly measurements of PM_{10} concentrations and emissions (five days per season for four seasons, from fall 2008 to summer 2009). The mean plume rises for fall 2008, winter 2008, spring 2009 and summer 2009 were 16.2 m (SE = 11.2 m) 7.9 m (SE = 9.5m) 16.5 m (SE = 12.4m), and 14.3 m (SE = 10.0m), respectively. The relationships between plume rises and various factors were tested. While the diurnal patterns of the plume rises were not consistent among different selective days, the daily variation of the plume rise was found to be related to the variations of daily ventilation rates. Plume rise for weekends were significantly higher than those for weekdays in fall. Multiple linear regression showed a significant positive relationship (p-value = 0.0134) between wind speed and the plume rises. Ambient RH and total volume flow were also found to be slightly (p-value = 0.171 and 0.217, respectively) related to the plume rises.

Through this study, both CFD and AERMOD were found to be good tools for AFO plume rise modeling. They can simulate the scenarios quicker than actually doing the experiments, saving time and costs. Meanwhile, the results as well as the inputs were all well-formed for further analysis. However, model is not the real experiment and need to be validated through field measurements. The real cases are often more complicated. Thus, the combination of field work and modeling would be a better choice.

4.2 RECOMMENDATIONS FOR FUTURE WORK

For the study CFD modeling, the following suggestions are recommended for future work:

1. The current field measurement plan only include 5 (sensors) * 4 (heights) *3(rings) = 60 points for each group of data. This is not enough to generate a satisfying 3D contour plot of the fluid field. More points are suggested for field measurements.
2. Other methods of measuring the fluid field, including remote sensing technologies are recommended. Comparisons among the results measured by different methods would also be necessary.
3. Field tests with various factors such as temperature differences and lower RPM scenarios in the future can be used to compare with the predictions of CFD model.
4. More simulations with different background wind speeds and directions are needed.

For the application of AERMOD, future work can be done in the following aspects:

1. Since the input files of other source types, i.e. the cross ventilated and naturally ventilated houses in the AERMOD were either adopted from literature, or assumptions-based,, field measurements of those sources would increase the accuracy of the model predictions.
2. In order to find more valid and accurate plume rises, 1) more days and hours could be selected; 2) meteorological data from other sources may be used for those hours when the original meteorological data was missing; 3) adjustments of the ambient PM concentrations, such as taking the traffic into consideration, should be done.
3. Data from more seasons could be used to find a more reliable seasonal pattern of the plume rises.

4. The measurement of ground temperature should be considered as a factor affecting plume rises.
5. Further statistical analysis other than multiple linear regression could be done for testing the impact of various factors on the magnitude of plume rises. Furthermore, other ways of measuring and modeling plume rise as well as plume shape could also be tried. And the results of different modeling methods can be compared if they were simulated under similar environment.
6. The assessment of AERMOD in application of ground level emission should also be a concern of future work. For instance, AERMOD assumes Gaussian (or bi-Gaussian) dispersion of concentrations across the plume while it may not be the case for ground level emissions.

REFERENCES

ACGIH. 2004. *Industrial ventilation-a manual of recommended practices* (25th Edition). American Conference of Governmental Industrial Hygienists, Oh.ISBN1882417429.

Alič, G., B. Širok and M. Hočevar. 2010. Method for modifying axial fan's guard grill and its impact on operating characteristics. *Forsch Ingenieurwes*. 74:87-98.

Allen, G., C. Sioutas, P. Koutrakis, R. Reiss, F.W. Lurmann, and P.T. Roberts. 1997. Evaluation of the TEOM method for measurement of ambient particulate mass in urban areas. *Journal of the Air and Waste Management*. Association 47:682 –689.

Asman, W. A.H. 1998. Factors influencing local dry deposition of gases with special reference to ammonia. *Atmos. Environ.*32(3):415-421.

Awasthi, S., M. Khare, and P. Gargava. 2006. General plume dispersion model (GPDM) for point source emission. *Environmental Modeling & Assessment*. 11:267-276.

Bennett, M., S. Sutton and D. R. C. Gardiner. 1991. Measurement of wind speed and plume rise with a rapid-scanning LIDAR. *Atmos. Environ.* 26A(9): 1675-1688.

Bennett, M., S. Sutton and D. R. C. Gardiner. 1992. An analysis of LIDAR measurement of buoyant plume rise and dispersion at five power stations. *Atmos. Environ.* 26A(18): 3249-3263.

Blanes-Vidal, V., E. Guijarro, S. Balasch and A. G. Torres.2008. Application of computational fluid dynamics to the prediction of airflow in a mechanically ventilated commercial poultry building. *Biosystems engineering.*100(1):1537-5110.

Bottcher, R.W. 2001. An environmental nuisance: Odor concentrated and transported by dust. *Chem. Senses.* 26(3): 327-331.

Briggs, G. A.. 1969. Mathematical analysis of chimney plume rise and dispersion: Optimum formulas for buoyant plume rise. *Phil. Trans. Roy. Soc. Lond.* 265: 197-203.

Briggs, G.A.. 1971. Plume rise: a recent critical review. *Nuclear safety*. 12 (1), 15-24.

Briggs, G.A.. 1984. Plume rise and buoyance effects. *Atmospheric Science and Power Production.* Randerson, D., U.S. Dept. of Energy, 327-366.

Briggs, G.A., R.E.Britter, S.R.Hanna, J.A.Havens, A.G.Robins and W.H.Snyder. 2001. Dense gas vertical dilution over rough surfaces: results of wind tunnel studies. *Atmos. Environ.* 35: 2265-2284.

Bunton, B., P. O'Shaughnessy, S. Fitzsimmons, J. Gering, S. Hoff, M. Lyngbye, P. S.Thorne, J. Wasson, and M. Werner. 2006. Monitoring and modeling of emissions from concentrated animal feeding operations: Overview of methods. *Environ. Health Perspect.* 115(2): 303-307.

Burkholder, J., B. Libra, P. Weyer, S. Heathcote, D. Kolpin, P. S. Thorne and M. Wichman. 2007. Impacts of waste from concentrated animal feeding operations on water quality. *Environ Health Perspect*.115(2): 308–312.

Cambra-Lopez, M., T. Hermosilla, H. T. L. Lai, A. J.A, Aarnink and N. W. M. Ogink. 2011. Particulate matter emitted from poultry and pig houses: source identification and quantification. *Transactions of the ASABE*.54 (2): 629.

Carney, P. G. and V. A. Doddt. 1989. Comparison between predicted and measured values for the dispersion of malodors from slurry. *J. agric. Engng Res.*44: 67-76.

Charron, A., R.M. Harrison, S. Moorcroft, and J. Bookerb. 2003. Quantitative interpretation of divergence between PM_{10} and $PM_{2.5}$ mass measurement by TEOM and gravimetric (Partisol) instruments. *Atmos. Environ.* 38:415 – 423.

Contini, D. and A. Robins. 2001. Water tank measurements of buoyant plume rise and structure in neutral crossflows. *Atmos. Environ.* 35: 6105-6115.

Cooper, C. D., F. C. Alley.2002. *Air pollution control: a design approach*. Waveland Press, Prospect Heights, Ill.

Curran, T.P., B.A. Sheridan, E.T. Hayes and V.A. Dodd. 2002. Comparison of two dispersion models for odour nuisance prediction from pig units. In: ASAE Annual International Meeting, CIGR XVth World Congress, Chicago, IL, USA, 28th–31st July 2002

Gates, R.S., K.D. Casey, H. and Xin, E.E. Wheeler, and J.D. Simmons. 2004. Fan Assessment Numeration System (FANS) design and calibration specifications. *Transactions of the ASAE.* 47(5): 1709-1715.

Gidhagen, L., Johansson, C., et al., 2004.Simulation of NO_x and ultra-fine particles in a street canyon in Stockholm, Sweden. *Atmos. Environ.* 38 (14): 2029–2044.

Gifford Jr., F.A. 1976. Consequences of effluent releases. *Nuclear Safety* 17 (1), 68–86.

Gong, Y., Y. Zhang, H. Li and W. Wang. 2009. A study on airflow field of super-high speed pectination grinding Wheel Based on PIV. *Advances in Abrasive Technology*. 389-390: 332-337.

Gorgy, T.G.A. 2003. Validation of an air dispersion model for odor impact assessment. M.Sc. thesis, McGill University, Mon-treal, Que.

Green, D., and G.W. Fuller. 2006. The implications of tapered element oscillating microbalance (TEOM) software configuration on particulate matter measurements in the UK and Europe. *Atmos. Environ.* 40:5608–5616.

Hanna, S. R., G. A. Briggs and J. C, Chang. 1997. Lift-off of ground-based buoyant plumes. *Journal of Hazardous Material*. 59: 123-130.

Hanna, S. R., B. A. Egan, J. Purdum, and J . Wagler. 1999. Evaluation of ISC3, AERMOD and ADMS dispersion models with observations from five field sites. HC Report PO_2O, AOI, 1220 L St. NW, Washington, DC 20005–4070.

Harper, L. A., T. K. Flesch and J. D. Wilson. Ammonia emissions from broiler production in the San Joaquin Valley. *Poultry Science.* 89: 1802-1814.

Hayes, E. T., T. P. Curran and V. A. Dodd. 2006. A dispersion modeling approach to determine the odor impact of intensive poultry production units in Ireland. *Bioresource Technology*.97(15): 1773-1779.

Heber, A.J., W. Bogan, J.Q. Ni, T.T. Lim, J.C. Ramirez-Dorronsoro, E.L. cortus, C.A.Diehl, S.M. Hanni, C. Xiao, K.D. Casey, C.A. Gooch, L.D. Jacobson, J.A. Kozel, F.M. Mitloehner, P.M. Ndgwa, W.P. Rpbarge, L. Wang, R. Zhang. 2008. The nation air emission monitoring study: overview of barn sources. Presented at ILES VIII.

Henihan A. M., B. P. Kelleher, M. J. Leahy, E. Cummins and J. J. Leachy. 2003. Monitoring and dispersion modeling of emissions from the fluidized bed combustion of poultry litter. *Environmental monitoring and assessment*. 85(3): 239-255.Hiscox, A. L., D. R. Miller, B. A. Holmén, W. Yang and J. Wang. 2008. Near-field dust exposure from cotton field tilling and harvesting. *Journal of Environmental Quality.* 37: 551-556.

Holmes, N.S.and L. Morawska. 2006. A review of dispersion modeling and its application to the dispersion of particles: An overview of different dispersion models available. *Atmos. Environ*. 40:5902-5928.

Jaques, P.A., J.L. Ambs, W.L. Grant, and C. Sioutas. 2004. Field evaluation of the differential TEOM monitor for continuous $PM_{2.5}$ mass concentrations. *Aerosol Science and Technology* 38:49–59.

Jeppsson, K. H.. 2001. Diurnal variation in ammonia, carbon dioxide and water vapor emission from an uninsulated, deep litter building for growing/finishing pigs. *Biosystems Engineering*. 81(2): 213-223.

Kawamorita, T., H. Uozato and K. Shimizu.2012. Fluid dynamics simulation of aqueous humour in a posterior-chamber phakic intraocular lens with a central perforation. *Graefe's archive for clinical and experimental ophthalmology*.250 (6): 935-939.

Kim, M., J. A. Thurston and L. J. Hagen. 2007. Computational Fluid Dynamics (CFD) modeling to predict bioaerosol transport behavior during center pivot. Paper No. 074063. 2007 ASABE Annual International Meeting. June 17-20, 2007. Minneapolis, Minnesota.

Kun, L., W. Zhe, R. Han and Z. Ren. 2011. The numerical simulation of directional solidification process temperature field for large-scale frustum of a cone ingot. *Manufacturing Process Technology*. 189-193: 1476-1481.

Lee, J.H., P.K. Hopke, T.M. Holsen, and A.V. Polissar. 2005. Evaluation of continuous and filter-based methods for measuring $PM_{2.5}$ mass concentration. *Aerosol Science and Technology* 39:290 –303.

Li, Q-F., L. Wang-Li, Z. Liu and A. J. Heber. 2012a. Field evaluation of particulate matter measurements using tapered element oscillating microbalance in a layer house. *Journal of the Air & Waste Management.* Association, 62:3, 322-335

Li, Q-F., L. Wang-Li, B.W. Bogan, K. Wang, I. Kilic, J-Q.Ni. A.J. Heber. 2012b. National air emissions monitoring study-Southeast layer site: Part II- particulate matter. *Transaction of the ASABE.* In revision

Li, Q.-F., L. Wang-Li, J.T. Walker, S. B. Shah, P. Bloomfield and R.K.M. Jayanty. 2012c. Particulate matter in the vicinity of an egg production facility: concentrations, statistical distributions and upwind and downwind comparison. *Transaction of the ASABE.* Accepted.

Lim, T. T. and B. W. Bogan. 2007. Calculation and reporting of air emissions from barns. SOP. B4.

Linacre, E.andB. Geerts. 1999. Roughness length. The University of Wyoming, WY. Available at: http://www-das.uwyo.edu/~geerts/cwx/notes/chap14/roughness.html. Accessed 9 March 2012.

McGinn, S. M., H. H. Janzen and T. Coats. 2003. Atmospheric ammonia, volatile fatty acids and other odorants near beef feedlots. *J. Environ. Qual.* 32:1172-1182.

McGinn, S. M., T. K. Flesch, D. Chen, B. Crenna, O. T. Denmead, T. Naylor and D. Rowell. 2010. Coarse Particulate Matter Emissions from Cattle Feedlots in Australia. *J. Environ. Qual.* 39:791–798.

Mentor Graphics. 2009. Governing Equations Flow Simulation 2009 Technical Reference. Wilsonville, O.R.: Mentor Graphics.

Meroney, R. N.. 1978. Lift off of buoyant gas initially on the ground. *Journal of Industrial Aerodynamics*.5(1979): 1-11.

Michioka, T., A. Sato, T. Kanzaki and K. Sada. 2007. Wind tunnel experiment for predicting a visible plume region from a wet cooling tower. *Journal of Wind Engineering and Industrial Aerodynamics.* 96: 741-754.

Morton, B. R., G. I. Taylor and J. S. Turner, 1956: Turbulent gravitational convection from maintained and instantaneous sources. *Proc.Roy.Soc.London*, A234, 1-23.

Muramalla, K., Y. Chen and A. Hechanova. 2005. Simulation and optimization of homogeneous decomposition of sulfur trioxide gas on a catalytic surface. *Heat Transfer Division of the American Society of Mechanical Engineers*. 376-1: 201-207.

National Research Council. 2003. Air emissions from animal feeding operations: current knowledge, future needs. *The National Academies Press*, Washington D.C.

Ngwabie, N. M., K. H. Jeppsson, G. Gustafsson and S. Nimmermark. Effects of animal activity and air temperature on methane and ammonia emissions from a naturally ventilated building for dairy cows. *Atmos. Environ.* 45: 6760-6768.

Novel, Christian. 2004. Chimney and smoke. Dreamstime.com. Available at: http://www.dreamstime.com/chimney-and-smoke-imagefree209716. Accessed on 15 August 2012.

Pasquill, F. 1961. The estimation of the dispersion of windborne material. *Meteorology Magazine* 90 (1063), 33–40.

Powers, W. J., C. R. Angel and T. J. Applegate. 2005. Air emissions in poultry production: Current challenges and future directions. *Journal of Applied Poultry Research*. 14(3): 613-621.

Purdue University. 2006a. Quality Assurance Project Plan for the National Air Emisisons Monitoring Study (Barn component). Purdue University, West Lafayette, IN.

Purdue University, 2006b. Measurement of barn inlet and exhaust particulate matter (TSP, PM_{10}, $PM_{2.5}$) concentration using the Thermo Electron (Rupprecht and Patashnick) TEOM Series 1400A PM monitor. Standard operation procedure P1. Purdue Ag Air Quality Lab.

Purdue University. 2007. Site monitoring plan for Southeast layer site. Purdue Ag Air QualityLab

Li, Q., L. Wang-Li, Z. Liu and A. J. Heber. 2012. Field evaluation of particulate matter measurements using tapered element oscillating microbalance in a layer house. *Journal of the Air & Waste Management Association*. 62:(3), 322-335

Quinn, A.D., M. Wilson and A.M. Reynolds, S.B. Couling and R.P. Hoxey. 2001. Modeling the dispersion of aerial pollutants from agricultural buildings – an evaluation of computational fluid dynamics (CFD). *Computers and Electronics in Agriculture*. 30:219-235.

Redwine, J. S., R. E. Lacey, S. Mukhtar and J. B., Carey. 2002. Concentration and emissions of ammonia and particulate matter in tunnel-ventilated broiler houses under summer conditions in Texas. T*ransactions of the ASAE*.45 (4):1101-1109.

Robins, A., I. Castro, P. Hayden, N. Steggel, D. Contini and D. Heist. 2000. A wind tunnel study of dense gas dispersion in a neutral lboundary layer over a rough surface. *Atmos. Environ.* 35: 2243-2252.

Roumeiliotis, T. S. and B. J. Van Heyst. 2008. Summary of ammonia and particulate matter emission factors for poultry operations. *Journal of Applied Poultry Research*. 17: 305-314.

Roumeiliotis, T. S., B. J. Dixon and B. J. Van Heyst. 2010. Characterization of gaseo us pollutant and particulate matter emission rates from a commercial broiler operation part I: Observed trends in emissions. *Atmos. Environ.* 44: 3770-3777.

Sarr, J. H., K. Go ťa and C. Desmarais. 2010. Analysis of Air Pollution from Swine Production by Using Air Dispersion Model and GIS in Quebec. *J. Environ. Qual.* 39: 1975 – 1983.

Seedorf, J., J. Schulz and J. Hartung. Outdoor measurements of airborne emission of staphylococci from a broiler barn and its predictability by dispersion models. *Environmental Exposure and Health*. 85: 33-42.

Schauberger, G., Pringer, M., and Petz, E. 2000. Diurnal and annual variation of the sensation distance of odor emitted by live-stock building calculated by the Austrian odor dispersion model (AODM). *Atmos. Environ.*34: 4839–4851.

Singal, S. P., B. S. Gera and D. R. Pahwa. 1994. Application of sodar to air pollution meteorology. *Journal of Remote Sensing*. 15(2): 427-441.

Tecplot, Inc. 2011.Tecplot 360 User's Manual. Bellevue, W.A.: Tecplot, Inc.

Turner, D.B.. 1970. *Workbook of atmospheric dispersion estimates: an introduction to dispersion modeling*. Available at

http://gate1.baaqmd.gov/pdf/1691_Workbook_Atmospheric_Dispersion_Estimates_1971.pdf. Accessed on 15 November, 2012.

USDA/NASS. 2005. Livestock and poultry-production and value 2004 summary. U.S. Department of Agriculture (USDA), National Agricultural Statistics Service (NASS).

USDA. 2011. Agricultural income and finance outlook. U.S. Department of Agriculture (USDA), Economic Research Service (ERS). Available at: http://usda01.library.cornell.edu/usda/ers/AIS//2010s/2011/AIS-12-14-2011.pdf. Accessed on 29 May 2012.

U.S. EPA, 1990. Ambient air monitoring reference and equivalent methods designation, U.S. Federal Register, Washington.

U.S. EPA.1995.Emissions factors & AP 42, compilation of air pollutant emission factors. U.S. EPA. Available at: http://www.epa.gov/ttn/chief/ap42/index.html. Accessed 6 June 2011.

U.S. EPA. 2004a. Air emission characterization and management. Supporting documentation for the EPA regional science workshop on animal feeding operations (AFOs).*Science and technical support needs* Dec. 2004: 6-9. Print.

U.S. EPA. 2004b. AERMOD: Description of model formulation. Available at http://www.epa.gov/ttn/scram/7thconf/aermod/aermod_mfd.pdf. Accessed on 13 November 2012.

U.S. EPA, 2005. Air quality compliance agreement for animal feeding operations. Available at http://www.epa.gov/compliance/resources/agreements/caa/cafo-agr-0501.html. Accessed on 14 July 2011.

U.S. EPA. 2008. Large Animal Feeding Operations: Reducing Their Impact on Air Quality." *Enforcement Alert.* Aug. 2008: 1-4. Print.

U.S. EPA, 2010. National Ambient Air Quality Standards (NAAQS). U.S. Environmental Protection Agency (U.S. EPA). Available at: http://www.epa.gov/air/criteria.html. Accessed 9 March 2012.

U.S. EPA. 2012a. Clean Air Act (CAA). U.S. Environmental Protection Agency (U.S. EPA). Available at: http://www.epa.gov/air/caa/. Accessed 29 May 2012.

U.S. EPA. 2012b. Development of Emissions-Estimating Methodologies for Broiler Operations (Draft).U.S. Environmental Protection Agency. Available at: http://www.epa.gov/airquality/agmonitoring/pdfs/afobroilereemreport2012draftnoapp.pdf. Accessed 29 May 2012.

U.S. GAO. 2008. Concentrated animal feeding operations: EPA needs more information and a clearly defined strategy to protect air and water quality from pollutants of concern. Washington, D.C.: Government Accountability Office. Available at: http://www.gao.gov/new.items/d08944.pdf. Accessed 11 November 2010.

Wang-Li, L., Q. Li, K. Wang, B.W. Bogan, J-Q. Ni, E.L. Cortus, and A.J. Heber. 2012. National air emissions monitoring study-Southeast layer site: Part I-site specifics and monitoring methodology. *Transaction of the ASABE.* In 2nd review.

Wang, K., I. Kilic, Q. Li, L. Wang-Li, W. L. Bogan, and A. J. Heber. 2010. National air emissions monitoring study: emissions data from two tunnel-ventilated layer houses in North Carolina-Site NC2B. Final Report. Purdue University. West Lafayette, IN.

Wang, T., Q. Zheng, R. Yu and Z. Li.2009.Modeling of copper wire bonding ball transient temperature behavior.2009 International Conference on Electronic Packaging Technology and High Density Packaging (1-4244-4658-9, 978-1-4244-4658-2).345-348.

Wang, X., R. Chen and Y. Zhou. 2011. The Flow Field Analysis and Optimization of Diagonal Flow Fan Based on CFD. *Advanced Materials Research*. 201-203, 2657-2660.

Weil, J. C., L. A. Corio and R. P. Brower. 1997. A PDF dispersion model for buoyant plumes in the convective boundary layer. *J.Appl.Meteor.* 36: 982-1003.

Weil, J. C., 1985: Updating applied diffusion models. *J.Climate Appl.Meteor.,* 24(11), 1111-1130.

Wendt, J. F. and Anderson, J. D. 2009. Basic philosophy of CFD. In Computational fluid dynamics: An introduction (pp. 5-8). Verlag Berlin Heidelberg: Spinger.

Yadigaroglu, G., and H. A. Munera. 1987. Transport of Pollutants - Summary Review of Physical Dispersion Models. *Nucl. Technol.* 77:125-149.

Ying, M., L. Wang-Li and Q. Li. 2011.Backward Gaussian dispersion modeling for estimating Plume Rise of Air Emissions from Animal Housing Systems. Paper No. 1110693. *2011 ASABE Annual International Meeting. August 7-10, 2011*. Louisville, Kentucky.

Zhao, L., Y. Zhang, X. Wang, G. L. Riskowski and L. L. Christianson. 2011. Development of particle image velocimetry techniques for measurement of room airflow patterns in ventilated airspaces. Presented at 1999 ASABE annual conference. Paper No. 994156. Ontario, Canada.

APPENDICES

APPENDIX A —TECPLOT RESULTS

TECPLOT RESULTS FOR FIELD DATA SET ONE

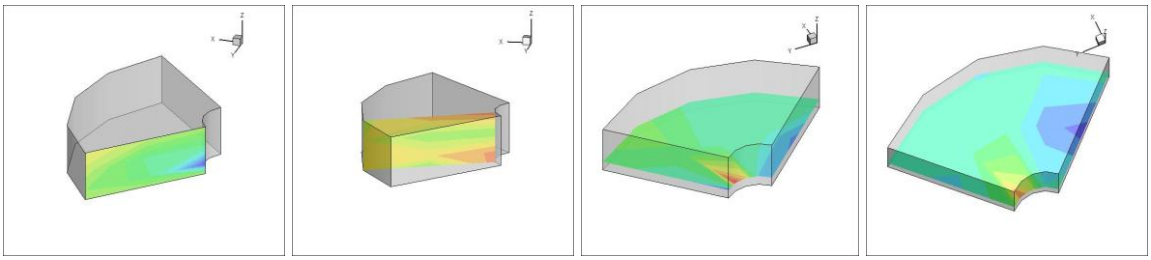

Figure a-1 Contour plots of the vertical velocity "w" for testing group 1-01 to 1-04

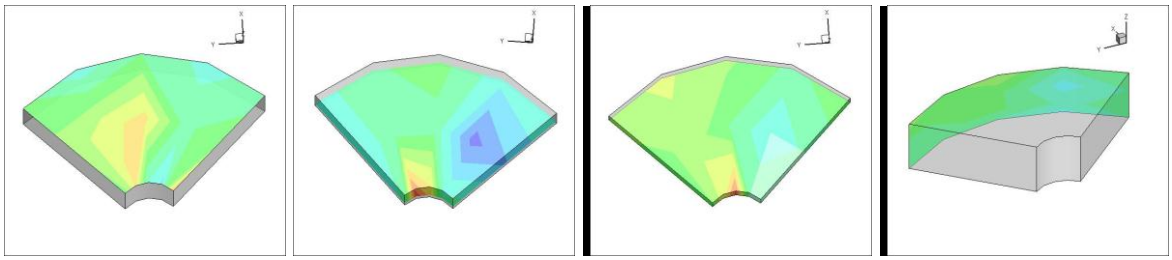

Figure a-2 Contour plots of the vertical velocity "w" for testing group 1-05 to 1-08

TECPLOT RESULTS FOR FIELD DATA SET TWO

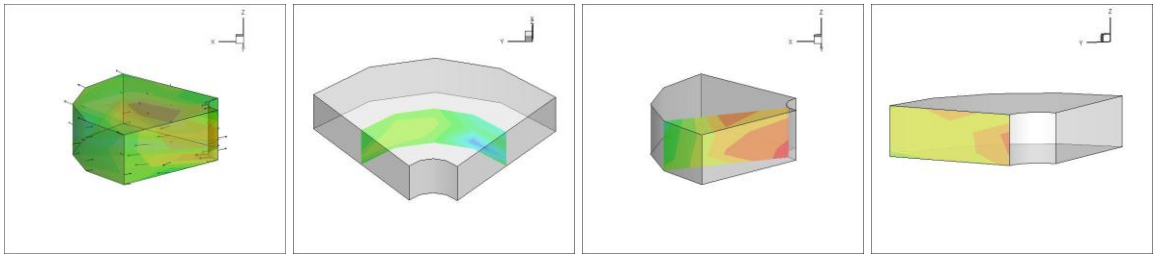

Figure a-3 Contour plots of the vertical velocity "w" for testing group 2-01 to 2-04

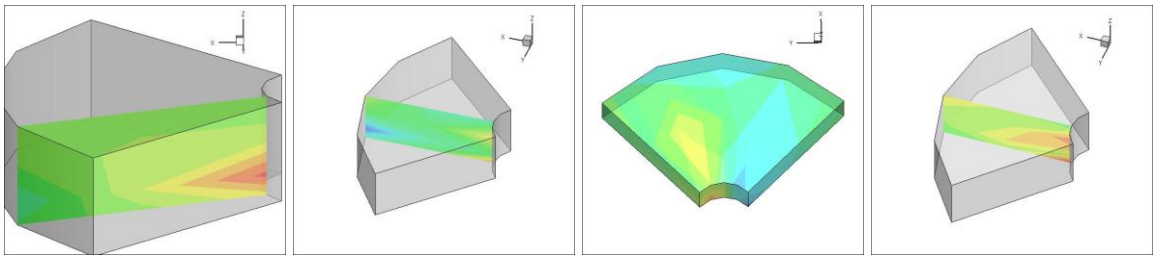

Figure a-4 Contour plots of the vertical velocity "w" for testing group 2-05 to 2-08

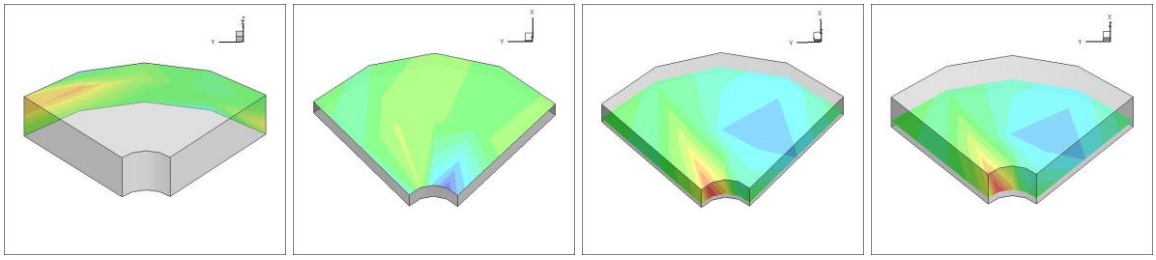

Figure a-5 Contour plots of the vertical velocity "w" for testing group 2-09 to 2-12

TECPLOT RESULTS FOR FIELD DATA SET THREE

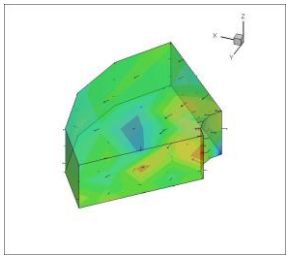

Figure a-6 Contour plots of the vertical velocity "w" for testing group 3

APPENDIX B—FLOEFD RESULTS

RESULTS OF FLOEFD SIMULATING IMPACTS OF VARIOUS TEMPERATURE DIFFERENCES

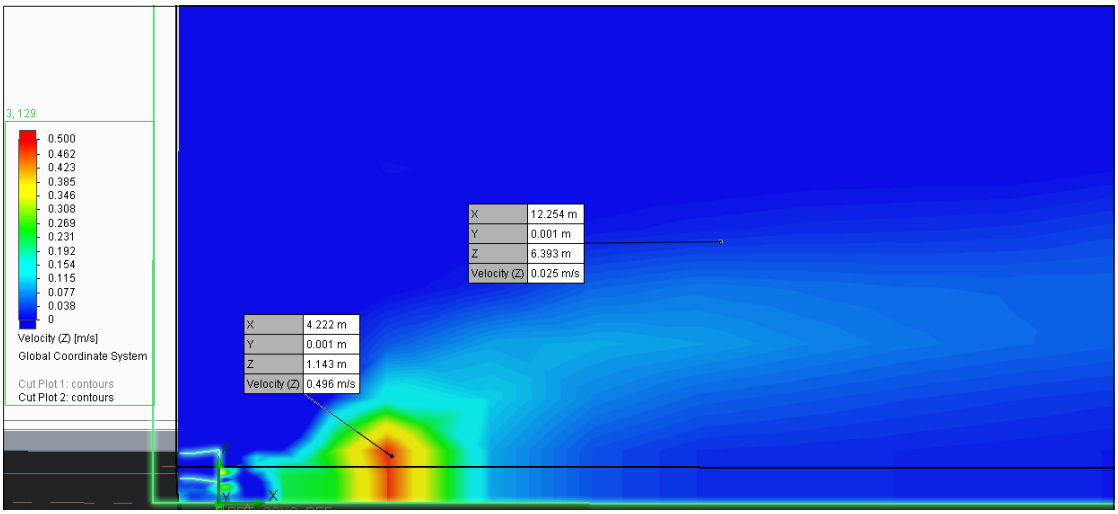

Figure b-1 Side view of the "w" velocity when ΔT = 0℃

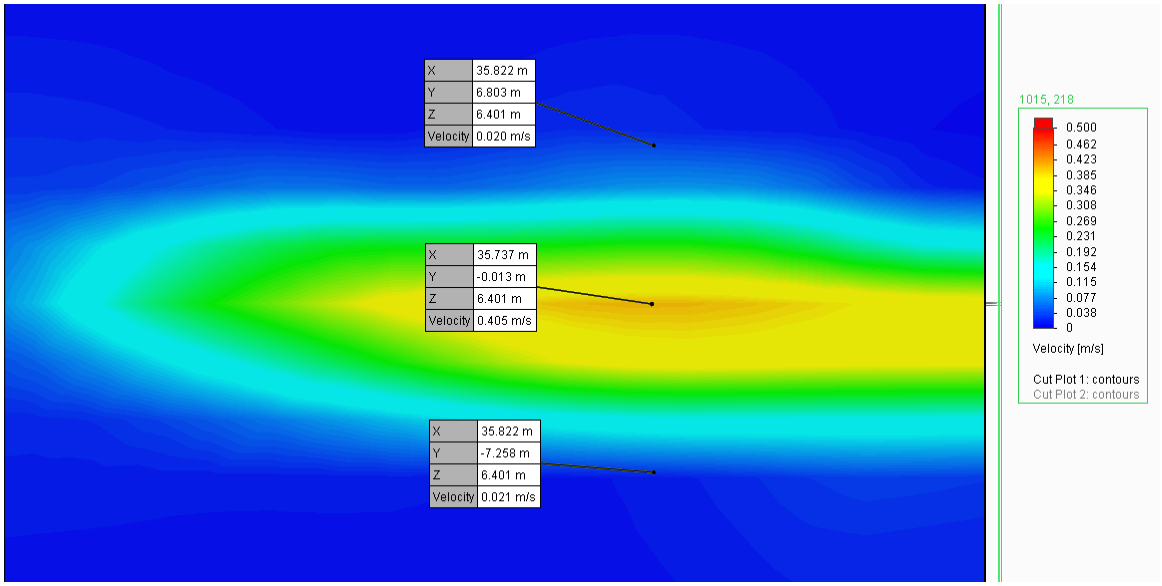

Figure b-2 Top view of the flow speeds when ΔT = 0℃ at a horizontal plane 6.40m above the ground

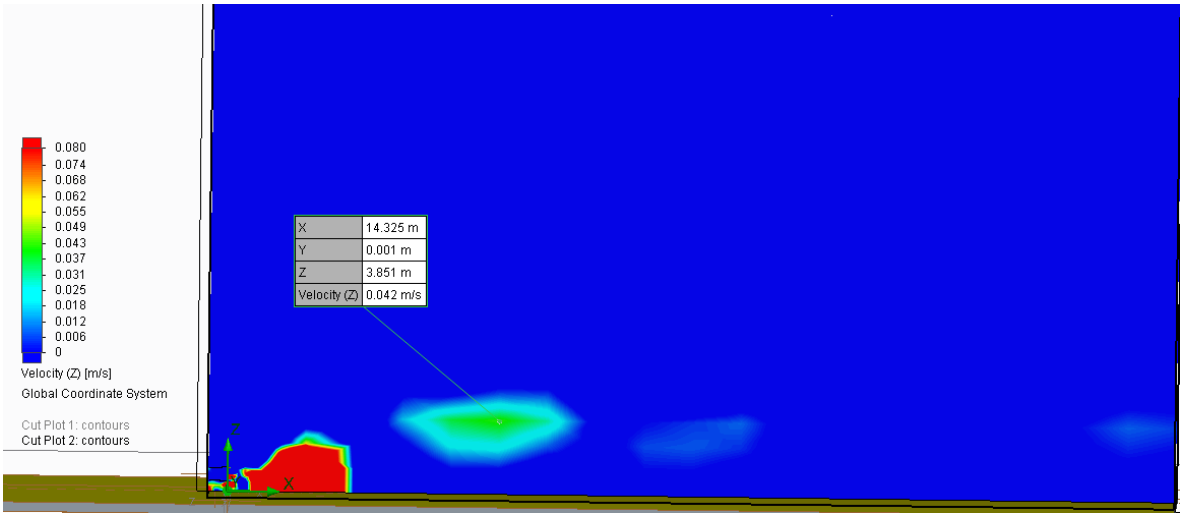

Figure b-3 Side view of the "w" velocity when ΔT = -10℃

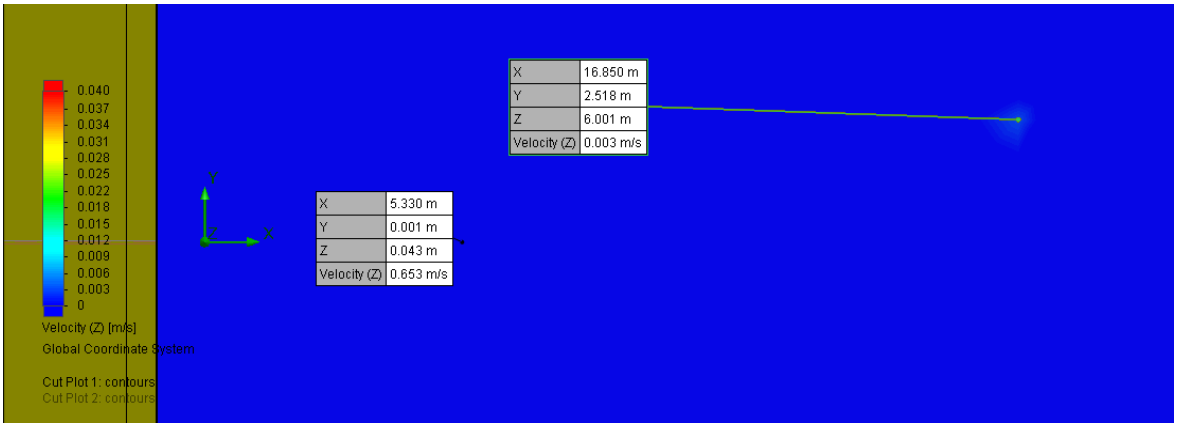

Figure b-4 Top view of the "w" velocity when ΔT = -10℃

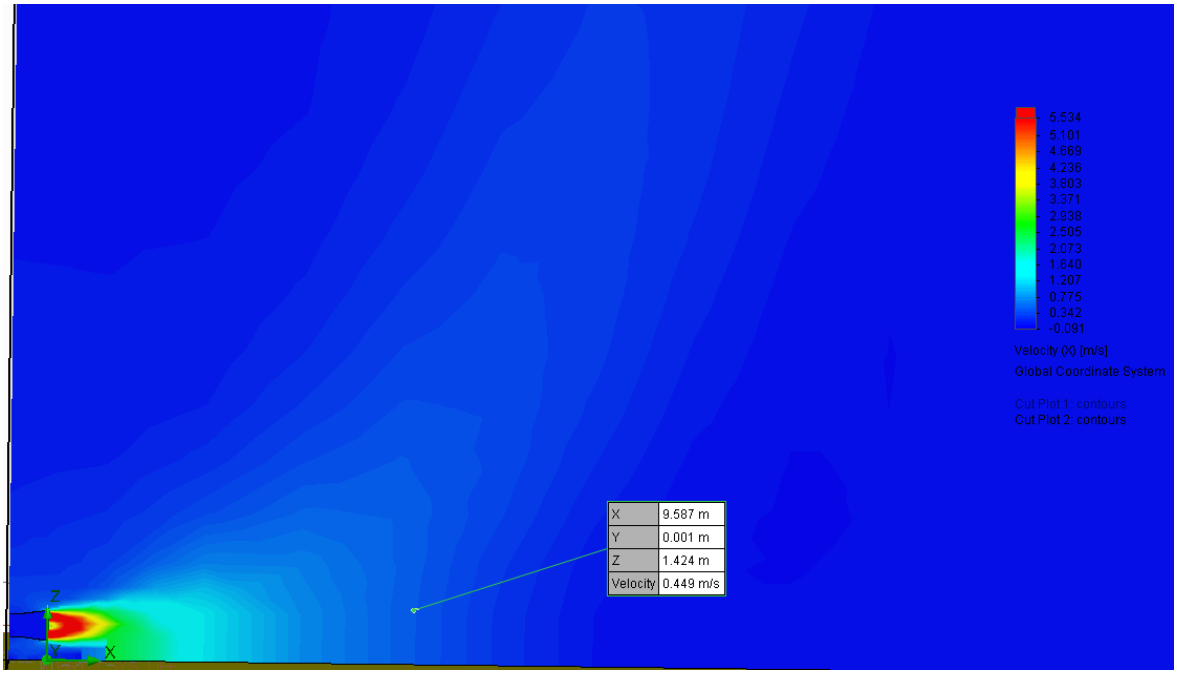

Figure b-5 Side view of the "u" velocity when ΔT = 10℃

FLOEFD RESULTS SIMULATING VARIOUS BACKGROUND WINDS IN X DIRECTION

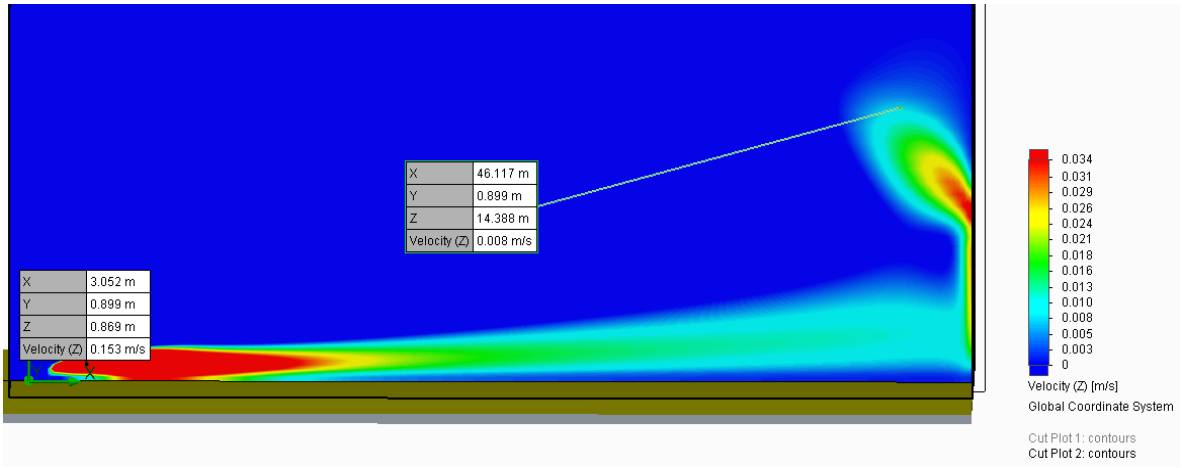

Figure b-6 Side view of the "w" velocity when V_x = -0.05 m s^{-1}

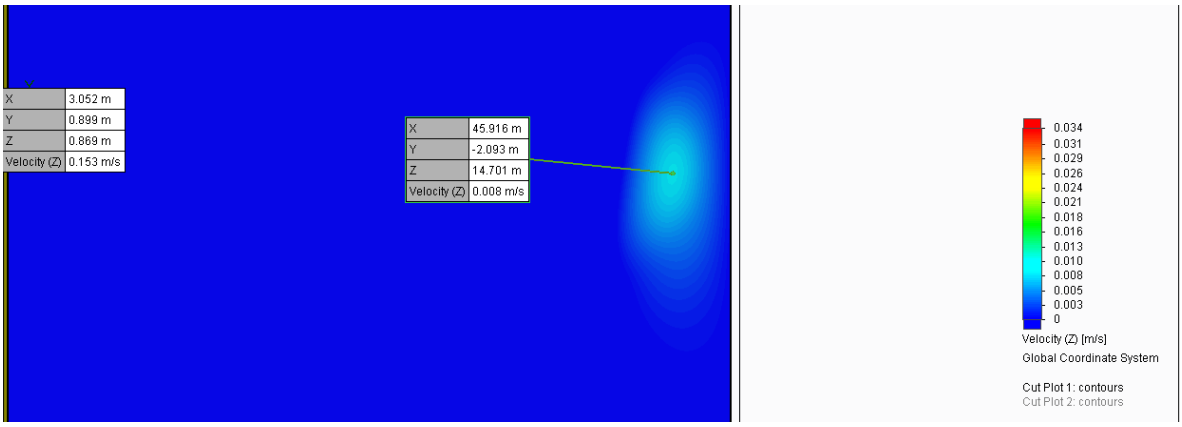

Figure b-7 Top view of the "w" velocity when V_x = -0.05 m s^{-1}

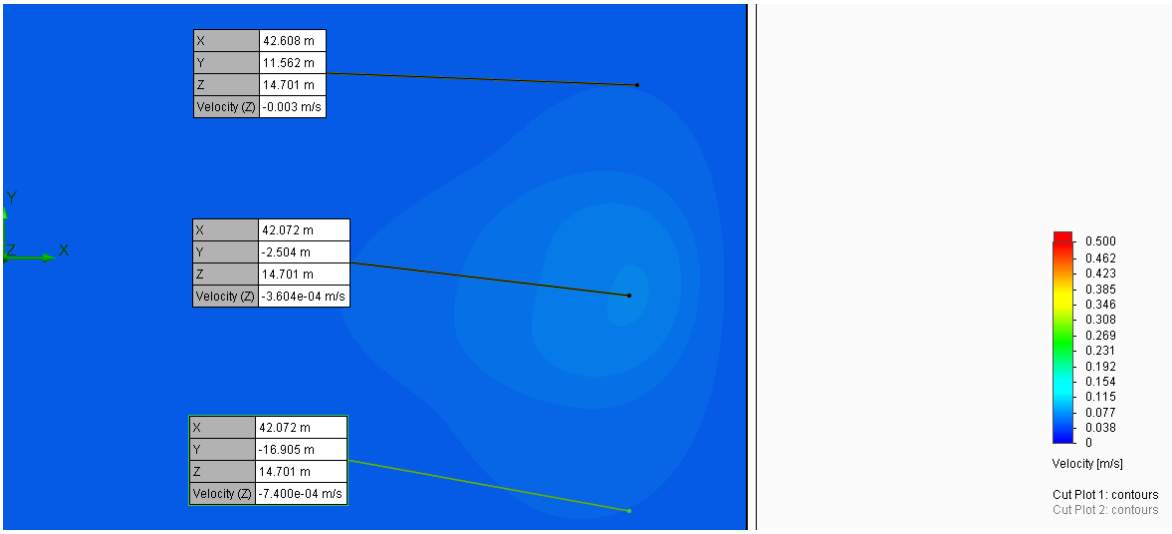

Figure b-8 Top view of the flow speeds when V_x = -0.05 m s^{-1} at a horizontal plane 14.70 m above the ground

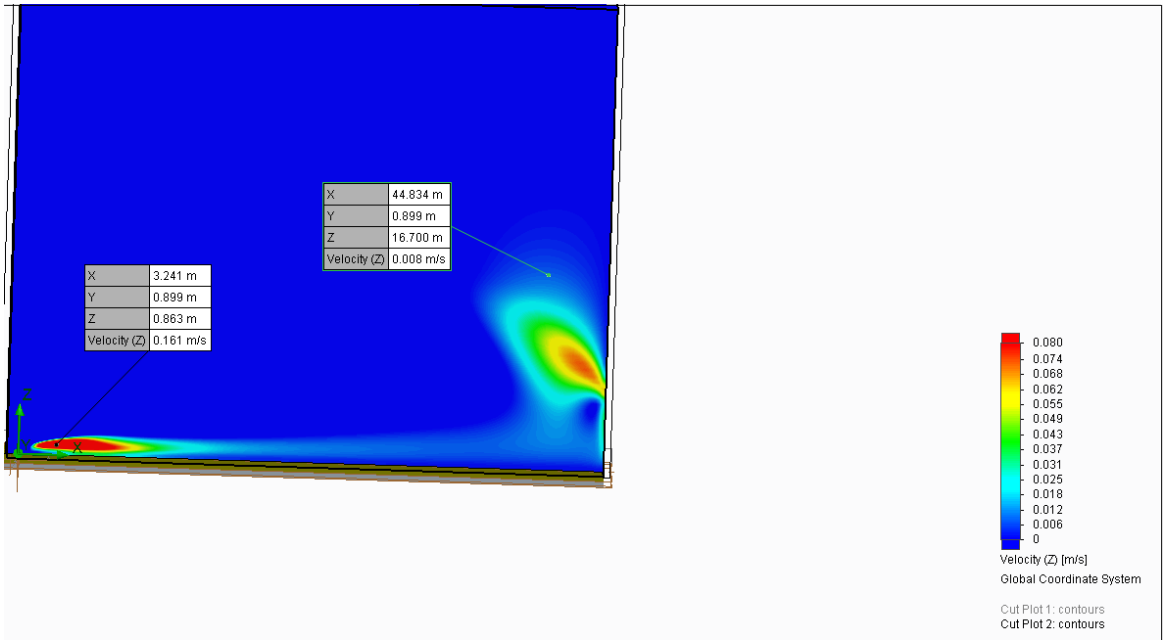

Figure b-9 Side view of the "w" velocity when V_x = -0.10 m s^{-1}

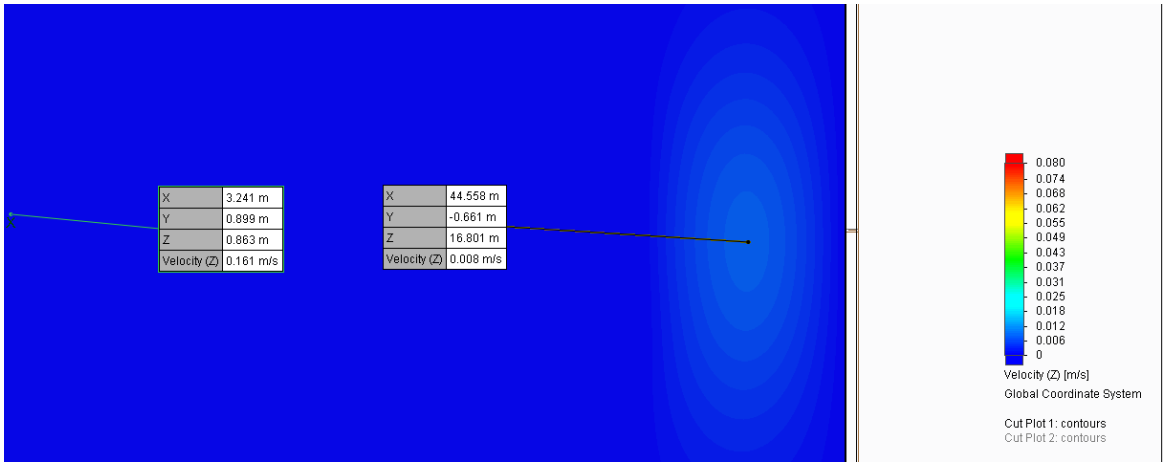

Figure b-10 Top view of the "w" velocity when V_x = -0.10 m s^{-1}

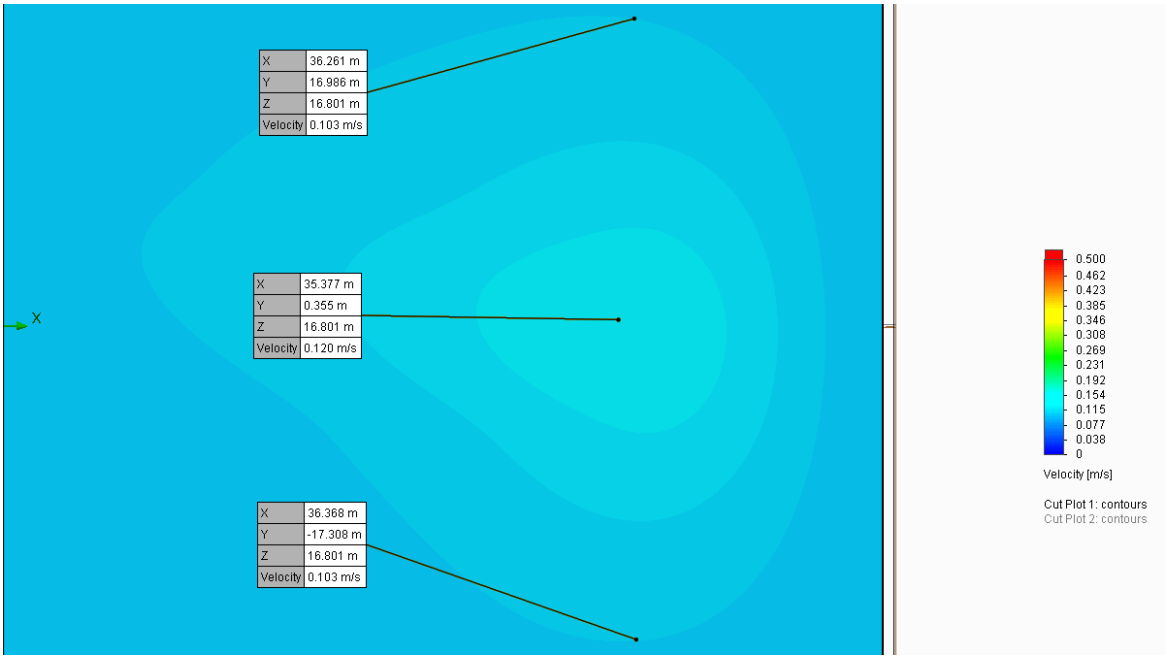

Figure b-11 Top view of the flow speeds when V_x = -0.10 m s^{-1} at a horizontal plane 16.80 m above the ground

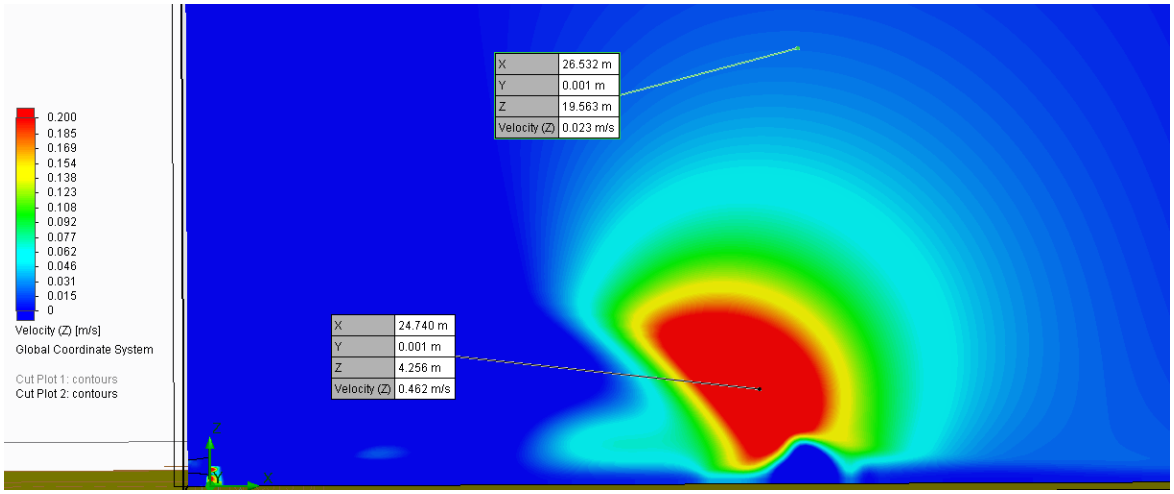

Figure b-12 Side view of the "w" velocity when V_x = -1.00 m s^{-1}

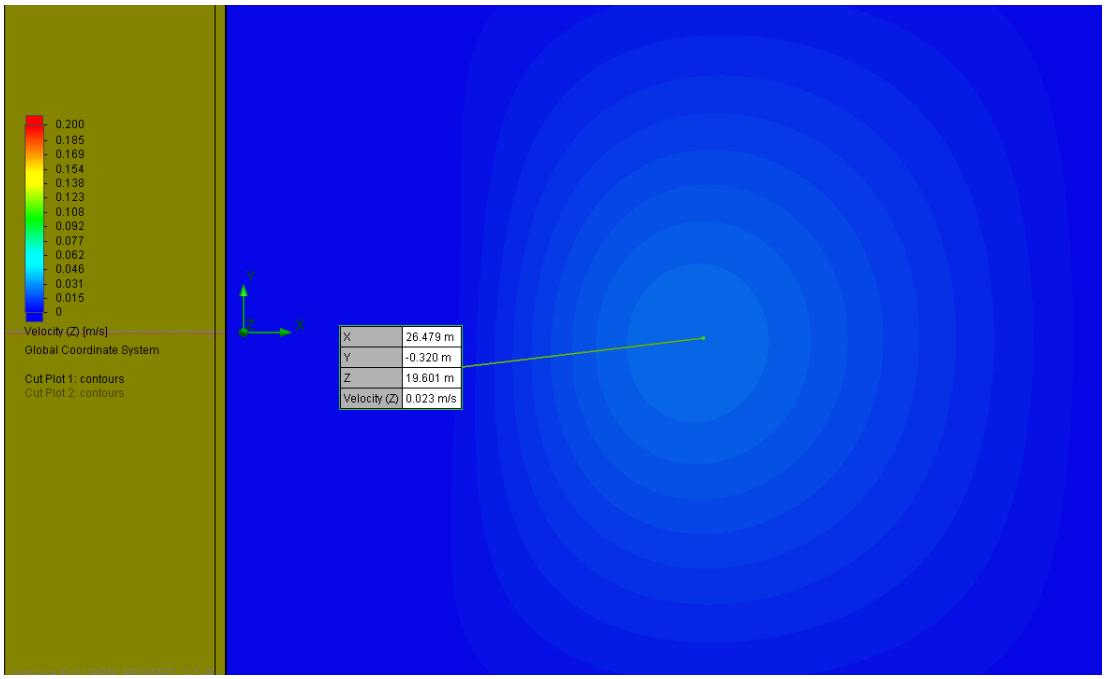

Figure b-13 Top view of the "w" velocity when V_x = -1.00 m s^{-1}

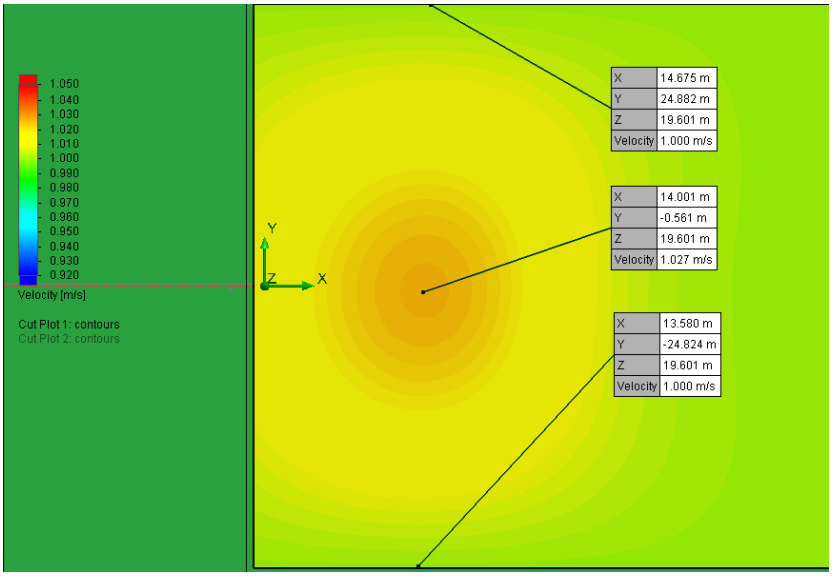

Figure b-14 Top view of the flow speeds when V_x = -1.00 m s^{-1} at a horizontal plane 19.60 m above the ground

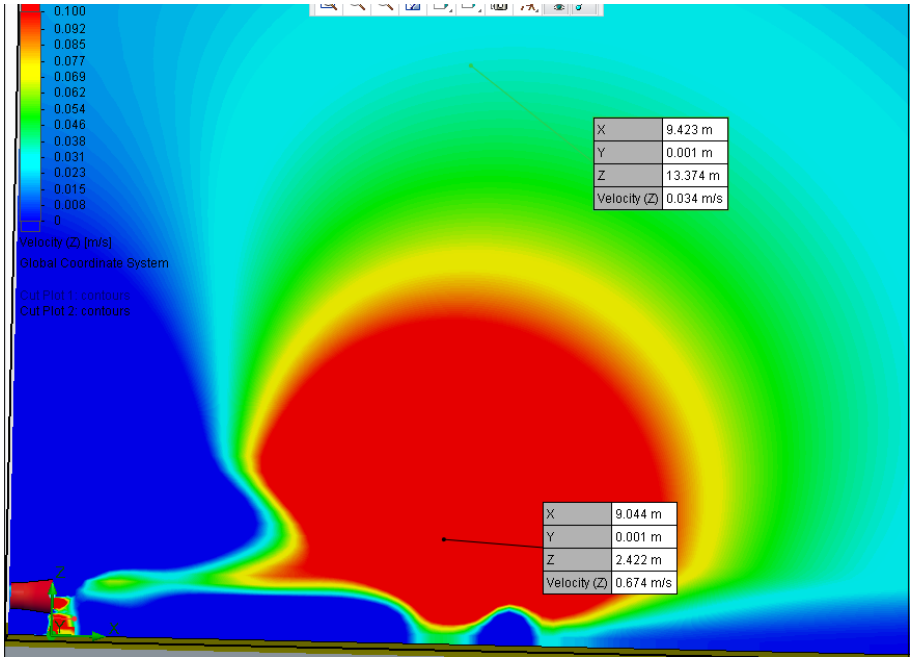

Figure b-15 Side view of the "w" velocity when V_x = -2.50 m s^{-1}

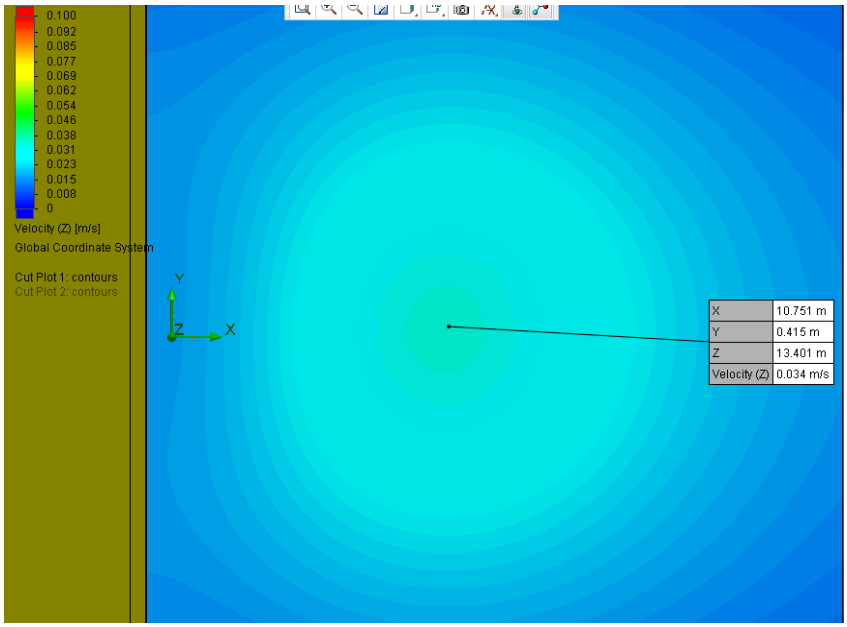

Figure b-16 Top view of the "w" velocity when V_x = -2.50 m s^{-1}

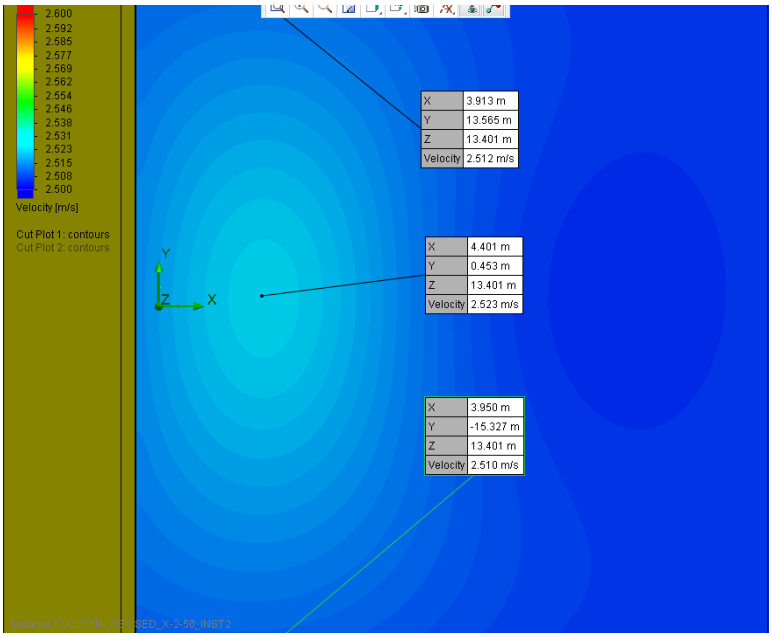

Figure b-17 Top view of the flow speeds when V_x = -2.50 m s^{-1} at a horizontal plane 13.40 m above the ground

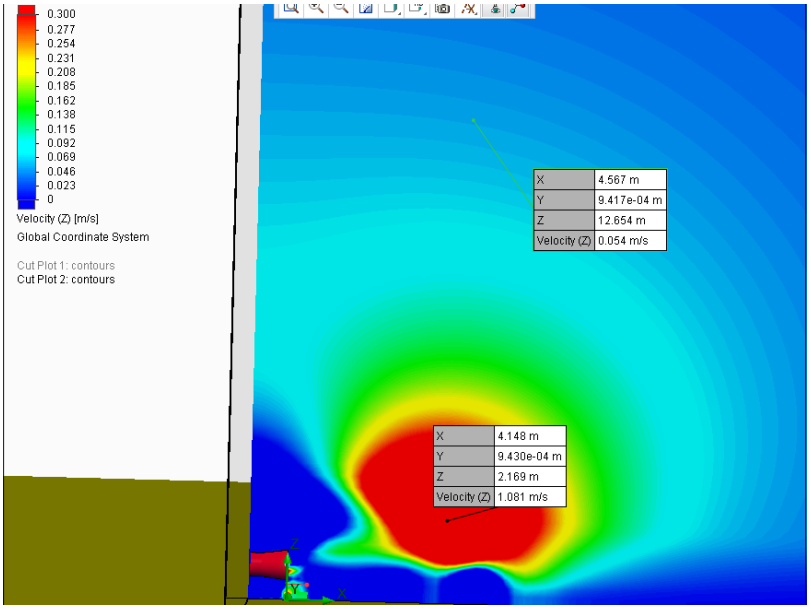

Figure b-18 Side view of the "w" velocity when V_x = -4.00 m s^{-1}

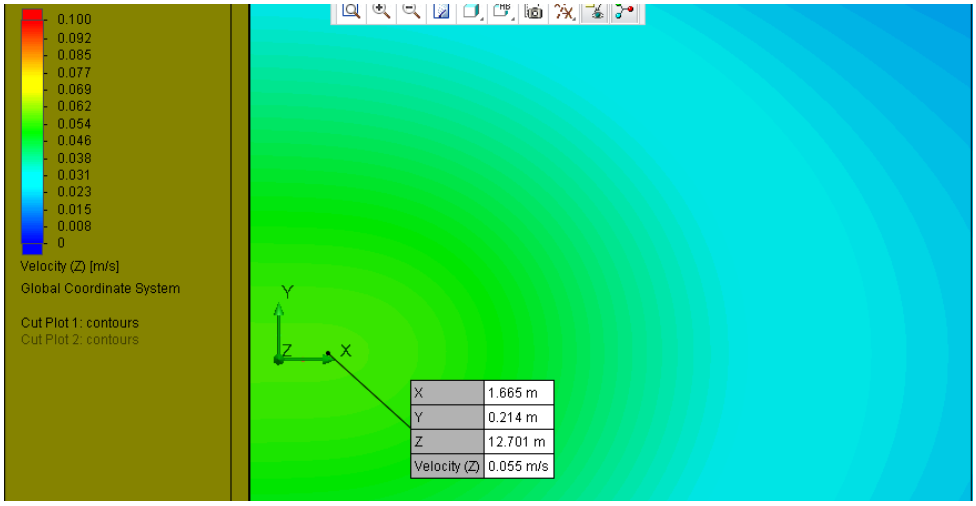

Figure b-19 Top view of the "w" velocity when V_x = -4.00 m s^{-1}

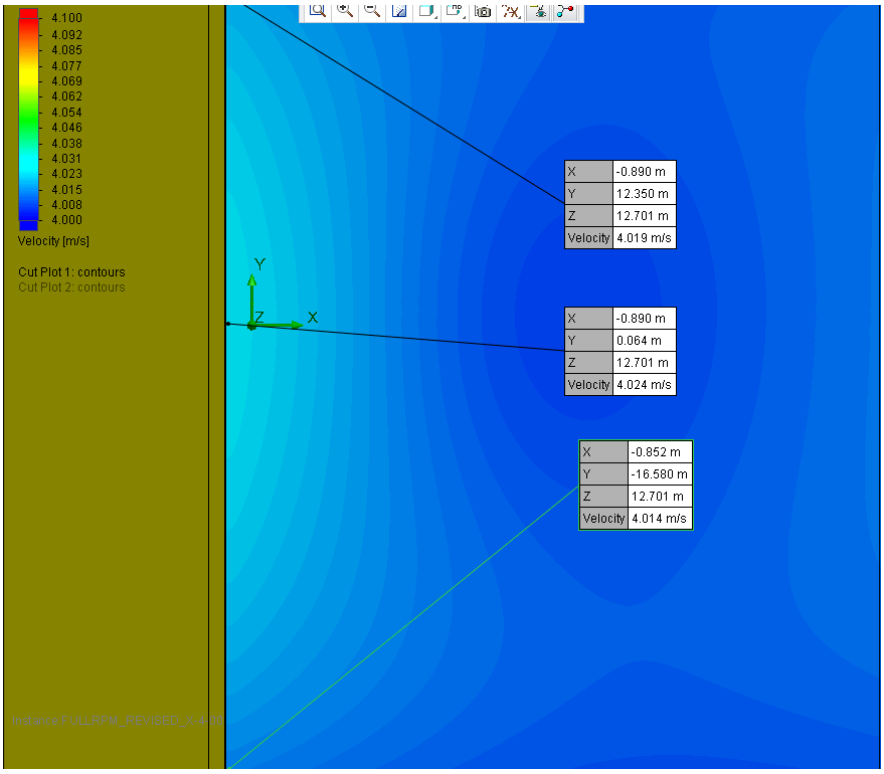

Figure b-20 Top view of the flow speeds when V_x = -4.00 m s^{-1} at a horizontal plane 12.7 m above the ground

FLOEFD RESULTS SIMULATING IMPACTS OF VARIOUS BACKGROUND WINDS IN Y DIRECTION

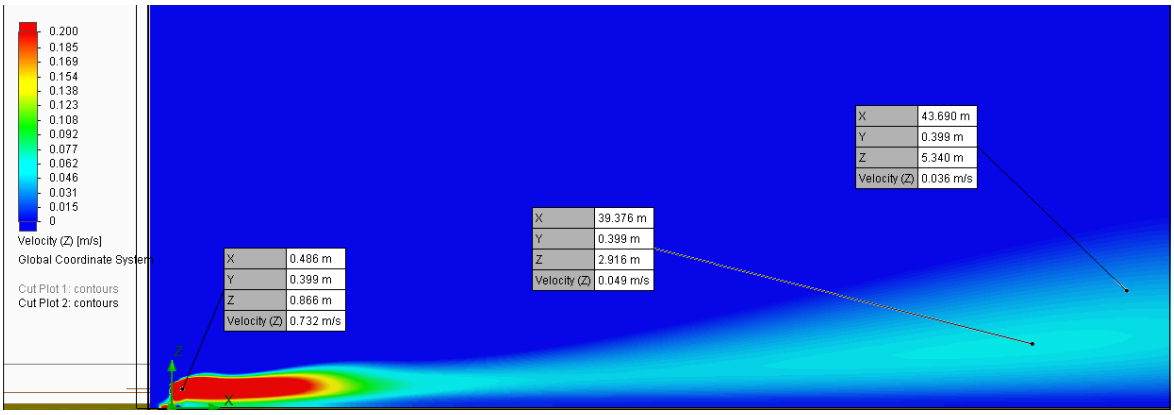

Figure b-21 Side view of the "w" velocity when V_y = -0.05 m s^{-1}

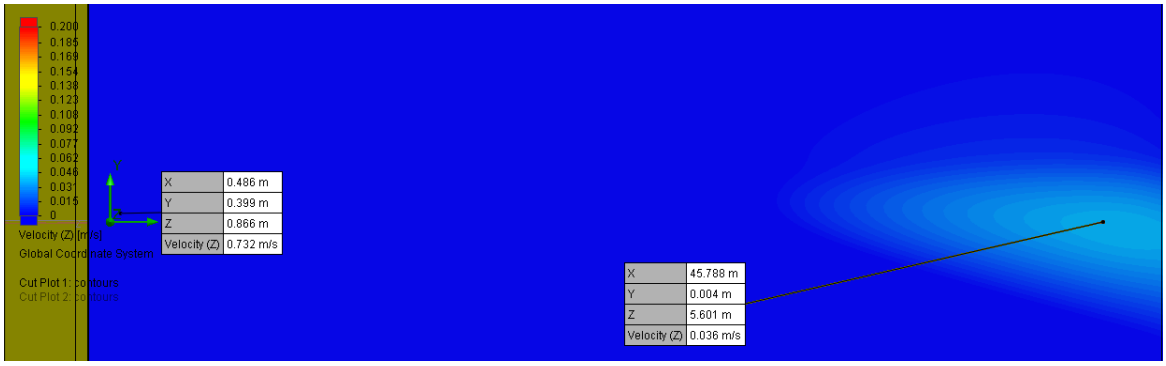

Figure b-22 Top view of the "w" velocity when V_y = -0.05 m s^{-1}

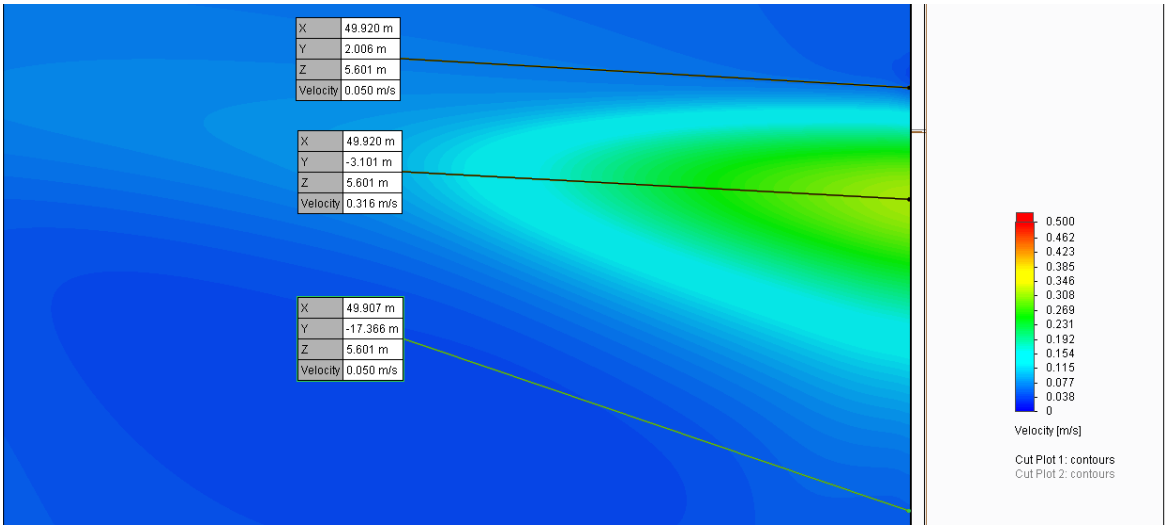

Figure b-23 Top view of the flow speeds when V_y = -0.05 m s^{-1} at a horizontal plane 5.60 m above the ground

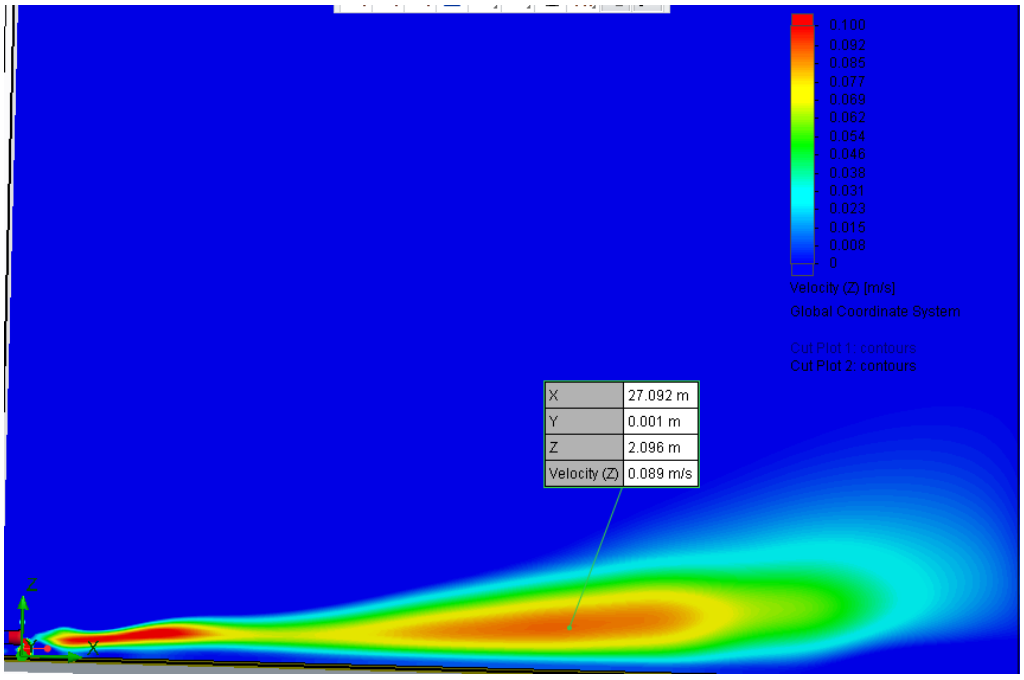

Figure b-24 Side view of the "w" velocity when V_y = -0.10 m s^{-1}

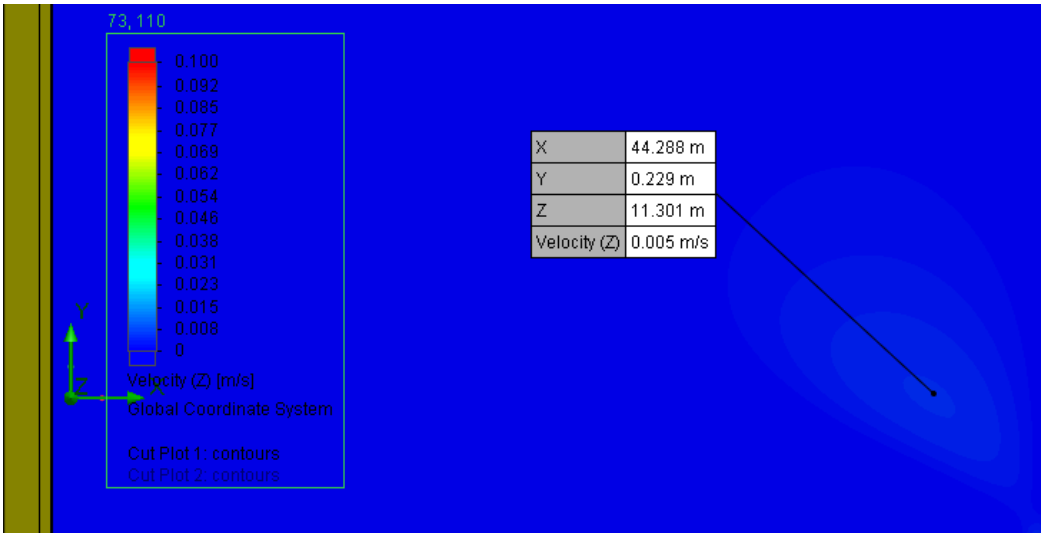

Figure b-25 Top view of the "w" velocity when V_y = -0.10 m s^{-1}

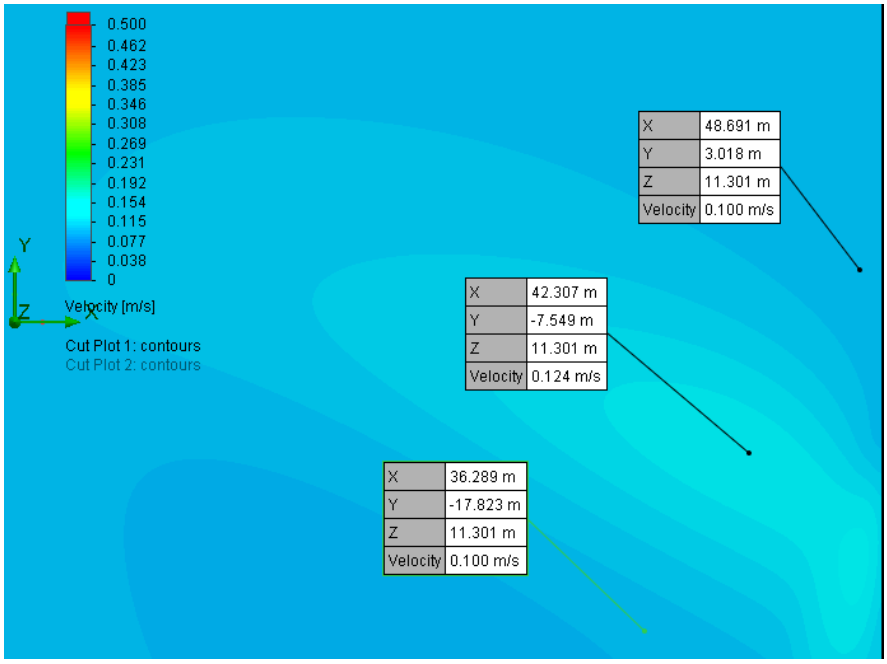

Figure b-26 Top view of the flow speeds when V_y = -0.10 m s^{-1} at a horizontal plane 11.30 m above the ground

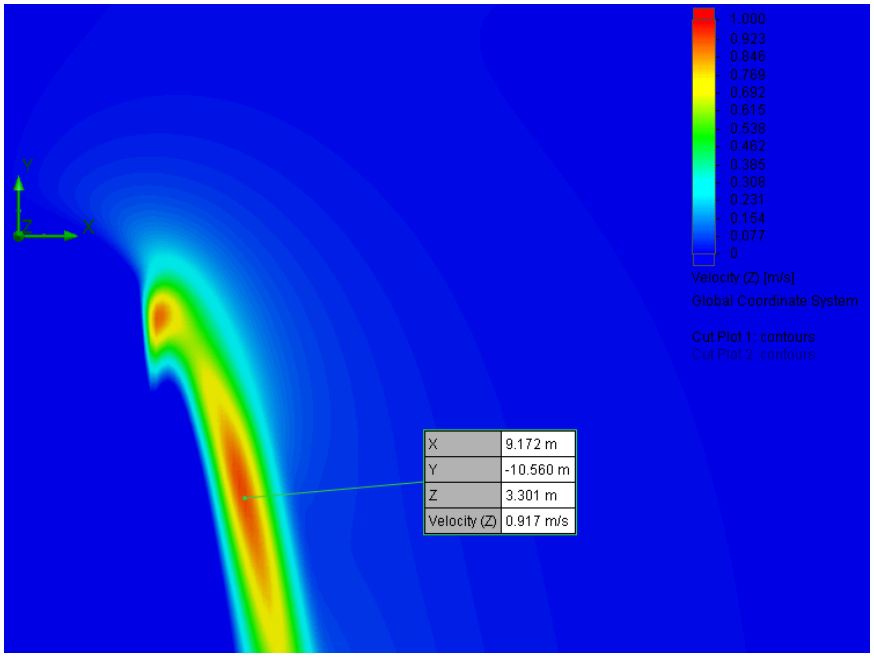

Figure b-27 Top view of the "w" velocity at z = 3.3 m when V_y = -1.00 m s^{-1}

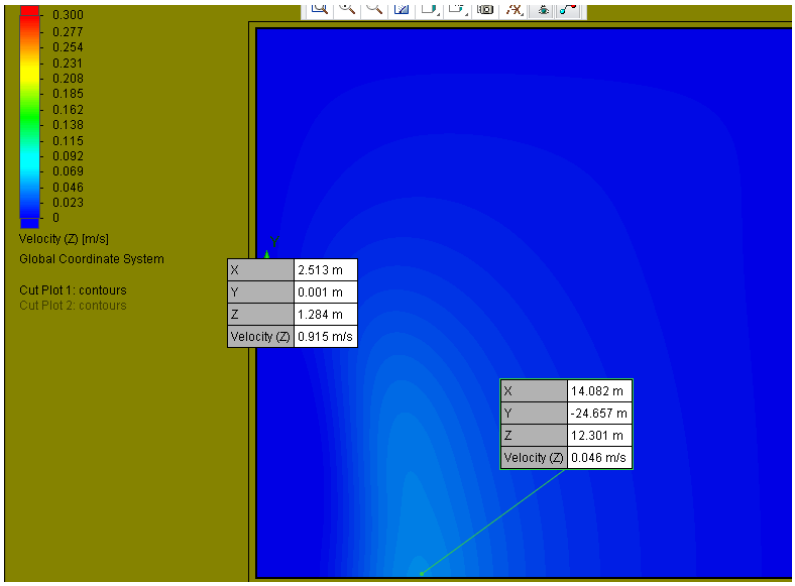

Figure b-28 Top view of the "w" velocity at z = 12.3 m when V_y = -1.00 m s^{-1}

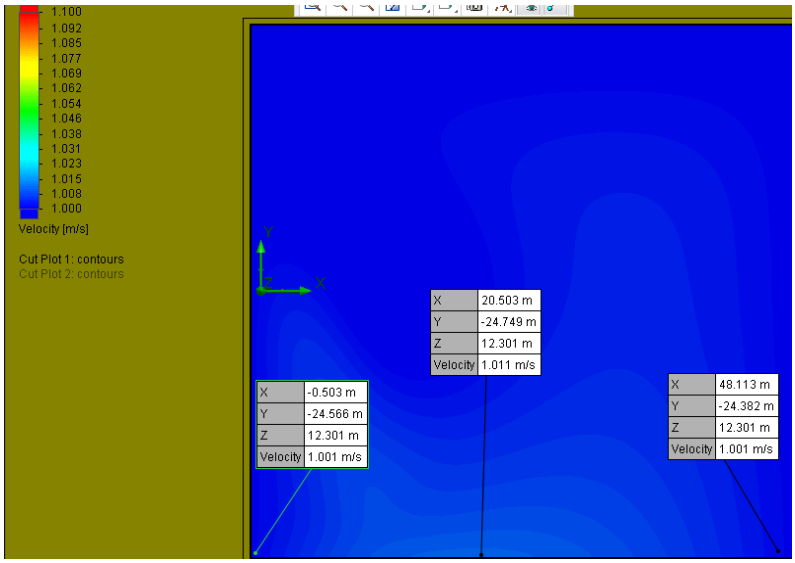

Figure b-29 Top view of the flow speeds when V_y = -1.00 m s^{-1} at a horizontal plane 12.30 m above the ground

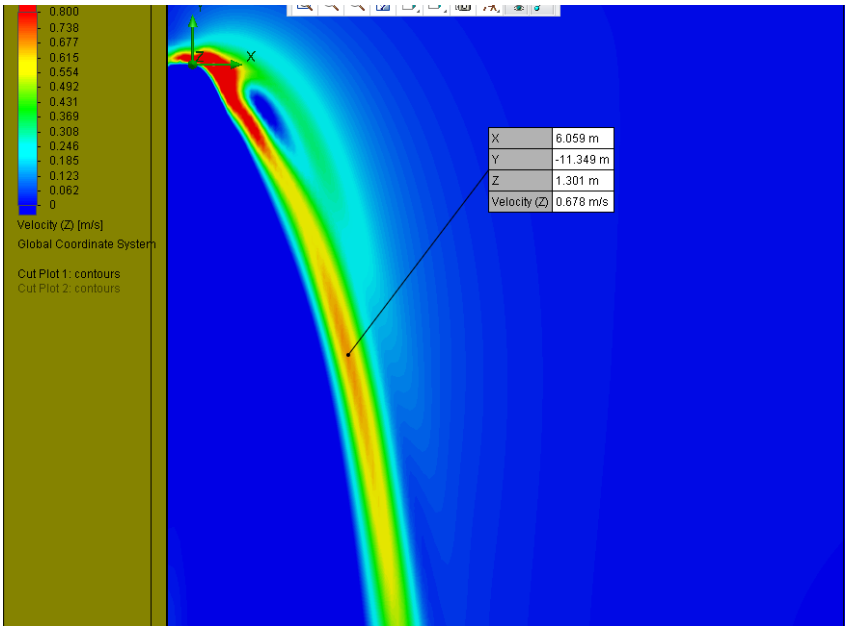

Figure b-30 Top view of the "w" velocity at z = 1.3 m when V_y = -2.50 m s^{-1}

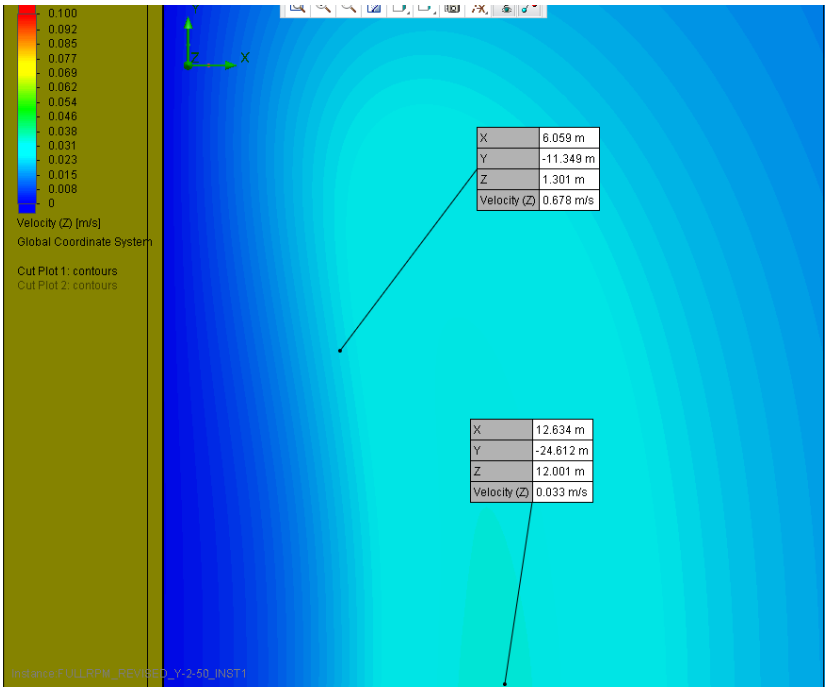

Figure b-31 Top view of the "w" velocity at z = 12.0 m when V_y = -2.50 m s^{-1}

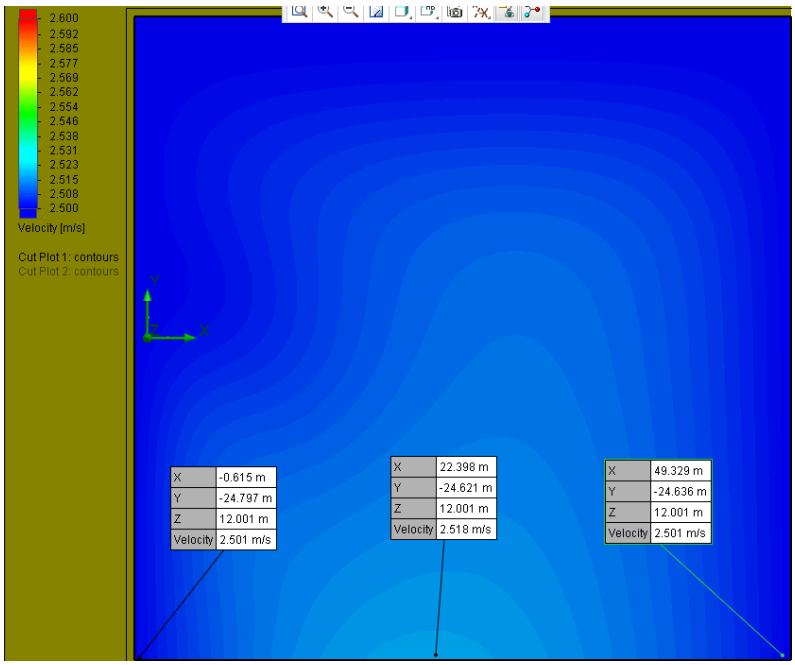

Figure b-32 Top view of the flow speeds when V_y = -2.50 m s^{-1} at a horizontal plane 12.00 m above the ground

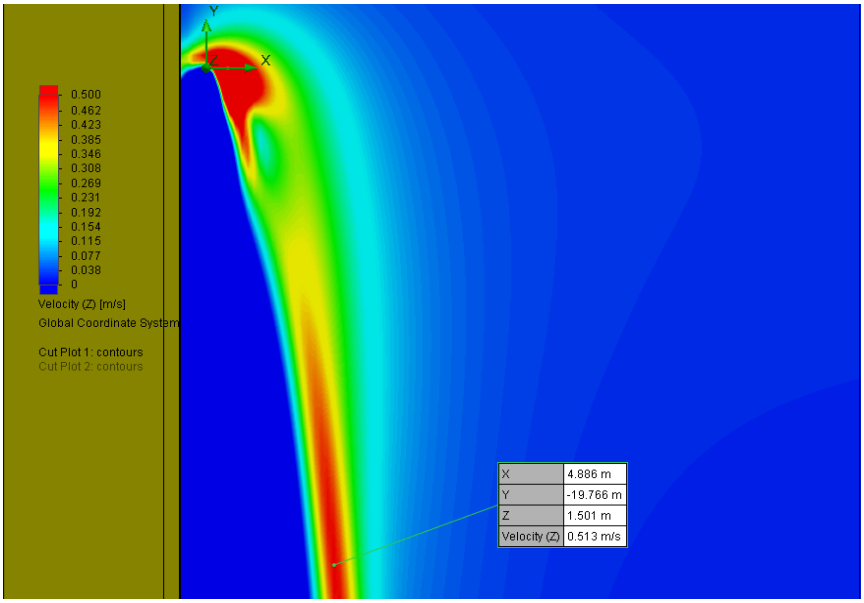

Figure b-33 Top view of the "w" velocity at z = 1.5 m when V_y = -4.00 m s^{-1}

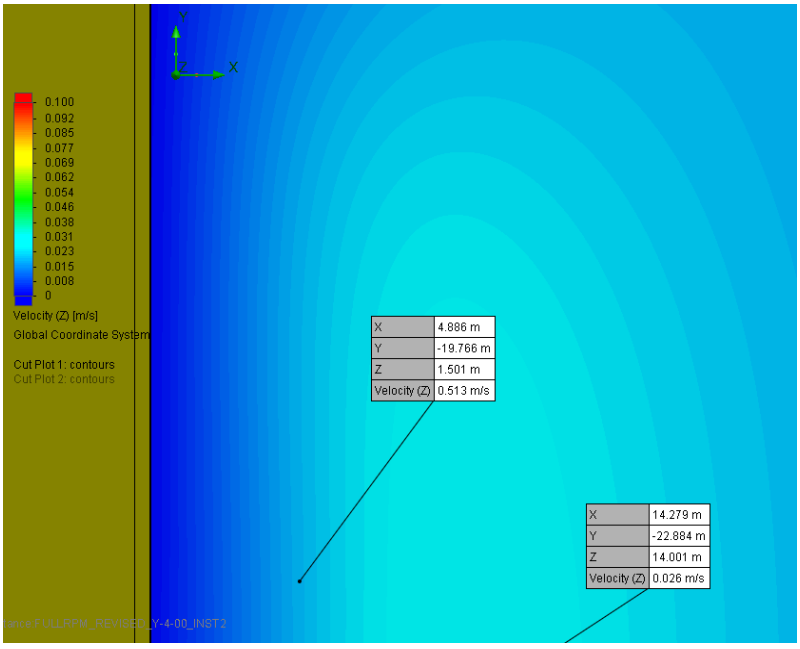

Figure b-34 Top view of the "w" velocity at z = 14.0 m when V_y = -4.00 m s^{-1}

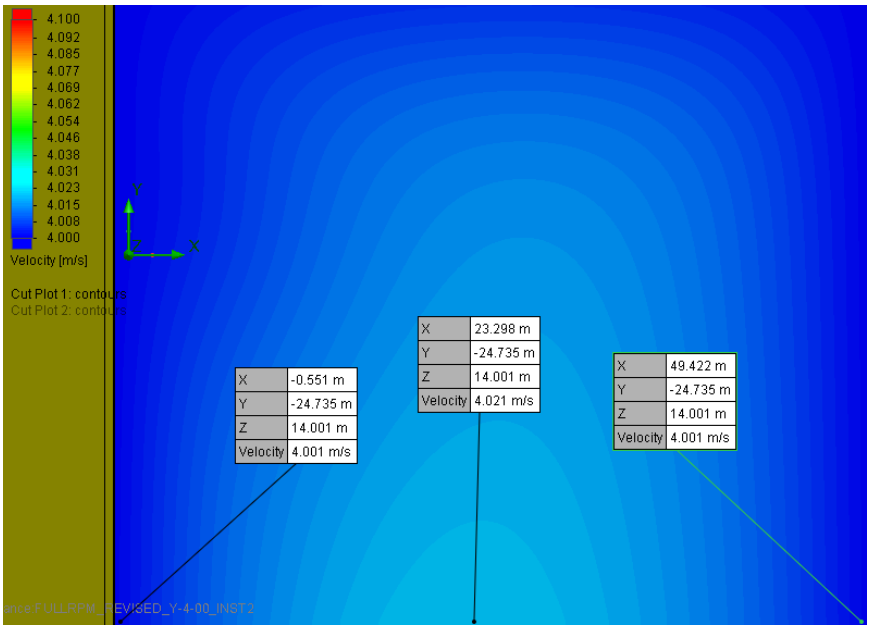

Figure b-35 Top view of the flow speeds when V_y = -4.00 m s^{-1} at a horizontal plane 14.00 m above the ground

APPENDIX C—AERMOD RESULTS

Table c-1 Summary of plume rises resulted from AERMOD simulations in fall 2008

Time	Δh_{max} (m)	$\Delta h_{adjusted}$ (m)	Wind direction	Wind speed (m s^{-1})	Ambient T (℃)	Source T (℃)	ΔT (℃)	Ambient RH (%)	Cloud cover (%)	Solar radiation (w m^{-2})	Q (m^3 s^{-1})
2008/10/11 0:00	66.5	22.0	130	2.41	293.00	298.83	5.83	82.00	10.00	0.00	1325.25
2008/10/11 5:00	66.0	27.4	140	2.83	291.90	298.26	6.36	81.00	0.00	0.00	1483.21
2008/10/11 6:00	70.0	30.7	129	2.86	291.60	298.27	6.67	81.00	0.00	14.56	1568.09
2008/10/11 11:00	72.0	42.4	124	3.76	295.40	299.38	3.98	63.00	9.00	262.44	2179.18
2008/10/11 18:00	61.0	14.5	140	1.67	293.20	298.23	5.03	70.00	0.00	0.00	1057.53
2008/10/11 19:00	61.2	16.0	139	1.84	292.60	298.29	5.69	72.00	0.00	0.00	1084.92
2008/10/11 20:00	59.0	20.7	146	2.56	291.90	298.87	6.97	75.00	0.00	0.00	1220.11
2008/10/11 21:00	43.5	12.9	138	2.04	291.70	299.02	7.32	77.00	0.00	0.00	1070.77
2008/10/11 23:00	62.0	20.2	138	2.21	290.60	298.76	8.16	77.00	0.00	0.00	1099.60
2008/10/12 10:00	28.0	13.1	165	3.75	295.30	299.34	4.04	68.00	8.00	382.17	1953.43

Table c-1 Summary of plume rises resulted from AERMOD simulations in fall 2008 (continued)

2008/10/12 12:00	39.0	14.9	160	3.35	298.70	299.82	1.12	58.00	8.00	423.49	2306.96
2008/10/12 13:00	60.0	27.9	108	3.47	299.10	299.90	0.80	55.00	9.00	327.81	2458.55
2008/10/12 15:00	72.0	24.9	156	2.60	299.80	299.91	0.11	53.00	9.00	198.86	2328.79
2008/10/12 17:00	54.0	14.8	143	1.80	296.90	299.50	2.60	65.00	0.00	17.53	1464.58
2008/10/12 20:00	62.5	12.6	156	1.61	292.10	298.51	6.41	68.00	0.00	0.00	837.69
2008/10/12 21:00	11.0	1.4	114	0.85	290.70	298.71	8.01	73.00	0.00	0.00	495.84
2008/10/13 10:00	0.0	0.0	330	1.01	295.80	299.48	3.68	62.00	8.00	357.18	890.80
2008/10/13 13:00	3.0	1.4	273	1.16	299.40	299.95	0.55	51.00	8.00	378.00	1387.10
2008/10/14 14:00	8.0	4.8	284	1.76	301.40	302.28	0.88	30.00	0.00	300.35	1910.60
2008/10/15 23:00	4.0	1.9	55	0.35	291.80	299.05	7.25	83.00	0.00	0.00	291.42

Table c-2 Summary of plume rises resulted from AERMOD simulations in winter 2008

Time	Δh_{max} (m)	$\Delta h_{adjusted}$ (m)	Wind direction	Wind speed (m s^{-1})	Ambient T (℃)	Source T (℃)	ΔT (℃)	Ambient RH (%)	Cloud cover (%)	Solar radiation (w m^{-2})	Q (m^3 s^{-1})
2009/2/4 1:00	6.0	0.2	138	1.54	275.10	294.62	19.52	78.00	10.00	0.00	136.68
2009/2/4 5:00	0.0	0.0	113	2.97	273.90	294.44	20.54	59.00	10.00	0.00	323.77
2009/2/4 10:00	24.0	11.3	301	6.33	274.80	294.20	19.40	37.00	8.00	298.33	582.33
2009/2/5 17:00	0.0	0.0	49	1.46	272.80	293.09	20.29	31.00	0.00	24.68	509.89
2009/2/5 19:00	47.0	22.1	187	0.70	270.30	292.41	22.11	45.00	0.00	0.00	286.20
2009/2/5 20:00	7.0	0.1	128	0.79	269.10	291.94	22.84	53.00	0.00	0.00	225.30
2009/2/6 2:00	72.0	1.8	162	0.75	265.70	288.42	22.72	77.00	0.00	0.00	209.58
2009/2/6 8:00	59.0	27.3	310	2.32	271.00	291.62	20.62	59.00	8.00	114.40	441.75
2009/2/6 19:00	8.0	4.2	176	1.65	278.00	295.10	17.10	54.00	0.00	0.00	458.17
2009/2/6 21:00	3.0	1.3	159	0.87	274.40	293.56	19.16	65.00	0.00	0.00	248.75
2009/2/6 22:00	36.0	0.1	160	1.59	274.70	293.61	18.91	63.00	0.00	0.00	263.53

Table c-2 Summary of plume rises resulted from AERMOD simulations in winter 2008 (continued)

2009/2/7 1:00	27.0	14.3	185	1.76	275.20	293.02	17.82	63.00	0.00	0.00	226.64
2009/2/7 3:00	34.0	20.1	188	1.76	274.60	293.44	18.84	68.00	0.00	0.00	183.61
2009/2/8 9:00	32.0	14.6	341	3.85	288.40	299.28	10.88	44.00	8.00	210.62	462.09
2009/2/8 18:00	14.0	1.4	353	1.21	292.10	298.64	6.54	47.00	0.00	0.00	307.05

Table c-3 Summary of plume rises resulted from AERMOD simulations in spring 2009

Time	Δh_{max} (m)	$\Delta h_{adjusted}$ (m)	Wind direction	Wind speed (m s^{-1})	Ambient T (℃)	Source T (℃)	ΔT (℃)	Ambient RH (%)	Cloud cover (%)	Solar radiation (w m^{-2})	Q (m^3 s^{-1})
2009/4/12 0:00	10.5	8.3	14	0.68	280.50	295.17	14.67	84.00	0.00	0.00	196.72
2009/4/12 1:00	26.8	18.3	278	0.62	279.80	294.82	15.02	84.00	0.00	0.00	250.12
2009/4/12 3:00	12.0	10.4	105	2.22	281.60	294.88	13.28	67.00	0.00	0.00	784.89
2009/4/12 4:00	26.5	18.3	103	1.69	280.80	294.69	13.89	65.00	0.00	0.00	626.03
2009/4/12 7:00	24.0	17.2	112	3.86	282.20	295.11	12.91	52.00	9.00	168.11	1310.65
2009/4/12 9:00	51.0	24.4	116	3.21	284.80	295.44	10.64	41.00	8.00	397.21	1166.18
2009/4/12 13:00	0.0	0.0	54	2.32	289.30	296.00	6.70	27.00	8.00	537.12	720.72
2009/4/12 18:00	3.7	0.4	119	0.64	289.20	295.54	6.34	30.00	0.00	25.27	457.64
2009/4/13 4:00	77.0	10.9	148	1.00	279.40	294.52	15.12	76.00	0.00	0.00	417.13
2009/4/13 5:00	9.3	0.9	108	0.67	279.10	294.53	15.43	79.00	0.00	2.65	322.91
2009/4/13 10:00	48.0	33.0	202	2.31	286.30	295.00	8.70	67.00	10.00	138.28	486.25

Table c-3 Summary of plume rises resulted from AERMOD simulations in spring 2009 (continued)

2009/4/13 12:00	30.0	20.6	235	2.61	287.30	295.33	8.02	69.00	10.00	185.52	664.46
2009/4/16 1:00	16.0	7.5	98	3.59	280.70	294.91	14.21	75.00	10.00	0.00	1095.60
2009/4/16 12:00	7.0	6.2	124	5.82	290.30	296.26	5.96	29.00	8.00	542.81	2425.36
2009/4/16 14:00	36.0	25.1	130	5.07	291.90	295.80	3.90	27.00	8.00	456.28	2486.65
2009/4/16 15:00	46.0	29.5	113	4.59	292.40	295.76	3.36	26.00	8.00	360.67	2236.69
2009/4/16 16:00	14.0	7.9	118	3.95	292.30	295.43	3.13	26.00	8.00	246.85	2193.32
2009/4/16 17:00	55.0	32.7	123	3.96	291.40	295.73	4.33	27.00	9.00	126.46	1955.22
2009/4/16 22:00	28.0	15.7	202	1.07	282.90	295.66	12.76	53.00	0.00	0.00	216.25
2009/4/16 23:00	0.0	0.0	67	1.03	281.20	295.40	14.20	58.00	0.00	0.00	163.86
2009/4/17 3:00	0.0	0.0	13	0.69	275.20	294.02	18.82	79.00	0.00	0.00	200.43
2009/4/17 6:00	18.5	21.4	334	0.94	276.50	294.49	17.99	78.00	9.00	62.58	243.39
2009/4/17 13:00	6.5	4.2	346	1.86	295.30	297.48	2.18	27.00	8.00	521.69	1552.18
2009/4/17 17:00	14.0	8.9	349	1.29	296.50	297.89	1.38	25.00	9.00	126.16	1397.92
2009/4/17 21:00	1.0	0.7	304	2.19	288.90	295.15	6.25	46.00	0.00	0.00	885.37

Table c-3 Summary of plume rises resulted from AERMOD simulations in spring 2009 (continued)

2009/4/17 22:00	18.5	11.9	316	3.06	288.60	295.29	6.69	45.00	0.00	0.00	1251.83
2009/4/17 23:00	41.0	25.4	327	2.51	287.70	294.97	7.27	47.00	0.00	0.00	1078.71
2009/4/18 0:00	29.0	18.0	325	2.13	287.00	295.00	8.00	49.00	0.00	0.00	863.01
2009/4/18 1:00	39.0	24.2	314	0.78	285.80	295.06	9.26	54.00	0.00	0.00	462.56
2009/4/18 2:00	45.0	27.9	208	2.81	284.10	294.88	10.78	62.00	0.00	0.00	171.37
2009/4/18 8:00	61.0	37.8	332	2.90	290.60	296.18	5.58	44.00	8.00	292.73	1490.19
2009/4/18 12:00	43.0	28.0	350	2.37	299.30	299.49	0.19	28.00	8.00	547.73	1913.14
2009/4/18 15:00	77.0	47.8	318	2.58	300.80	301.28	0.48	25.00	8.00	349.28	2409.87

Table c-4 Summary of plume rises resulted from AERMOD simulations in summer 2009

Time	Δh_{max} (m)	$\Delta h_{adjusted}$ (m)	Wind direction	Wind speed (m s^{-1})	Ambient T (℃)	Source T (℃)	ΔT (℃)	Ambient RH (%)	Cloud cover (%)	Solar radiation (w m^{-2})	Q (m^3 s^{-1})
2009/6/18 1:00	47.0	6.1	265	1.29	294.90	302.14	7.24	84.00	10.00	0.00	976.76
2009/6/18 15:00	54.0	18.2	335	2.72	304.40	305.06	0.66	63.00	9.00	295.79	3155.90
2009/6/18 19:00	41.5	5.7	272	1.16	301.60	303.00	1.40	76.00	0.00	3.71	2208.32
2009/6/19 5:00	1.5	0.9	26	0.61	295.80	298.50	2.70	85.00	10.00	17.72	1172.71
2009/6/19 14:00	26.0	15.8	326	1.67	304.80	304.95	0.15	53.00	9.00	320.32	2400.81
2009/6/19 16:00	72.0	5.6	263	0.74	305.90	305.42	-0.48	53.00	10.00	193.57	1850.52
2009/6/19 19:00	41.0	5.9	280	1.11	302.20	303.59	1.39	71.00	5.00	1.50	2281.72
2009/6/19 21:00	12.0	7.3	303	2.05	301.10	302.31	1.21	72.00	0.00	0.00	2929.52
2009/6/19 22:00	40.0	24.3	292	2.25	300.60	301.92	1.32	73.00	0.00	0.00	2997.25
2009/6/20 2:00	57.5	9.3	336	1.29	299.10	300.90	1.80	79.00	0.00	0.00	2421.58
2009/6/20 12:00	30.0	14.5	337	3.96	305.60	306.46	0.86	62.00	9.00	334.95	3806.96

Table c-4 Summary of plume rises resulted from AERMOD simulations in summer 2009 (continued)

2009/6/20 19:00	57.5	10.8	342	1.62	304.00	305.36	1.36	64.00	0.00	5.92	2553.90
2009/6/21 14:00	72.0	29.4	74	4.77	305.50	305.72	0.22	43.00	9.00	397.64	2888.55
2009/6/21 20:00	56.5	10.7	109	1.38	299.20	300.66	1.46	64.00	0.00	0.00	2359.81
2009/6/22 9:00	72.0	43.2	74	3.31	300.20	300.81	0.61	58.00	9.00	352.55	2838.23
2009/6/22 16:00	33.0	20.0	78	2.31	303.30	303.65	0.35	52.00	9.00	217.38	2094.44
2009/6/22 18:00	19.5	11.8	324	2.72	302.80	303.16	0.36	56.00	10.00	58.30	1663.17
2009/6/22 20:00	30.5	18.4	185	0.63	298.30	300.27	1.97	75.00	0.00	0.00	1605.11
2009/6/22 23:00	23.0	14.1	184	1.14	295.60	298.89	3.29	83.00	0.00	0.00	1065.38

APPENDIX D—STATISTICAL CODES

SAS CODE OF SNK TEST IDENTIFYING DIFFERENCE OF PLUME RISES AMONG SEASONS

```
data season;
infile "C:\Users\mqying\Desktop\season.txt" firstobs=2;
input season$ plumerise;
run;
proc sort data=season;
  by season;
run;
proc univariate plot data=season;
  var plumerise;
  by season;
run;
proc glm data=season;
  class season;
  model plumerise = season;
  means season / SNK lines;
run;
```

R CODE OF MULTIPLE LINIEA REGRESSION MODEL FOR FACTORIAL ANALYSIS OF PLUME RISES

```
factor <-read.table(file="summary of result.txt",header=TRUE)
mult <-
lm(adjustedplumerise~winddirection+windspeed+ambientT+sourceT+deltaT+ambientRH+cl
oudcover+solarradiation+totalQ,data=factor)
summary(mult)
```